Distributed Control of Microclimate by Honeybee Colonies, Apis Mellifera, L.

Distributed control of microclimate by honeybee colonies, *Apis mellifera* L.

A DISSERTATION PRESENTED
BY
JACOB M. PETERS
TO
THE DEPARTMENT OF ORGANISMIC AND EVOLUTIONARY BIOLOGY

IN PARTIAL FULFILLMENT OF THE REQUIREMENTS
FOR THE DEGREE OF
DOCTOR OF PHILOSOPHY
IN THE SUBJECT OF
ORGANISMIC AND EVOLUTIONARY BIOLOGY

HARVARD UNIVERSITY
CAMBRIDGE, MASSACHUSETTS
APRIL 2018

Thesis advisor: Professor L. Mahadevan Jacob M. Peters

Distributed control of microclimate by honeybee colonies, *Apis mellifera* L.

Abstract

Social organisms often exhibit complex, ordered behaviors at the group level that are not observed in individuals. Such collective behaviors emerge from the iterative interactions between individuals, each of which sense and respond to local stimuli. Many group behaviors in social insects arise not from direct interactions between individuals but from distributed interactions with a shared environment, a process known as *stigmergy*. In classical examples of stigmergy, an individual deposits a cue in the environment, such as a clump of pheromone-laden building material, which in turn influences the behavior of the next individual to encounter the deposition. These local manipulations lead to self-organization of large scale patterns such as complex nest architecture. In these examples, the interactions between individuals and the environment are local. However, stigmergic behaviors can also involve interactions with a dynamical physical processes in the environment such as airflow, elastodynamics or heat transfer. In such instances, non-local physical interactions play a role. In this thesis I use both experimental and computational approaches to explore a class of behaviors in honeybee colonies in which bees collectively modulate large scale physical processes through local manipulations of their shared dynamical environment. In Chapters 1 and 2, I investigate how temperature-dependent wing fanning behaviors in honeybees give rise to efficient large-scale flows during nest ventilation. In Chapter 3, I explore how honeybee swarm clusters change their collective morphology in order to maintain stability when exposed to dynamic mechanical perturbations. In Chapter 4, I explore how swarm clusters modulate their morphology to maintain thermal stability despite large fluctuations in ambient temperature. Taken together, this work suggests honeybees can coordinate large-scale physical processes through distributed local interventions. This may be a ubiquitous strategy in the evolution of complex systems.

Contents

Listing of figures

To Carlos. Without his persistent support and friendship I would not have had this opportunity.

Acknowledgments

My PhD experience has been a bit tortuous and as a result I have interacted with a lot of wonderful people.

I have learned that doing research requires us to constantly tackle problems that we lack the skill or expertise to solve. At first this perpetual feeling of unpreparedness was uncomfortable and even paralyzing for me, but after sharing an office with James Crall and Nick Gravish for a couple of years I have learned to operate under the assumption that the task at hand is doable. Thanks guys.

I would like to thank Stacey Combes for assembling an awesome team. The Combes lab was delightful place to work. Graduate school can be isolating, but the Combes crew–Callin, Mary, James, Nick, Sridhar, Susie, Andrew–often felt more like a family than a group of coworkers. It was hard to watch the lab dismantled, but I hope to reproduce that kind of camaraderie in a group of my own someday.

The staff at the Concord Field Station has been an important support for me. Lisa, Andra, Ken, Pedro and Somer have always been eager to help with any problem, even if they are unrelated to their jobs. The Biewener lab–Andy, Talia, Glenna, Kari, Brianna, Phil, Alison, Nicolai, Ivo, Chris–have also made me feel like I belong. This was especially important to me as the Combes lab slowly disbanded.

The field station itself is a unique place and projects like mine would not be possible without it. Honeybee work requires reconfigurable indoor and outdoor space which is rare on campus. It also requires an exceptionally tolerant groundskeeper. There are a few nooks and crannies at CFS that tend to accumulate strange experimental devices from previous students and projects. There have been many occasions where my experiments have been saved or even inspired by things found in these rummage piles. I hope that Harvard will hold on to this place and the unique culture that has developed there.

The Lauder lab provided a temporary home base for me while I was transitioning between lab groups. I learned a lot about instrumentation and how to take a more systematic approach to experiments. I think I would have made a good fish scientist if I had joined the group earlier in my PhD. Thanks to George, Dylan, Kelsey, Kara, Chris, Valentina and Maggie for making me feel welcome.

I am pretty lucky to have had the opportunity to work with Maha. There are few group meetings where you can learn about super-massive black holes, origami tessellations, limb bud development and yogurt in one session. Even rarer are lab cultures in which these topics are considered related. From Maha I have learned how to identify the active ingredients in a system, describe their interactions and turn an otherwise unanswerable question into a solvable math problem. Perhaps the most important thing that I have learned from Maha is the richness that one can discover by probing phenomena that might otherwise seem intuitive and familiar. I used to worry that all of the interesting topics are taken, but now they are everywhere. Thanks Maha.

Several of the projects in this dissertation were done through close collaboration with Orit Peleg. I think that we both accomplished more together than we ever could have on our own. I am grateful to Orit for this and have learned a lot from her over the past few years.

Jim MacArthur was a critical resource for me during my PhD. I have learned a lot by working with him to develop the instrumentation needed to execute my experiments.

Ben de Bivort asked several difficult questions during my qualifying exams and committee meetings that identified a few major gaps in my knowledge. I never would have read about control theory or wondered about the role of inter-individual variation in collective control strategies without these conversations. Both topics have provided useful context for my work.

Finally I would like to thank my committee as whole–Ben, Andy, George and Maha–for the encouragement, criticism and guidance during this process.

List of Authors

The following authors contributed to Chapter 1: Nick Gravish and Stacey A. Combes.
The following authors contributed to Chapter 2: Orit Peleg and L. Mahadevan.
The following authors contributed to Chapter 3: Orit Peleg, Mary Salcedo and L. Mahadevan.
The following authors contributed to Chapter 4: Orit Peleg and L. Mahadevan.

0

Introduction

Large groups of organisms often exhibit complex, ordered behaviors at the group level that are not observed in individuals (e.g., coordinated evasive maneuvers in schooling fish[71], synchronization of flashing fireflies[8], complex nest construction in social insects[84]). Instead, these collective behaviors emerge from the interactions between individuals that each sense and respond to local stimuli. Due to the nonlinear nature of these systems, determining the underlying rules that govern the behavior of individuals does not necessarily provide insight into the workings of the group level behavior; that is, the outputs of the system are not directly proportional to the inputs. This conundrum makes the study of these systems inordinately difficult, but it also suggests intriguing possibilities for evolutionary change. For instance, subtle changes to the parameters that control the interactions between individuals (some of which are heritable) can lead to large changes insystem-level properties. This means that qualitatively different group behaviors may result from subtle changes to the same underlying mechanism, amplifying the phenotypic space available for evolution.

Self-organization affords biological systems complex functions that do not need to be explicitly

coded in the genome of individual organisms. Natural selection can act on self-organizing systems in several ways. For example, many self-organizing systems have multiple stable states, and changing parameters intrinsic to the system or within the environment can induce a phase transition between these states[11]. These parameters could be tuned by natural selection so that the function of the system transitions from one behavior in context A to another behavior in context B. For example, the cellular slime mold *Dictyostelium discoideum* hunts as a solitary amoeba when food resources abound, but aggregates through cAMP signaling when resources are sparse to form fruiting bodies[72]. Alternatively, natural selection might drive the system away from these bifurcation points so that the behavior is relatively stable over a large range of internal and external conditions[11]. For instance, workers in honeybee colonies with a multiply mated queen show broad variation in task response thresholds associated with colony-level thermoregulation[38]. As a result, the brood nest of such colonies are more thermally stable than those with queens that have mated only once, resulting in workers with more uniform task response thresholds. Natural selection might favor polyandry as a mechanism for maintaining the genetic diversity required to exhibit graded thermoregulatory responses and ultimately to achieve thermal stability over a broad range of ambient temperatures.

Not only does self-organization relieve the cognitive/computational burden required for individuals to control complex behaviors[16], it also allows them to overcome scaling constraints. For example, schools of juvenile golden shiners seek shaded water to avoid predators. However, the individual fish are so small (5cm) that they sense only scalar measures of the local light intensity. Individuals swim slower in low light and faster in bright light. This individual stimulus-response rule coupled with the cohesion and alignment of the group allows the group to track noisy, meter-scale light gradients to find dark water[4].

Collective behaviors are often described in terms of the behavioral algorithms that individuals execute in response to one another and the environment. The resulting interactions between individuals are presumed to give rise to complex global behaviors. However, these systems do not exist

in a vacuum. In fact, these behavioral interactions are often mediated by the environment in which they occur. For example, the ordered motion of groups of the swimming bacterium *Bacillus subtilis* is influenced not only by the interactions between self-propelled individuals but also by the large-scale fluid flows that they collectively generate[49]. The recognition that the interaction between active agents suspended in passive fluids can give rise to ordered, large-scale flows has spawned the booming field of soft active matter (reviewed by Marchetti et al.[50]). Soft active matter is a rich topic of study because complexity in these system arises not only due to nonlinear interactions between the active components (e.g., self-propelled particles) but also through the nonlinear physics associated with soft condensed matter (e.g., fluids, gels). Many studies in this field take a reductive view of biological agents in order to rigorously explore the complex physics. On the other hand, biologists often emphasize the behavioral interactions between organisms while considering physical interaction with the environment to be negligible.

In many instances, however, the explicit function of group behaviors is to shape or control the micro-environment. In such cases information may be propagated not through direct interactions between neighboring individuals, but through distributed, recursive interactions with their common environment. For instance, colonies of the ant *Lasius niger* build large, complex nests without central coordination or direct interactions between ants. Individuals pick up building material, infuse it with pheromone, and deposit it somewhere else. Workers are more likely to deposit building material where others have previously deposited pheromone-laden material. This positive feedback and the depletion of pheromone-free building material leads to the emergence of pillars[44]. This process - in which one individual's modification of the environment stimulates future actions by other individuals - is called stigmergy[28].

From a narrow view of stigmergic nest building behaviors, it can appear that the environment is functionally inert. Because the material being manipulated is a hard solid, the physical interactions are simple: pick it up here and set it there. However, Theraulaz et al.[81] note that many nests

built by social insects have features, such as helical ramps, that appear to be related to large-scale air flows, which influence the form the nest structure takes and are in turn influenced by the resulting structure. Large scale flows are known to play a role in nest ventilation in many social insect species (reviewed by Jones and Oldroyd[39]). For instance, colonies of the fungus-harvesting termite *Odontotermes obesus* build large, unoccupied mounds above their nests. These mounds are heated by the sun during the day and cooled by ambient temperatures at night. Temperature gradients within this fluted mound, which are imposed by daily heating and cooling cycles, drive large scale flows that facilitate respiratory gas exchange[45].

Observable examples of the interaction between building behavior and flow are limited because such interactions occur over long time scales in cluttered environments. However, there are several notable laboratory experiments that suggest a role for flow in patterning building behavior, and vice versa. For example, the ant *Messor sanctus* tends to form piles of their corpses[42]. Individual ants pick up corpses where they are sparse and deposit them where they are dense, leading to a spatial pattern that coarsens until only a few stable corpse piles remain[83]. Jost et al.[42] placed a group of ants in an experimental arena that was blanketed with randomly dispersed corpses and induced a laminar airflow through the arena. Ants were more likely to remove corpses from regions of high wind and place them in regions of low wind. This resulted in the elongation of the leeward side of corpse piles and further channelization of airflow. This example suggests that large-scale patterns within insect nests could emerge from the interaction between a stigmergic building process and airflow, but it does not suggest any function for the airflow in this system. Several theoretical studies, however, have suggested that if (1) an individual-level behavior is responsive to flow-mediated cues such as pheromones or temperature, and (2) such behaviors in turn manipulate the flow, then global behaviors can arise that control this flow for adaptive functions such as ventilation or thermoregulation[6,61,62].

In this dissertation, I investigate three collective behaviors in which individual honeybees, act-

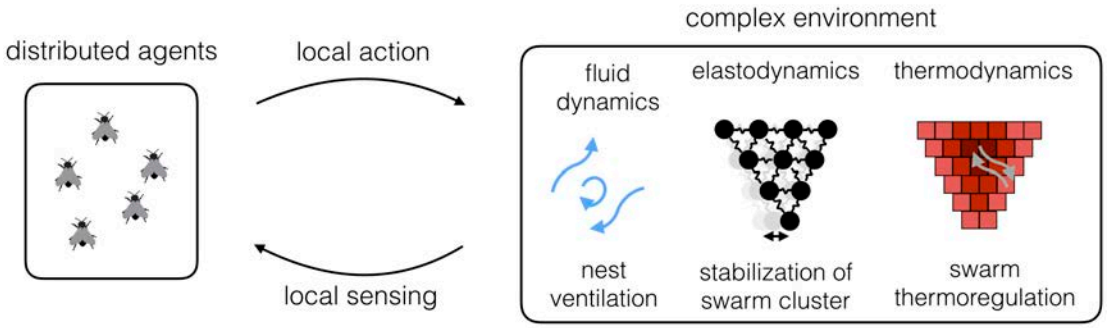

Figure 1: Schematic of dynamic interaction with environmental forces and flows.

ing as independent, distributed agents, sense and act upon their local environment, giving rise to colony-scale physiological processes that are mediated by forces and flows (Fig. 1). In Chapters 1 and 2, I examine how individual bees fanning their wings in response to high air temperatures can give rise to efficient, hive-scale airflows that effectively regulate nest temperature. The global flow patterns that arise result not from direct behavioral interactions between bees, but from non-local interactions mediated by fluid dynamics. In Chapters 3 and 4, I examine mechanical stabilization and thermoregulation of honeybee swarm clusters. In Chapter 3, I explore how honeybee swarm clusters change their collective morphology in order to improve their mechanical stability when faced with physical perturbations. In this loaded network of bees, long-range elastodynamic interactions play a role in coordinating the morphological response. In Chapter 4, I explore how swarm clusters change their morphology to maintain thermal stability in response to ambient temperature fluctuations. In this system, the local stimulus-response behaviors of individuals are coordinated in part by heat transfer through a dynamic, porous medium. Taken together, this body of work suggests that honeybees can manipulate large-scale physical processes to solve physiological problems through distributed local interventions. This may be a ubiquitous strategy in the evolution of complex systems.

1

Wings as impellers: Honeybees co-opt flight system to induce nest ventilation and disperse pheromones

1.1 Introduction

Insect wings have undergone approximately 285 million years of evolution as flight appendages[18]. The evolution of flight contributed to the dramatic diversification of insects in the Carboniferous period and has subsequently allowed winged insects to colonize nearly every terrestrial ecosystem[18]. Researchers often assume that flight performance is the only selective pressure driving the evolution of the flight apparatus. However, many winged insects have evolved secondary functions for wings. When at rest, insect wings can provide physical protection (e.g., forewings of beetles and grasshoppers[85]), help to absorb or dissipate heat (e.g., butterfly wings[73]), provide camouflage, or signal to conspecifics and potential predators. The wings can also be moved for non-flight functions such drawing air past the antennae to sense pheromones[48], producing sounds (e.g. stridula-

tion), or for alternative forms of locomotion, such as skating across water surfaces (e.g, stoneflies[51]). Although these alternative functions of wings are well known, few studies have examined how the physical demands of these non-flight functions differ from those of flight – a critical step in understanding how the various selective forces acting on the insect flight apparatus have contributed to its current form.

Here, we investigate the mechanics of a critical, non-flight use of the wings in social Hymenoptera—ventilatory fanning. Honey bees, bumblebees, paper wasps, yellow jackets, hornets and some stingless bees flap their wings while standing on the surface or at the entrance of their nests. This behavior presumably induces airflow through and around the nest that promotes convective cooling and/or gas exchange[40]. When nest temperatures or carbon dioxide concentrations rise above a threshold, honey bees assemble at the entrance of the nest and fan their wings, driving temperature and/or CO2 values back below the threshold[38,74] (Fig. 1). This behavior is critical to the success and fitness of the colony, as failure to regulate brood temperature can lead to cognitive deficiencies in adulthood[37]. Considering that ventilation is crucial to healthy brood development, and that they invest so much time in a behavior that is likely to be energetically costly, we posit that there is a strong selective pressure on the flight system to accommodate this non-flight behavior.

Wing fanning also plays an important role in chemical communication among honey bees. During entry into a new nest site, honey bees broadcast volatile pheromones produced by the Nasonov gland at the tip of their abdomen. Bees that have located the entrance of the nest raise their abdomens and fan their wings, driving airflow across the Nasonov gland, which disperses pheromones that signals the location of the nest entrance to the rest of the swarm[3]. This "scenting" behavior is also used for other purposes, such as to direct disoriented workers back to the nest entrance after a nest disturbance[70].

Stationary wing fanning is a unique challenge for a winged insect. Fanning is used to impel (or blow) air along a solid, two-dimensional surface without displacing the insect's body, whereas

Figure 1.1: A group of honey bees fanning at the entrance of a man-made hive. Note that fanning bees are oriented with their abdomens pointed away from the nest entrance, drawing air out of the hive.

the flapping motions associated with flight are used to propel the insect through an aerial, three-dimensional world, generating air flows and forces that offset its weight and direct its motion. Insect wings have undergone several hundred million years of evolution as flight appendages that generate flow in a three dimensional, aerial environment. In contrast, ventilatory fanning in Apis presumably arose only after the appearance of eusociality in corbiculate bees, approximately 87 mya[12], and co-opting propulsive wings to serve as impellers presents several physical challenges. First, the primary direction of fluid movement generated by the wings must be shifted from downward (as in flight), to horizontal (as in fanning). Second, the kinematics of flapping must be altered to avoid disadvantageous contact with the solid surface, which could cause wing damage[56], reducing flight performance and survival[13,19,55]. In this study, we explored three aspects of stationary wing fanning to better understand the selective pressures that this behavior may place on the flight system: 1) kinematic differences between wing fanning and flight, 2) the magnitude of air flow produced by

an individual fanning bee, and 3) the potential role of wing-wing and wing-ground interactions in generating ventilatory flows.

1.2 Methods

High-speed filming

All filming was performed on honey bees from domesticated, outdoor hives at the Concord Field Station in Bedford, MA. 13 fanning bees performing ventilation behavior at the entrance of a beehive were filmed at 5000 fps using two Photron SA-3 cameras. The cameras were focused on a small focal volume (approximately $8 \times 8 \times 8$cm) at the nest entrance. The hive was placed on a 2-axis rail system so that when a fanning bee was identified, the hive could be re-positioned to center the fanning bee within the focal volume of the cameras (Fig. 2A). Before each round of filming, a 3D calibration was obtained by capturing a still photo of a calibration object with 14 markers with known spatial relationships. The calibration frames were analyzed using DLTdv5 MATLAB program[31]. Because the calibration object was level, we were able to reference the horizontal plane in our video analysis. Filming of fanning behavior was conducted from 12-3pm on 09/20/2013. Bees were exposed to full sun during filming and the ambient temperature ranged from $23 - 26°$C (recorded by the weather station at Hanscom Airforce Base).

A similar camera set-up was used to film 8 individuals performing Nasonov scenting behavior at 7500 fps. Approximately 500 workers from an artificial swarm of honey bees were placed at the entrance of an empty hive structure containing the swarm's queen. Upon locating the nest entrance, workers paused, lifted their abdomens, and began to fan their wings, driving air across the exposed Nasonov gland. Filming of Nasonov scenting behavior was conducted on 08/14/2013 between 2 and 5pm. Videos were captured in full sun and the ambient temperature ranged from $21 - 23°$C (recorded by the weather station at Hanscom Airforce Base).

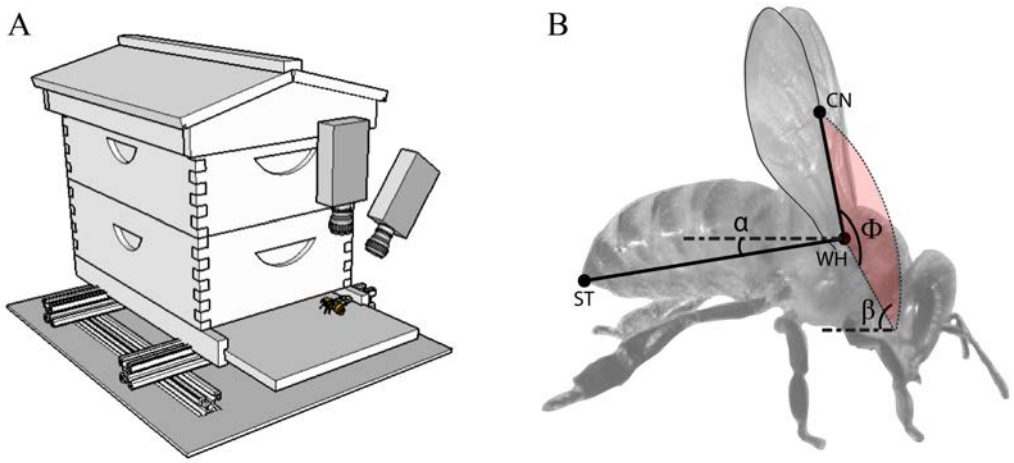

Figure 1.2: (A) Camera set-up used to film ventilatory fanning behavior. Two high-speed video cameras were focused on a point near the nest entrance and calibrated. When a bee began to fan, the entire hive was translated on a rail system so that the fanning bee was visible in the focal volume of the cameras. A similar set-up was used to film Nasonov scenting behavior. (B) Landmarks and kinematic parameters measured on fanning and scenting bees. The costal notch (CN) on the leading edge of the forewing, the wing hinges (WH) on both sides, and the sting (ST) were digitized in each video frame. These landmarks were used to calculate abdomen angle (α), stroke amplitude (Φ), and stroke plane angle (β)). Note that when the sting is positioned below the wing hinges (as in the illustration), abdomen angle is reported as negative.

Quantification of kinematics

The costal notch on the leading edge of one wing, both wing hinges, and the sting (tip of the abdomen) were digitized during five successive wing strokes using the DLTdv5 MATLAB program [31]. The positions of these landmarks were used to calculate the stroke amplitude, frequency, stroke plane angle, and abdomen orientation of fanning and scenting bees. Wing stroke parameters were quantified using methods described by Altshuler et al.[1], so that our data could be directly compared to previously obtained measures for honey bee flight kinematics (Fig. 2B).

Stroke plane angle was determined by performing a regression on the path of the leading edge of the wing for 5 successive wing beats, and calculating the angle between this line and the horizontal plane. This metric describes the orientation of the plane through which the wing sweeps while flapping. Wing position was calculated as the instantaneous angle of the wing within the stroke plane, with the wing defined by a vector running from the wing hinge to the costal notch on the leading edge. Stroke amplitude was calculated as the difference between the maximum and minimum wing position angles, averaged over 5 wing strokes. Flapping frequency was determined by conducting a fast Fourier transform on the time series of wing positions over 5 strokes. The stroke-averaged angular velocity (rad s^{-1}) of the wing was calculated by dividing the stroke amplitude by the average duration of a half stroke. Abdomen angle was calculated as the angle between the horizontal plane and a line connecting the midpoint between the wing hinges with the sting in the initial frame of the video (note that an analogous measurement during hovering flight was not available for comparison). Bees did not adjust their posture noticeably during the five strokes analyzed from each video.

Statistical analysis

For each kinematic parameter evaluated (flapping frequency, stroke amplitude, stroke plane angle, and abdomen angle), we tested the null hypothesis that the median values of each flapping behavior

(fanning, scenting, and hovering when available) were equal, using a Kruskal-Wallis test. In cases where the null hypothesis was rejected and data was available for all three behaviors, we conducted multiple comparisons among the behavioral modes using the Tukey method, to determine which behaviors exhibited differences in the kinematic parameter.

Flow visualization

We performed qualitative flow visualization of Nasonov scenting behavior, but were unable to use this technique for ventilatory fanning, due the difficulties involved in inducing ventilation behavior in the laboratory. We visualized the flow generated by Nasonov scenting behavior in a transparent acrylic tunnel ($5 \times 5 \times 50$ cm) extending from a previously occupied hive, using a 532 nm sheet laser (Optotronics, Class IIIB, 2 Watts) and a high speed camera (Photron SA-3) filming at 5000 fps. The hive box was seeded with suspended olive oil droplets, which diffused out of the box through the tunnel. The laser sheet was oriented downward toward the tunnel such that the laser sheet bisected the tunnel along the long axis. Particles moving along this plane were illuminated and visible to the camera.

Groups of 10 bees were placed in the tunnel. When the bees smelled the odor emanating from the nest box, they initiated Nasonov scenting behavior. Once wing fanning commenced, the hive/tunnel and the bees were re-positioned such that the laser illuminated a sagittal section of the air surrounding a fanning bee. An orthogonally positioned high-speed camera was used to film the motion of the particles.

1.3 Results

Comparison of wing kinematics and body posture

Our comparison of wing kinematics during ventilatory fanning behavior, scenting behavior, and hovering flight reveal that these behaviors involve kinematically distinct flapping modes (Table 1). Honey bees flap their wings at significantly lower frequencies during ventilatory fanning behavior than during scenting behavior or hovering flight (p = 0.0112 and 0.0007, respectively; Fig. 3A). In addition, stroke amplitude is significantly higher during fanning behavior than during hovering (p = 0.0076, Fig. 3B). During scenting behavior, bees exhibited substantial variation in stroke amplitude ($70 - 125°$), but the median of the distribution did not significantly differ from that during ventilatory fanning or hovering (p $= 0.0835$ and p $= 0.5207$). The angular velocity of the wing during fanning, scenting and hovering was not significantly different. Both fanning and scenting bees flapped their wings through an anteriorly rotated stroke plane angle ($> 50°$) relative to that of hovering bees (p $= 0.0024$ and 0.0138, respectively; Fig. 3C). However, despite maintaining a similar stroke plane angle, fanning and scenting bees exhibited significantly different body postures. On average, the abdomen angle of scenting bees was more than $15°$ higher than that of fanning bees (p $= 0.0018$, Fig. 3D).

Flow visualization and velocity measurements

Our flow visualizations revealed that scenting honey bees draw air in from a broad area upstream, and accelerate it backwards in a narrow jet that runs approximately parallel with the surface to which the bees are clinging (Fig. 4A, Movie 1). A substantial portion of the upstream air appears to be drawn downward from above the bee. The flow visualization videos also revealed that scenting bees shed a vortex at the end of the upstroke. When viewed in the sagittal plane, this vortex flows along

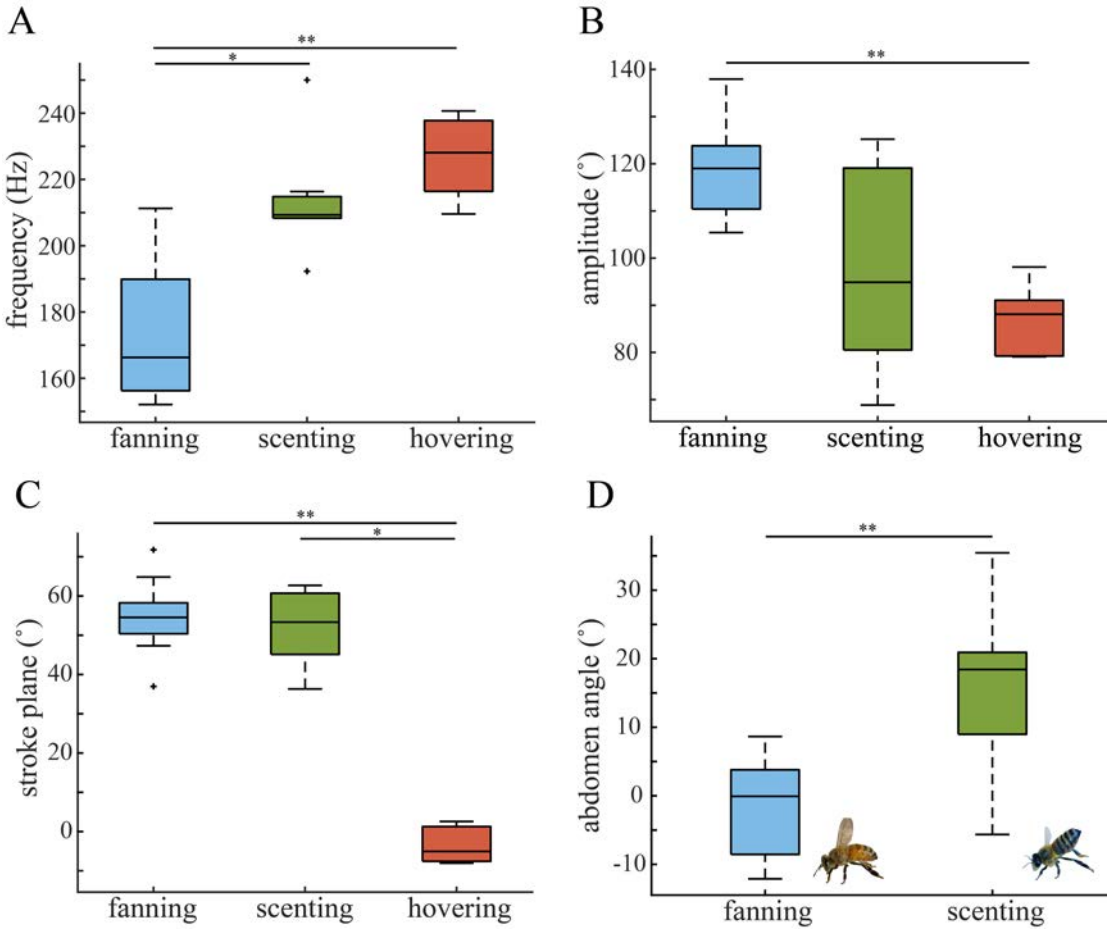

Figure 1.3: Flapping frequency (A), stroke amplitude (B), stroke plane angle (C), and abdomen angle (D), plotted according to the type of wing-flapping behavior (* indicates p < 0.05, ** indicates p < 0.01). Values for hovering flight were calculated from Altschuler et. al. ([1]) and Vance et. al. ([86]) no corresponding measures of abdomen angle during hovering were available. Sample sizes are provided in Table 1 and indicate the number of individuals from which each parameter was measured.

the dorsal surface of the abdomen and into the wake of the bee, persisting for approximately 1.5 body lengths. By digitizing the position of this vortex within the sagittal plane over 25 successive wing strokes of one bee (Fig. 4B), we calculated an average flow speed of 0.94 ± 0.11 m/s (mean ± SD). Because the vortex is traveling along the boundary between a low flow region (above) and the fast-moving current (below), we suspect that this is a slight underestimate of the flow speed generated by this bee during scenting.

Qualitative observations of wing-wing and wing-ground interactions

From the high-speed videos used for kinematic analysis and flow visualization, we made several unexpected observations of wing-wing and wing-ground interactions. In scenting bees, we observed wing-wing interactions during dorsal stroke reversal in some videos (Fig. 4A). In these cases, the leading edge of the forewings would come into contact with each other at the end of the upstroke. The point of contact would then shift chordwise towards the trailing edge, as the leading edges began to pull apart at the start of the downstroke (see Movie 2). This wing-wing interaction is reminiscent of the clap-and-peel mechanism observed in many small insects that fly at low Reynolds numbers, which enhances lift[53]. In some of the videos, we did not see any physical contact between the wings; we cannot address whether this difference is due to inter-individual variation in behavior or due to behavioral flexibility within an individual. We were also unable to determine whether wing-wing contact occurs during ventilatory fanning, because the contact was only visible with the use of a laser sheet during flow visualization. However, because the stroke plane angle is similar during both behaviors, and stroke amplitude is often higher during fanning, we suspect that wing-wing interactions occur at least some of the time during ventilatory fanning as well.

In addition to wing-wing interactions during the dorsal stroke reversal, we also observed that the forewings commonly contact the ground during ventral stroke reversal, in both fanning and scenting bees (Fig. 4B). At the end of the downstroke, the wing first contacts the ground at the leading

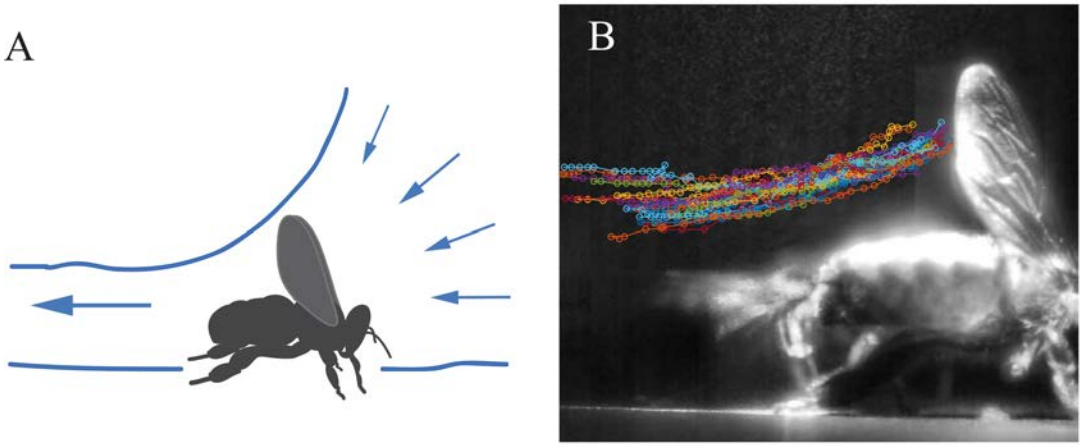

Figure 1.4: (A) A qualitative illustration of the flow generated by a scenting bee. This schematic was drawn after observing flow visualization videos available in the supplemental materials (see Movie 1). (B) Digitized positions of the location of a vortex shed at the end of the upstroke, as it moves downstream during Nasonov scenting behavior. Each colored line indicates the path of a single vortex during one wing stroke. Vortex paths during 25 successive wing strokes are plotted on the image. The vortex was visualized by illuminating particles suspended in the air with a laser sheet oriented along the sagittal plane of the scenting bee (see Movie 1). Note that the individual in this figure has an abdomen angle that is below average for scenting bees.

edge, and the point of contact shifts chordwise towards the trailing edge as the leading edge rises to begins the upstroke. Thus, bees appear to "roll" the wings along the ground, from the leading edge to the trailing edge, which may help minimize damage caused by the collision.

1.4 Discussion

Honey bees perform two non-flight, wing-flapping behaviors that are critical to the survival of the colony. Fanning behavior is used to ventilate the nest, in order to maintain a microclimate optimal for brood development (Seeley and Heinrich, 1981). Scenting behavior is used to drive air over the Nasonov gland and disperse pheromones that are key to communication in many contexts, such as coordinating the arrival of naive bees to a new nest site[3]. In both behaviors, the wings are used as

impellers, driving airflow past a stationary bee that is gripping a surface, rather than as propellers, generating downward flow to support a bee's weight in the air. This study demonstrates that these ventilatory fanning behavior is kinematically distinct from flight, and suggests that bees may employ unsteady flow mechanisms (e.g., clap-and-fling and wing-ground interactions) during these behaviors.

WING KINEMATICS

Neuhaus and Wohlgemuth[60] filmed 2 fanning honey bees and measured their flapping frequencies (121 and 150 Hz) which were substantially lower than that of flying flying honey bees[60]. They also measured amplitude (90 and 120°) for these bees, but they expressed lower confidence in these measurements because it was difficult to obtain video from appropriate angles and they were limited to 2D projections of the wing motion. Despite their limited sample size and methodological challenges, Neuhaus and Wohlgemuth suspected that the kinematics of fanning and the kinematics of flight are different enough that they should be considered a distinct behaviors[60]. We were able to rigorously test this hypothesis with a larger sample size and with the use of 3D calibrations.

Indeed, one of the most striking kinematic differences we found between wing fanning behaviors and flight was in flapping frequency. Flapping frequency of ventilatory fanning behavior (173.9 ± 20.4 SD) was significantly lower than that reported for hovering flight (226.8 ± 12.8 SD). Scenting behavior had an intermediate mean flapping frequency (213.4 ± 16.4 SD), which was significantly higher than during ventilatory fanning, but not significantly different from that during flight. The large differences we measured between the flapping frequencies of ventilatory fanning and hovering flight were surprising because the wings and flight motor of insects (especially those with asynchronous flight muscles, such as hymenopterans and dipterans) are classically described as a damped oscillator[29]. The lack of substantial variation in flapping frequency for many species is consistent with this hypothesis[29], and suggests that flapping frequency may be constrained to the natural fre-

quency of the flight system[21]. However, our study reveals that honey bees performing ventilatory fanning routinely flap their wings at a frequency that is approximately 30% lower than during flight. Despite this reduction in frequency, fanning and scenting bees generate wing angular velocities that are similar to that of hovering flight. We also observed substantially more variation in flapping frequency during fanning behavior than was previously observed in flying honey bees[1]. These observations suggests that bees may have more control over flapping frequency than previously thought.

The frequency of a damped oscillator system can be controlled by (1) changing the mass of the load or (2) changing the stiffness of the system. Honey bees are known to have a complex wing-thorax articulation and the transmission of force from the flight muscles and the wings is mediated by steering muscles and a series of sclerotized skeletal elements called pteralia[59]. Little is known about the role of this complex articulation in flight control in honey bees, but it is possible that bees could change the gearing ratio of the lever arm (i.e., the wing) by adjusting this articulation, changing the effective mass of the wing and ultimately the natural frequency of the flight system. In addition, the steering muscles could also be used change the stiffness of the thorax-wing system in order to alter flapping frequency. This mechanism is widely accepted in the Diptera, but it is typically thought to cause only small changes to flapping frequency[21,58,41]. It is also possible that gripping the substrate during fanning behavior could contribute to changes in thorax stiffness or damping, which could lower flapping frequency. In general, variation in flapping frequency and the control of this variation has not yet been fully appreciated. Studying behaviors that exhibit broad variation in frequency, such as fanning and scenting behaviors in honey bees, could provide insight into how flapping frequency is modulated.

The reduced frequency during fanning behavior relative to hovering flight may also be related to differences in constraints on flapping frequency for these two behaviors. The aerodynamic constraints imposed by flight may be more significant in determining flight kinematics than those of the mechanical system. During flight, insects must generate enough lift to offset their body weight,

whereas this constraint is removed when bees are performing flapping behaviors while holding on to a surface. It is possible that flight occurs at a narrow range of frequencies not due to control constraints (imposed by mechanical resonance at a natural frequency), but rather due aerodynamic constraints (i.e., by the need to generate significant amounts of force as effectively as possible). In the absence of these aerodynamic constraints, fanning and scenting bees may be free to tune their flapping frequency to meet other demands.

Our results on stroke amplitude lend some support to this idea. The distinctive high-frequency, low-amplitude wing stroke observed in flying honey bees–which is thought to maximize lift production via rotational mechanisms[1]–shifts to a lower-frequency, high-amplitude stroke in bees performing ventilatory fanning. This suggests that the flapping frequency and stroke amplitude observed in flying bees may optimize lift production via unsteady mechanisms, whereas the kinematics observed during fanning may be optimized for a different goal, such as maximizing the speed of air flow or the metabolic efficiency of flapping.

Wing-wing and wing-ground interactions

Many tiny insects, including white-flies and thrips, as well as larger insects, such as butterflies, use wing-wing contact at the dorsal stroke reversal to enhance lift[89,20,78]. During the end of the upstroke the wings clap together, and at the start of the downstroke they fling (or peel) apart. As the wings peel apart, air is sucked across the top surface of the wings, helping to induce circulation around the wing[53]. This pattern of wing kinematics has not previously been described in honeybees during flight in natural conditions, but it has been shown to occur during flight in heliox, suggesting that honeybees may be able to employ this mechanism when high aerodynamic force is required[86]. Our findings show that bees employ this kinematic device when performing Nasonov scenting (and likely also during ventilatory fanning) behavior.

One of the primary risks that might be associated with fanning and scenting behaviors is poten-

tial wing damage, as both behaviors require bees to flap their wings near the surface on which they are clinging. Given that high-frequency collisions with surfaces (e.g., vegetation) are known to cause wing wear[35,23,56] and wing wear leads to reduced flight performance and increased mortality[13,19,55], one might expect bees to reduce their stroke amplitude during these behaviors to avoid contact with the surface. However, we observed just the opposite; bees typically increase their stroke amplitude during fanning, and the wings often contact the ground at ventral stroke reversal, during both Nasonov scenting and ventilatory fanning behavior. The high-frequency collisions that occur between the wings and the surface are likely to cause considerable wing wear in honey bees, and possibly in other social hymenopterans that perform ventilatory fanning. In fact, we noticed that many of the individuals that we filmed had distal wing wear. One factor that may ameliorate this damage is the "rolling" motion that we observed, as the wings contact the ground first at their leading edge and the point of contact rolls gradually towards the more fragile trailing edge. It is also possible that this rolling of the wing along the substrate generates additional flow by forcing a bolus of air (trapped between the wing and the substrate during supination) from the leading edge to the trailing edge as if by peristalsis. In addition, as the wing peels away from the substrate suction would draw additional flow as the volume below the wing expands from the leading edge to the trailing edge.

Direction of impeller-induced flow and body posture

Our flow visualization results show that scenting honeybees draw in air from a broad area in front of and above their heads, and re-direct this air into a concentrated jet that flows parallel to the surface to which the bees are clinging (see Movie 1). The ground likely contributes to the resultant flow direction by deflecting flow induced by the bees. Because scenting and fanning bees have similar stroke plane angles, we expect that bees performing ventilatory fanning also generate downstream flow parallel to the surface. This directionality is important to the group-level ventilation behavior, because while flow generated by an individual bee may persist for only a few body lengths, bees fanning

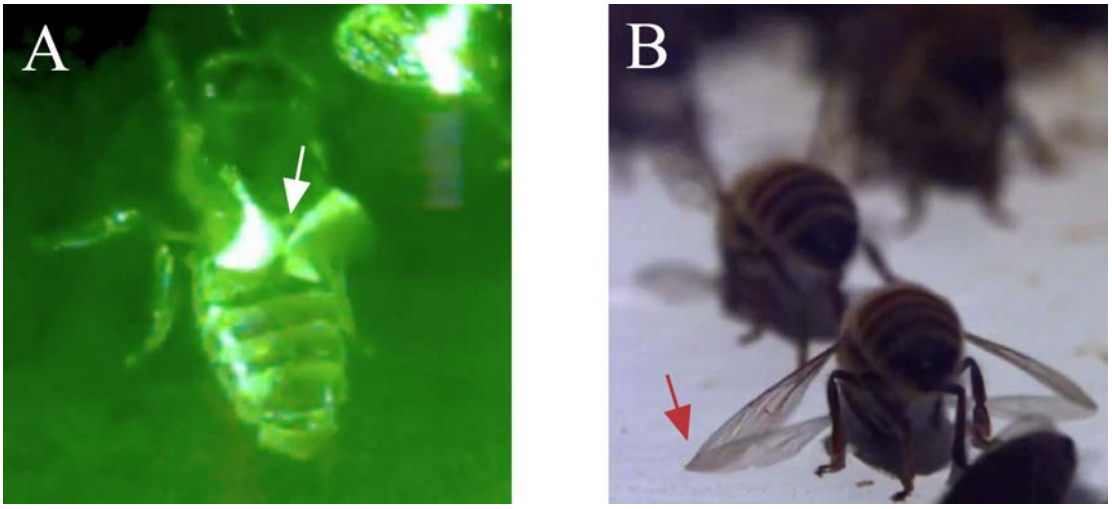

Figure 1.5: (A) A chordwise transect of the wings of a scenting honey bee are illuminated during the dorsal stroke reversal by a green laser sheet. The white arrow indicates contact between the wings (see Movie 2). This clap-and-peel behavior is not observed during flight in honey bees. (B) A still frame from a from a high-speed video of ventilatory fanning behavior. The red arrow indicates contact between the wing and the ground.

downstream can prevent the air from decelerating, and thus the group can achieve long-distance transport. If the flow were not parallel to the surface, this "bucket brigade" of air flow would not be possible (see Movie 3).

Although the ultimate goals of bees performing ventilatory fanning and those performing Nasonov scenting behavior are different, we found that the stroke plane angle employed during these two behaviors was strikingly similar. One obvious indicator of scenting behavior is that the bees raise their abdomens to expose the Nasonov gland, which is located near the tip of the abdomen. Before conducting this study, we suspected that by raising the abdomen scenting bees would achieve a more extreme stroke plane, allowing them to drive airflow upward, away from the surface to which they were clinging, which we thought might aid in broadcasting the pheromone. However, we found that while scenting bees do maintain a more elevated abdomen angle (15.8° ± 12 SD) relative to fanning bees (-1.9° ± 7.3), they do not flap their wings through a significantly different stroke plane angle. This suggests that scenting bees may raise their abdomen during scenting not to alter

the stroke plane angle, but rather to expose the Nasonov gland to the fast-moving air induced by the wings. If the abdomen were held near the ground as in fanning behavior, the Nasonov gland would be located be in the recirculation zone behind the body, and the concentration of pheromone in the air jet would likely be lower.

1.5 Conclusion

We have demonstrated that the flight system of honey bees performs several different functions, all of which are critical to the survival of the colony. Although the wings and thorax are often assumed to be specialized for flight, they routinely perform two additional tasks - ventilatory fanning and Nasonov scenting behavior - in which the flight system is used as an impeller. Ventilatory fanning behavior involves flapping frequencies and amplitudes that are significantly different from those employed during flight, and may subject the wings to irreparable damage. Its use as both a propeller and an impeller have likely imposed distinct (and possibly competing) selective pressures on the flight system, which may have influenced its evolution and contributed to its current form.

2

Self-organized ventilation in honeybee nests

2.1 Introduction

Many animal groups are able to solve complex problems using the collective action of individuals with limited sensory and cognitive abilities. These problems often involve spatial scales that are orders of magnitude larger than individuals that typically can sense and respond only locally. Thus, collectively organized solutions to problems such as complex navigation [4], predator avoidance [52] and distributed foraging [87] arise from the active interactions between individuals, which allow locally-sourced information to be integrated by the group [11].

Social behaviors in insects provide many such examples such as foraging recruitment, nest site selection and nest building. The solutions are often organized by a process called stigmergy in which individuals interacting with a common environment can lead to an emergent scheme or pattern without direct interaction [28]. In classical examples of stigmergy, individuals deposit static cues in

the environment such as pheromones, food stores or building materials that influence future behaviors by other individuals through positive feedback or recruitment which lead to the emergence of pheromone trails or architectural features such as walls, piles or pillars[11]. In less commonly studied class of behaviors, individuals interact with a dynamical physical process, such as flow, to structure their behavior. Experiments on corpse clustering by the ant *Messor sanctus*[43] and nest tube blocking in leaf-cutting ants *Acromyrmex ambiguus*[5] have demonstrated that depositing materials in the environment can modify airflow which can in turn influence future depositions. Several theoretical studies have suggested that if an individual-level behavior is responsive to flow-mediated cues and such behaviors manipulate flow, global behaviors can arise that control this flow for adaptive functions such as ventilation or thermoregulation[6,61,62].

A particular instance of this local-global behavior is seen in the context of thermoregulation and ventilation in honeybee colonies (> 10000 bees) that live in congested enclosures such as tree hollows or other pre-existing cavities, where they face the continuous challenge of maintaining relatively stable temperatures ($\sim 36°C$) and respiratory gas concentrations[76,40]. Active ventilation is a natural solution to both problems as it circumvents the limits imposed by impervious walls, small entrances (relative to nest volume) and large colony size. This allows for colony-level gas exchange with the environment and prevents buildup of heat and CO_2 within the nest[74,46]. Indeed, groups of honey bees orient themselves with their abdomens facing away from the nest and actively pull air out of the nest by fanning their wings at the nest entrance. However, conservation of mass requires that air drawn from the nest must be balanced by air flowing into the nest. Southwick and Moritz[77] observed that colonies in hives with small round entrances (2 cm diameter, 3.14 cm^2 area) exhibit tidal ventilation in which honeybees actively draw air out of the nest entrance for a while and then stop, allowing air to passively flow back into the nest. They also suggested that bees might select nest sites with larger entrances to allow for unidirectional or bidirectional air flow. Since nest entrances in feral colonies have a range of shapes and sizes that spans more than an order of magnitude[76], a nat-

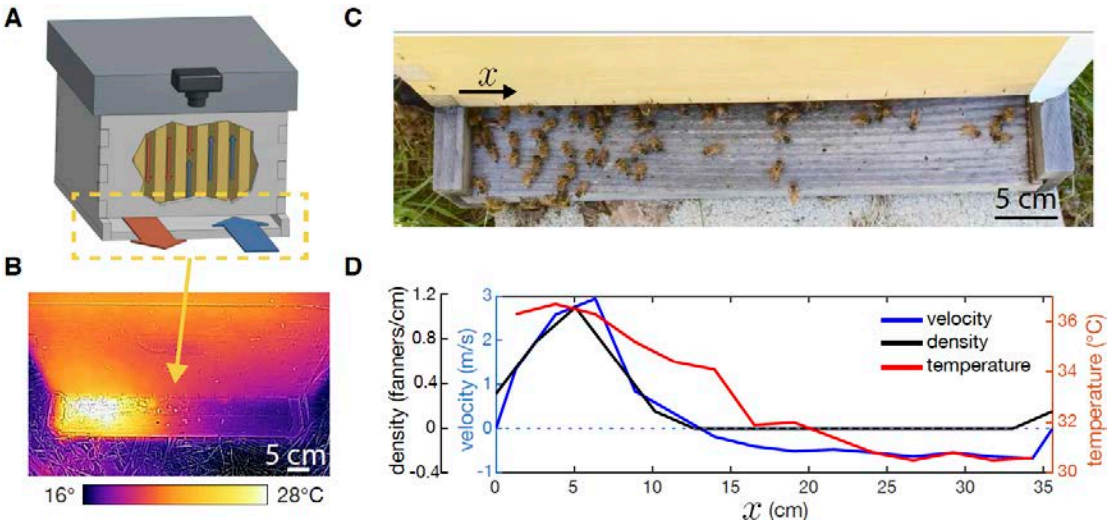

Figure 2.1: A) A schematic illustrating the path of air through the hive as induced by fanning bees. Warm, stale air is drawn out of the entrance by fanning bees and relatively cool ambient air enters passively where fanning bees are absent. The camera indicates the viewing angle in B and C. B) A thermal image of the hive entrance at night when fanning bees are actively fanning. Notice inflowing air at the right of the entrance has cooled the wood and the outflowing air induced by fanning bees on the left has warmed the wood. C) Honeybees ventilating at the entrance of a hive. Note the dense group of fanning bees at the left of the entrance and the lack of fanning bees at the right of the entrance. D) The air velocity (blue) and temperature (red) along the nest entrance of a hive. Note that inflow is indicated by negative values and outflow is indicated by positive values. These data demonstrate that the temperature profile along the entrance can be used as a qualitative proxy for flow velocity.

ural question is if and how the mechanism described in[77], i.e. temporal modulation of in/outflow, generalizes to characterize ventilation dynamics in nests with moderate to large entrances.

2.2 Experimental observations

To answer this question, we quantify the fanning behavior of bees at a large nest entrance shown schematically in Fig. 1A. We used four Langstroth beehives (80 liters, 20000 – 40000 bees each) with a single slit-like rectangular nest entrance (2 cm $\times$ 36 cm) that we monitored over time. In order to quantify the influence of the distribution of fanning bees along the entrance on the induced flow pattern, we counted the number of fanning bees in each of fifteen bins along the entrance (see Fig. 1D and SI Movie S3). Although there are fanning bees just inside the entrance, we counted only the

visible ones, which serve as a proxy for local fanning intensity. Simultaneously, we used a directional VelociCalc anemometer to measure the flow speed perpendicular to the entrance at the boundaries between the bins, with flow being positive outwards, and negative inwards. Flow direction was measured by placing a wool fiber at each position; if its motion was imperceptible or non-directional, no velocity value was recorded (see SI Movie S1). A thermocouple attached to the tip of the anemometer allowed us to measure the temperature at each location, which can also be qualitatively visualized using an infrared camera (Fig. 1B). All measurements were carried out five times a day over the course of three consecutive days. In Fig. 1D, we show the density of fanning bees, air velocity and air temperature as a function of the position along the entrance for one of the hives observed (see SI Fig. S1 and Fig. S2 - for the complete data set involving multiple bee hives).

We observed correlated variations in density, velocity and temperature at the entrance across space and time. In contrast with the observed rapid temporal modulation of ventilation behavior in nests with small openings[77], our observations show that for larger entrances, ventilation behavior is spatially modulated (i.e., in/outflow separated in space) but temporally steady, at least over times when the ambient temperature was steady. This dynamic adaptation to the physiological needs of a colony demands a dynamic explanation that links the behavior of individuals distributed at the hive entrance to the observed correlations between fanner density, air velocity, and air temperature in space and time.

2.3 Mathematical model

Honeybee colonies show broad inter-individual variation in the temperature thresholds that induce fanning, in part because of their high genetic diversity[38,14]. This variation can lead to emergent task allocation via the so-called task threshold model[82], which states that when the demand for a task is large, more individual bees will respond due to the broad variation in the task thresholds[14]. This

variation is higher in colonies with a queen which has mated multiple times[38], and promotes the temporal stability of thermoregulation. Furthermore, honeybees that are heated in a laboratory setting are more likely to fan at a given temperature when they are in a group than when they are alone[14]; independent of group size, individuals showed broad variation in temperature thresholds. In the largest group size considered (10 individuals), the mean temperature at which bees begin to fan was near the preferred hive (i.e., brood) temperature ($\sim 36°\mathrm{C}$).

Our minimal framework for the spatiotemporal organization of fanning starts by characterizing the local fanning response of individual bees to the local air temperature. We must also account for fluid flow which is induced by the bees and which carries the signal to which the bees are responding (i.e., heat derived from the hive). For simplicity, we consider the case when the hive and environmental temperatures are constant and focus on the dynamics of the bees at the entrance. To link bee behavior, air temperature and airflow we need to quantify how (i) the distribution of fanning bees, $\rho(x,t)$, (ii) the local air temperature, $T(x,t)$, and (iii) the local flow velocity, $v(x,t)$ vary with time t along the nest entrance. Because the nest entrance in this hive has a high aspect ratio (short but wide) we can model the entrance x as a 1D line (see Fig. 2A).

Consistent with the task threshold model, we assume that the probability of a bee stopping and initiating fanning behavior is determined by the local temperature[14]. Therefore, the local density of fanning bees, $\rho(x,t)$ changes according to the equation

$$\frac{\partial \rho}{\partial t} = (k_{\text{on}} - k_{\text{off}})\, T, \quad \rho(x,t) \in [0, \rho_{\text{max}}] \tag{2.1a}$$

where k_{on} is the rate at which bees initiate fanning behavior, k_{off} is the rate at which they cease fanning behavior, and ρ_{max} is the maximum density achievable (given spatial constraints at the nest

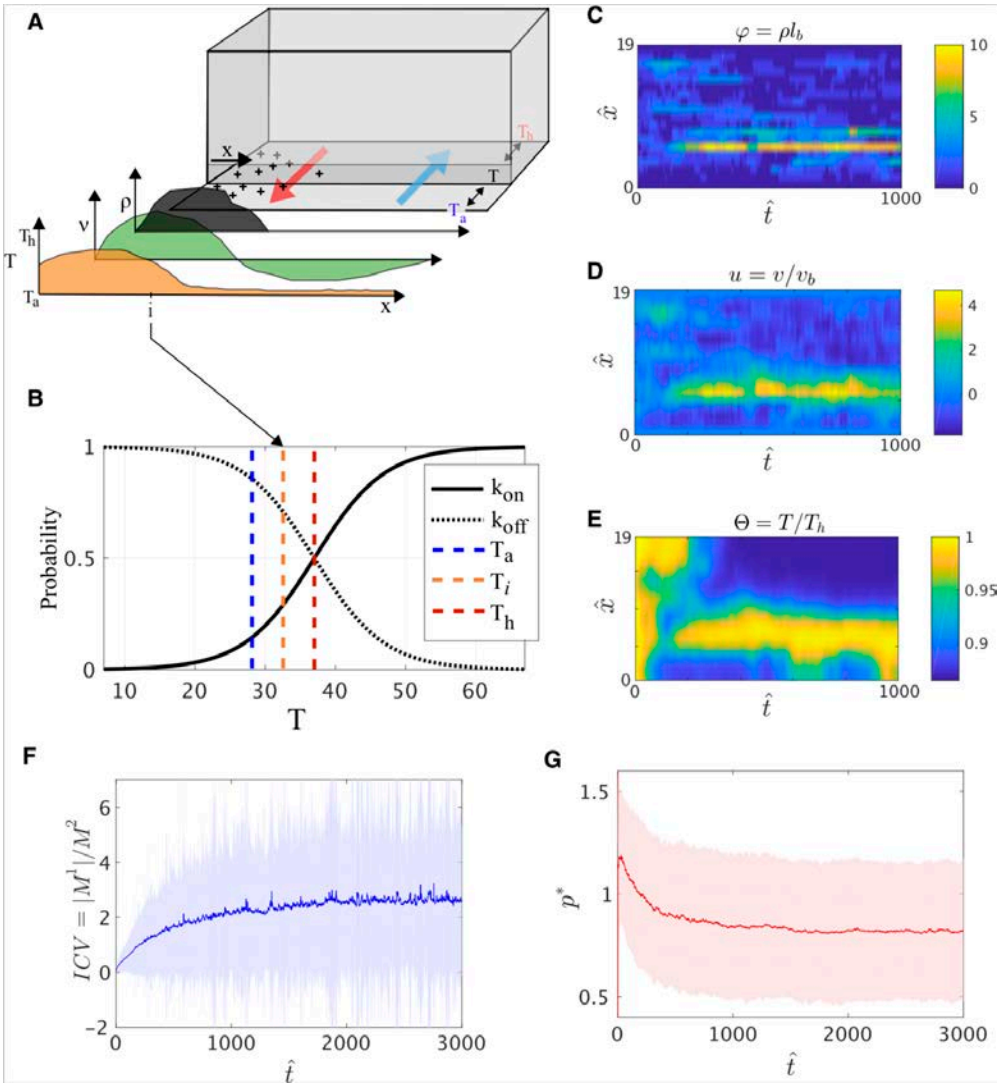

Figure 2.2: Theoretical model and numerical simulations. (A) Our model relates the density of fanners $\rho(x,t)$, air velocity $v(x,t)$, and air temperature $T(x,t)$ as a function of location along the nest entrance x at time t. Air drawn from the entrance by the bees has a $+$ve velocity. (B) The probability that a bee will begin (stop) fanning k_{on} (k_{off}) is high at high(low) temperatures and low at low(high) temperatures. (C) The density of fanning bees $\rho(x,t)$, (D) local air temperature $v(x,t)$ and (E) the local air velocity over the first 1000 steps of a representative numerical simulation, with initial conditions corresponding to a uniform fanner density, the hive temperature 36°C along the entire entrance and no initial velocity. Ambient temperature was fixed at 28°C. (F) The mean inverted coefficient of variation (ICV) is plotted for the first 3,000 time steps of 1000 simulations. Error bands indicate standard deviation. High ICV indicates that fanners are highly clustered. (G) The scaled power P^* lost to friction throughout the simulation. As fanners become more clustered, the amount of fluid friction is reduced, indicating that self-organization leads to increased ventilation efficiency.

entrance). These rates are assumed to be sigmoidal functions of the local air temperature, i.e.

$$k_{\text{on}} = k_0 \frac{\tanh(m(T - 36^\circ\,\text{C})) + 1}{2} \tag{2.1b}$$

and

$$k_{\text{off}} = k_0 - k_{\text{on}} \tag{2.1c}$$

where k_0 is an inverse time scale of the order of a few seconds, and m controls the slope of the sinusoidal function (see Fig. 2B), and is fit to approximately reproduce the variation in observed temperature thresholds[14] (see SI). Although, recent studies of fanning behavior in controlled laboratory settings suggest that the thermal response thresholds for fanning are affected by group size[14], presence/absence of larvae[15], and heating rate[?], our minimal representation of the fanning response as a switch-like behavior allows us to focus on the interaction with airflow and temperature.

To characterize the air flow, we assume that each bee generates an outward air flow with velocity v_b. Because the nest has just one opening, air that is actively drawn from the the entrance must be balanced by air flowing passively into the entrance elsewhere in order to ensure conservation of mass. Flow conservation at the entrance demands that (see SI for a simple derivation of this relation)

$$v(x,t) = l_b v_b \left[\rho(x,t) - \frac{1}{L}\int_0^L \rho(x,t)dx\right] + D_v \frac{\partial^2 v(x,t)}{\partial x^2} \tag{2.2}$$

where D_v is a scaled momentum diffusivity (with dimensions of squared length), L is the size of the nest entrance, l_b is a characteristic length scale derived from the fanning driven pressure gradient and fluid friction. The first two terms characterizes the difference in the local density of fanning bees from the average density over the entire length of the entrance and conserves the volume of air in the hive (since the net flow rate vanishes). The last term is associated with local fluid friction and ensures that fanning behavior not only drives local flow but also to entrains the airflow laterally, and

penalizes large velocity gradients, e.g., reversals in flow direction. Together, the global inhibition from conservation of volume and lateral flow entrainment due to friction may lead to emergent spatial patterning (for a detailed description see Fig. S10).

Finally, to characterize the dynamics of the local air temperature along the entrance, we assume that air temperature is governed by the local velocity and temperature difference between the entrance temperature and the upstream temperature, and can be described by a modification of Newton's law of cooling (neglecting complex flow dependences, see SI):

$$\frac{\partial T(x,t)}{\partial t} = -cv(x,t)\Delta T + D_T \frac{\partial^2 T(x,t)}{\partial x^2}, \tag{2.3}$$

$$\Delta T = \begin{cases} T_h - T, & \text{if } v \geq 0. \\ T_a - T, & \text{if } v < 0. \end{cases}$$

where c is a characteristic inverse length (chosen so that Newtonian cooling due to fanning dominates lateral diffusion), T_a, T_h are the ambient and hive temperature, and D_T is the thermal diffusivity.

The variables in our model can be rescaled using the following definitions: $\hat{x} = x/l_b, \hat{t} = tv_b/l_b, u = v/v_b, \phi = \rho l_b, \Theta = T/T_a$, which leads to a dimensionless set of our original equations with four dimensionless parameters: (i) L/l_b, a dimensionless measure of the entrance length (ii) D_v/l_b^2, a measure of the effect of fluid friction, (iii) $D_T/v_b l_b$, a scaled thermal diffusivity (inverse Peclet number) and (iv) cl_b, a length scale associated with bee fanning. In addition, we have two parameters that characterize each of the sigmoids associated with the switching of the fanning response (see SI for scaled equations and boundary conditions).

To complete the formulation of the model, we need to specify boundary conditions for the temperature and velocity of the airflow. The air velocity v is assumed to be zero at the ends of the nest

entrance, while the temperature was assumed to satisfy the Robin boundary condition

$$\alpha(T_0 - T_a) + (1-\alpha) l_b \left.\frac{\partial T}{\partial x}\right|_{x=0} = 0 \tag{2.4}$$

where T_0 is the temperature at the boundary and α is a dimensionless parameter that we use to characterize the thermal conductivity of the boundary (i.e., the walls on either side of the entrance): $\alpha = 0$ corresponds to the a perfect lyinsulating boundary while $\alpha = 1$ corresponds to a perfectly conducting boundary (see Fig. S5).

We used MATLAB to solve the initial boundary value problem (1-4) using a finite difference scheme in space and a Runge-Kutta method in time, using the following values for the parameters: width of the nest entrance $L = 0.38$ m, wingspan of a bee $l_b = 0.02$ m, air velocity generated by an individual fanning bee $v_b = 1$ m/s[67]. The diffusion coefficients D_v and D_T were fit to match observed behavior ($D_v = 1 \times 10^{-4}$ and $D_T = 4 \times 10^{-5}$; see Fig. S3 for a sweep of these parameters). All simulations were executed with the following initial conditions: 1) fanning bee density initially given a uniform distribution with one fanning bee per bin (1 bin $= l_b$), 2) local air velocity was zero along the length of the entrance, and the local air temperature was initially T_h.

Fanning bees initially formed multiple clusters allowing for spatial separation of inflow and outflow (Fig. 2c). Over time, several dominant clusters grew as other smaller clusters petered out. By $\hat{t} = 1000$ ($\sim$ several minutes), a single dominant cluster emerged leading to one region of outflow and 1 – 2 regions of inflow. This condition appeared to be stable, however when the simulations were run over long times, $\hat{t} > 10^4$ ($\sim$ several hours), the dominant cluster drifted in space. We quantified this clustering of fanning bees using the inverse of the coefficient of variation of the density of fanning bees, i.e. ICV $= |M_1|/M_2$, where M_i is the i^{th} moment of the density. If ICV is large, the bees are highly clustered. We also quantified the amount of power lost to fluid friction using the dimensionless parameter $P^* = \int (\partial u/\partial \hat{x})^2 \, d\hat{x}$. As shown in Fig. 2F and 2G, clustering

of fanners was inversely related to the amount of fluid friction in the system, suggesting that self-organization leads to more efficient ventilation by reducing friction (or shear) at the nest entrance.

To explore the role of m, the parameter which controls the variation in the temperature threshold associated with the behavioral switch functions K_{on} and K_{off}, we carried out representative simulations for various values of m and a fixed ambient temperature, $T_a = 32°\text{C}$. In Fig. 3A, we see that when m is extremely low ($m = 0.01$), fanning behavior is weakly coupled to temperature and no distinct fanning group forms, with poor ventilation efficiency. When m is extremely high ($m = 1$), fanning behavior occurs only over a narrow range of temperatures. At moderate m ($m = 0.1$), a stable fanning group forms over a broad range of temperatures, except when $T \approx T_{\text{hive}} (\Delta T < 2)$. We used this value for all subsequent figures as it best fits data on the diversity of fanning temperature thresholds reported in the literature[14,38]. Because m is the only behavioral parameter in our model, it is likely that natural selection has acted on this parameter to ensure efficient ventilation.

To explore the effect of boundary insulation, we used different values of $\alpha = 0.1, 0.55, 1$ and ambient temperatures $T_a = 15, 25, 35°\text{C}$ (Fig 3B). When $\alpha \ll 1$, corresponding to a strongly conducting boundary, the fanning group is more likely to occupy the center of the nest entrance. This occurs because heat is being continually lost to the environment through the boundary (if $T_a < T_h$) and the warmest region of the entrance where bees are most likely to fan is the center of the entrance. When $\alpha \approx 1$, the system loses no heat through the boundary. Therefore, when the fanning group is positioned at near the boundary, heat diffuses toward the opposite side of the entrance (where inflow is occurring) but not through the boundary. This condition is relatively stable and the fanning bees are more likely to continue fanning near the boundary than they are to drift away from the boundary. Varying T_a changes the range of temperatures over which the behavioral switch function can act and therefore has a dramatic effect not only on the number of bees fanning and the maximum flow speeds, but also on the spatial organization. In Fig. 4A, we see that

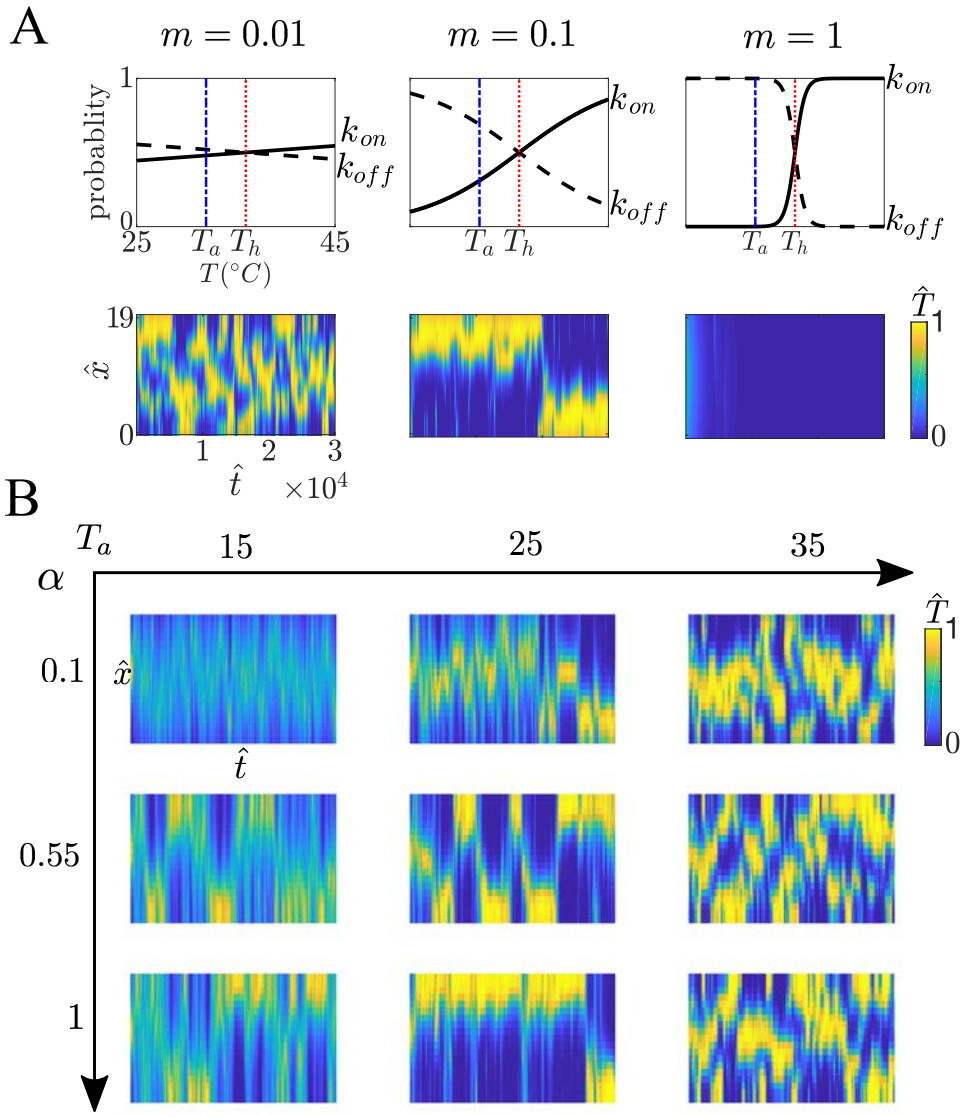

Figure 2.3: (A) Effect of slope of behavioral switch functions on ventilation dynamics for a fixed ambient temperature, $T_a = 32$. K_{on} and K_{off} prescribe the probability of a given bee to begin fanning or cease fanning at a given local air temperature. The slope of these functions is controlled by the parameter m. (B) Effects of ambient temperature T_a and boundary conductivity α on ventilation dynamics. The parameter α controls the thermal conductivity of the boundaries of the nest entrance. When α is near 0, the boundary is perfectly conductive and the position of fanning bees and the warm outflow that they generate tends to be found near the center of the nest entrance. When α is near 1, the boundary is perfectly insulated. Under this condition, the bees tend to fan more at one boundary of the nest entrance or the other. $\hat{x} \in [0, 19]$ and $\hat{t} \in [0, 3 \times 10^4]$.

when $T_a < T_h$ ($\Delta T \geq 10°$C), the cluster drifted relatively freely. However, at higher T_a the cluster tended to cling to the boundaries of the entrance with occasional spontaneous switching from side to side. As T_a approached T_h ($\Delta T \leq 2°$C), the dominant cluster broke up to form multiple ephemeral clusters.

Our model demonstrates that the interaction between fanning bees and the flow field in which they are embedded allows for emergent clustering of fanning bees and ultimately leads to ordered, efficient airflow through the nest entrance without a leader or central coordination. An explicit prediction of the model is that the dominant cluster should drift in space over long time scales and that this drift is qualitatively different at various temperatures.

2.4 Experimental tests of the theory

In order to test these theoretical predictions, we developed a method to continuously monitor the position of fanning bees at the nest entrance and the resultant flow pattern in the field under naturally varying conditions over many days. In the absence of our ability to continuously measure air velocity simultaneously at many positions within a cluttered and dynamic environment, we used temperature as a proxy for flow direction at the nest entrance (see Fig. 1D). We placed custom 32-sensor arrays above the nest entrances (1.8 cm $\times$ 37 cm) of three additional Langstroth beehives enabling us to sample local air temperature with high spatial and temporal resolution (1.17 cm sensor spacing, 10 second sampling intervals, Fig. 3B). Short videos were taken of the entrance of one of these hives every 10 minutes during daylight hours and the position of visible fanning bees was recorded (see SI Movie 2 – 3, SI).

The ambient temperature oscillated according to a 24 hour diurnal cycle (Fig. 3C) with variation in minimum and maximum daily temperatures throughout the observation period. The total number of fanning bees visible at the nest entrance tracked these oscillations and fanning intensity

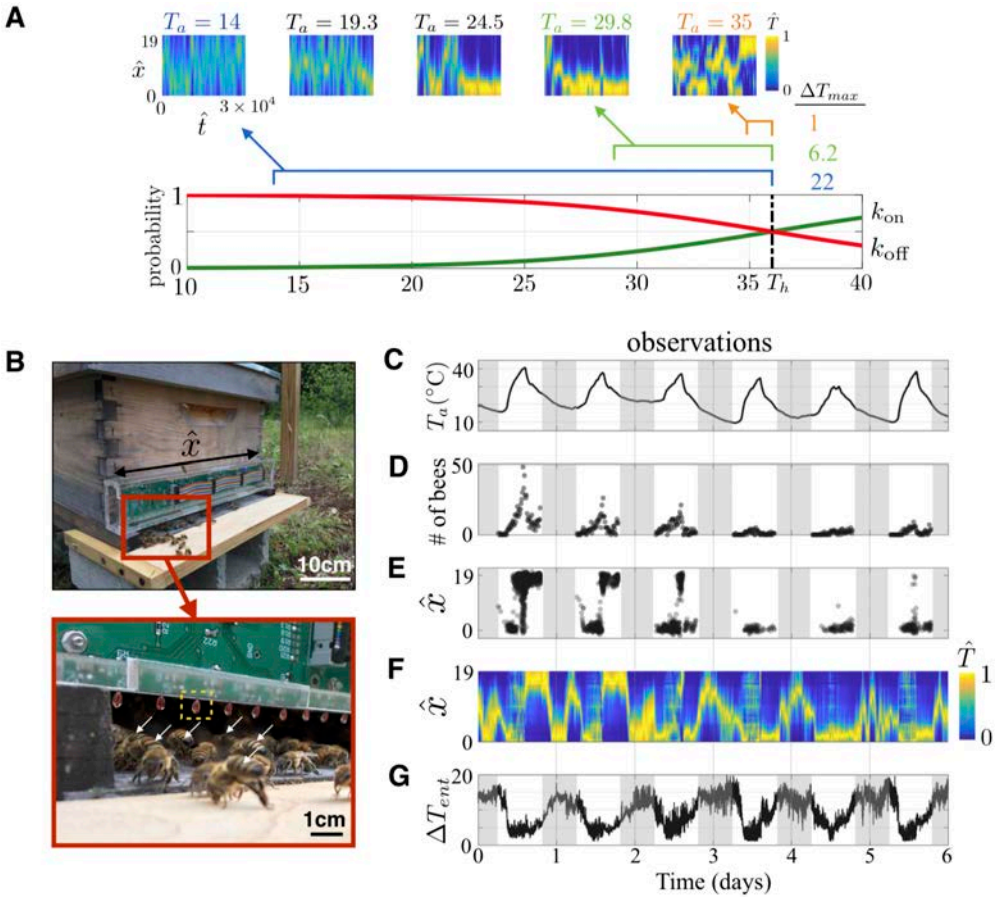

Figure 2.4: Predicted and observed ventilation dynamics over long time scales. A) Numerical simulations predict that the position of the fanning group will drift over long time scales (30,000 time steps, $T_h = 36°\text{C}$, $D_v = 1 \times 10^{-4}$, $D_t = 4 \times 10^{-5}$, $m = 0.1, c = 0.05, \alpha = 0.2$). At low temperatures ($T_a = 15$ - $20°\text{C}$), the fanners tend to occupy the center of the nest entrance and drift in space. At higher temperatures ($T_a = 25.5$ - $30.8°\text{C}$) the fanning group clings to the boundary of the nest entrance. When ambient temperature approaches hive temperature ($T_a = 36°\text{C}$), no singular, persistent fanning group emerges. (B) The temperature sensors along the entrance allow a true measure of air temperature in the flow stream. Fanning bees are indicated with white arrows. (C) The diurnal oscillations in ambient temperature closely tracked fanning intensity. (D) Total fanning bee number over time - gray regions indicate dark hours when it was difficult to record fanning behavior directly. (E) The position of the fanning bees indicates that single fanning group forms except when T_a is very close to T_h. During warm hours the fanning group tends to cling to the boundaries of the nest entrance. (F) The local air temperature shows that the position of the fanners is associated with warm, out-flowing air. The position of the fanning group (and outflow) tends to drift during the night when T_a is low. The entrance temperature has been normalized ($\hat{T} \in [0, 1]$). (G) The range of local air temperatures measured at any instance in time ($\Delta T_{\text{ent}} = T_{\text{max}} - T_{\text{min}}$) is also reported.

was higher on warmer days (Fig. 3D). The position of fanning bees during warm daylight hours revealed that the fanners tend to form well-defined clusters which tend to cling to the boundaries of the nest entrance (Fig. 3E). On warmer days, the ambient temperature would approach the nest temperature at midday and the fanning group would brake up into multiple, less-defined clusters. When the ambient temperature fell again, a single cluster would again emerge. For the hive depicted in Fig. 3 (Hive 1), the dominant fanning group often occupied the east side of the entrance during the morning and the west side of the entrance during the afternoon. This suggests that under some conditions, solar radiation may impose an environmental asymmetry that can bias the position of the fanners. This was not the case for Hives 2 and 3, suggesting that this is not the only factor determining the position of the fanners. The air temperature profile along the nest entrance reflected the distribution of fanning bees. Fig. 3F maps the normalized air temperature ($\hat{T} \in [0, 1]$) at each time step so that the entire dataset can be represented with one heat map. The difference between the minimum and maximum temperature at the nest entrance ($\Delta T_{\text{ent}} = T_{\text{max}} - T_{\text{min}}$) is also plotted in (Fig. 3G). The position of the dominant fanning group as indicated by the warm, outflowing air tended to drift away from the boundaries during the night when ambient temperatures were low as predicted by the model.

The nuances of the ventilation behavior are inevitably affected by the particular environmental conditions experienced by a colony, and yet the qualitative predictions made by our model are born out in the observed behavior in naturally fluctuating conditions. When T_a is lower than T_h a single cluster of fanners forms and tends to drift in space. As T_a increases the cluster tends to fix to a boundary. Which boundary the cluster fixes to may be biased by asymmetries in the environment. Finally, as T_a approaches T_h, the cluster breaks up into multiple or less defined clusters. Our observations are in agreement with theoretical predictions and suggest that collective nest ventilation is not just a product of the bee behavior, but arises from the local flow-mediated interactions between individual bees and of the resultant hive-scale fluid dynamics.

2.5 Conclusions

There are two behavioral components of this process that are critical to self-organized ventilation. First, the bees must (and do) fan air out of rather than into the nest entrance. This allows the bees to sense the upstream nest temperature. If the bees fanned into the nest entrance, they would have no information about the state of the hive. Interestingly, another cavity nesting honeybee species, *Apis cerana*, fans into the nest entrance[63]. This species likely uses an alternate strategy to the one described here or occupies nests with a small nest entrance in which spatial organization is not required[77]. Second, the switch function which determines the probability that a bee will fan at a given temperature, and has likely been tuned through natural selection. If the slope of this function is too shallow, fanning behavior is weakly coupled to temperature and no organization will emerge (see Fig. S5A,E). If the slope is too steep, fanning behavior can occur only over a small range of temperatures (see Fig. S5C,G). Indeed, colonies that have high genetic diversity have more variation in individual temperature thresholds for fanning and are therfor able to achieve a more stable hive temperature through time[38]. We have shown that this diversity is also critical to the stability of spatial patterning of fanning behavior which is required for efficient ventilation.

Our study demonstrates how harnessing the dynamics of the physical environment allows for large scale organization of a physiological process. This differs from classical stigmergy, which facilitates coordination by integrating spatially static information over longer time scales.

Honeybees sense local air temperature (which is coupled to speed and direction of airflow) and drive airflow when temperatures are high. Because the individuals are embedded in a common flowfield, their behavior is influenced by nonlocal interactions mediated by flow. The self-organization of fanners into groups which efficiently partition inflow and outflow, reduce friction and avoid antagonistic fanning behavior is ultimately the result of flow-mediated information processing that integrates locally sourced information over large spatial scales even in the absence of direct interac-

tion between neighboring individuals. This ability to manipulate existing physical processes locally to create self-organized behavior on large scales may be a pervasive strategy in the evolution of complex systems.

3

Collective mechanical adaptation of honeybee swarms

3.1 Introduction

Collective dynamics allow super–organisms to function in ways that a single organism cannot, by virtue of their emergent size, shape, physiology and behavior[3]. Classic examples include the physiological and behavioral strategies seen in social insects, e.g. ants that link their bodies to form rafts to survive floods[80,24,54,68], assemble pulling chains to move food items[66], form bivouac[36], towers[68], as well as bridges and ladders to traverse rough terrain[25]. Similarly, huddling groups of "daddy longlegs", emperor penguins cluster together for thermoregulation purposes[90], etc. While much is known about the static forms which are seen in such situations, the stability of these forms to dynamic perturbation, and their global response in the context of adaptation is much less understood.

European honeybees, *Apis mellifera* L., show many of these collective behaviors during their

life cycle[75]. For example, during the reproductive cycle of bees: colonies reproduce through colony fission, a process in which a subset of the colony's workers and a queen leave the hive, separate from the parent colony, and form a cluster on a nearby tree branch[75]. In these swarm clusters (which we will refer to as clusters), the bees adhere to each other and form a large structure made of $\sim 10,000$ individuals and can be hundreds of times the size of a single organism (Fig. ??A). Generally, this hanging mass of adhered bees takes on the shape of an inverted pendant cone, however, the resultant shape is also influenced by the surface to which the cluster is clinging to (see two different examples in Fig. ??A). The cluster can stay in place for several days as scout bees search the surrounding area for suitable nest sites[75].

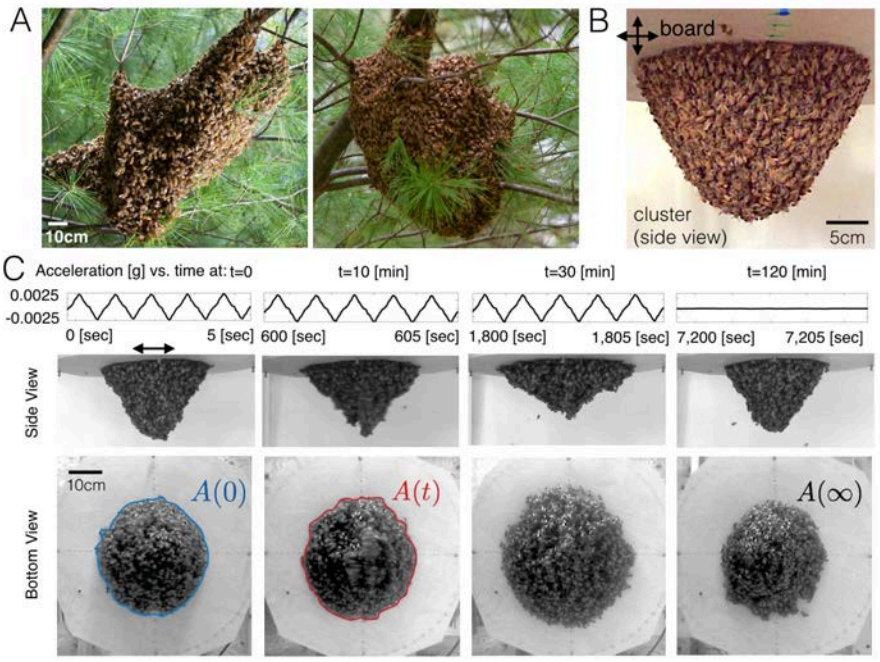

Figure 3.1: Experimental Setup: A) Horizontal shaking B) Vertical shaking. For the vertical shaking, the motor setup was rotated 90° to produce movement along the z axis.

The colony is never more exposed to the environment than during this stage and these clusters

show several striking behaviors to cope with the fluctuating thermal and mechanical environment. For instance, clusters tune their density and surface area to volume ratio to maintain a near constant core temperature despite large fluctuations in the ambient temperature[61,27,32]. Furthermore, at high temperatures, the swarm expands and forms channels which are presumed to aid in air circulation[32]. Additionally, in response to rain, bees at the surface arrange themselves to form "shingles", shedding moisture efficiently from the surface of the cluster[17]. Similarly, the cluster is mechanically stable; while it sways from side to side in the wind (e.g. see Movie S1), it could be catastrophic if the cluster breaks (when a critical load appears) as the bees would lose the ability to minimize surface area to prevent hypothermia, while still being mechanically stable. However, the mechanism by which a multitude of bees work together to create and maintain a stable structure that handles both static gravity and dynamic shaking stimuli (e.g. wind, predators), remains elusive. To understand this, we develop an experimental setup to quantify the response of a honeybee cluster to mechanical shaking over short and long times.

3.2 A mechanically adaptive honeybee cluster

To prepare a cluster, we attach a caged queen (see SI Sec. A) to a board and allowed a cluster to form around her (Fig. 1B). The bees at the base grip onto an area that is roughly circular. The board is controlled by a motor that can produce movement in the horizontal direction at different frequencies (0.5Hz – 5Hz) and accelerations (ranged $0 - 0.1$g). We apply both discontinuous shaking in which the acceleration is kept constant and the frequency is modified, and vice versa, continuous shaking in which the frequency is kept constant and the acceleration is modified (see Fig. 2).

For the case of horizontal shaking (for both discontinuous and continuous), the tall conical cluster swings to and fro in a pendular mode (one of the lowest energy modes of motion, see SI Sec. C), with a typical frequency of $\sim$ 1Hz. However, over longer durations (i.e. minutes), the bees adapt

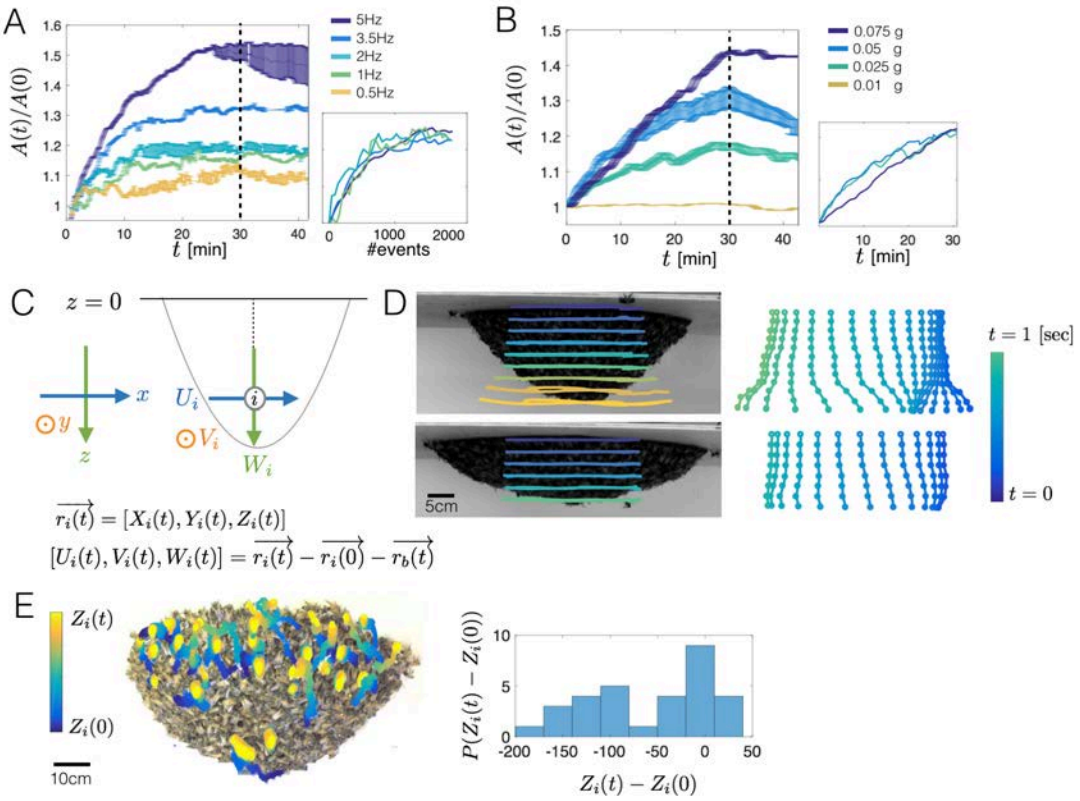

Figure 3.2: Quantifying adaptive response of the cluster: For all shaking frequencies, the base contact area of the cluster increases monotonically until a plateau is reached. Once shaking ceases, the cluster responds by gradually reverting to its original shape by increasing its contact area, but at a much slower rate. A) Ratio of the contact area of the base of the cluster divided by its original area $A(t)/A(0)$ as a function of time, for the discontinuous case. Colors represent results for different frequencies of periodic shaking. Inset shows that the scaled base area collapses onto a master curve when plotted vs. number of shaking events. Error bars correspond to standard deviation of three individual trials (see Table S1 for more information about trail repetitions). B) $A(t)/A(0)$ for continuous shaking shows the same qualitative behavior; note that when the acceleration is very small (0.01g), there is no response, i.e. there is a critical threshold of forcing below which the bees do not respond. C) Coordinate systems of the lab-frame and the displacement coordinates of the individual bees. D) Deformation of an elongated cluster before shaking began ($t = 0$, top) and a flattened cluster after shaking ($t = 30$ [sec], bottom) shows that displacement at the tip of the cluster is largest. On the right: time snapshots of a string of bees along the center of the cluster (See Movie S3). E) Trajectories of individual bees during 5 minutes of horizontal shaking show that when the cluster spreads out, surface bees move upwards. Color code represents time: the trajectory starts with blue and ends with yellow. Inset: probability distribution function of vertical displacement, showing a net upward trend.

by spreading themselves into a flatter conical form (Fig. 1B,C,D, Movie S2), while their total number remain constant (measured by the total weight of the cluster). The final shape flattens as the shaking continues for longer, or as frequency and acceleration of shaking increases. For the discontinuous shaking, when we plot the relative extent of spreading (scaled by a constant) as measured by $A(t)/A(0)$ for all different frequencies, as a function of number of shakes, the data collapses onto a single curve (Fig. 3.2A). This suggests that the cluster response scales with both the number and magnitude of shakes, but over much longer time scales than an individual event. The nature of this response is independent of the type of stimulus: when the shaking signal is continuous, we see a similar response (Fig. 2B). The graded adaptive response that scales with the number of shakes and is a function of applied displacements and frequencies, and the absence of any adaptation to very low frequencies and amplitudes (orange curves in Fig. 2B) suggests that there is a critical relative displacement (i.e. a threshold mechanical strain) needed to trigger this adaptation. Once the shaking stops, the cluster returns to its original elongated cone configuration over a period of $30 - 120$ minutes, a time that is much larger than the time for the cluster to flatten. This reversible cluster shape change to dynamic loading might be a functional adaptation that increases the mechanical stability of a flattened cluster relative to an elongated one.

To explore this suggestion quantitatively, we first define a lab-fixed coordinate system with axes as shown in Fig. 2C, with respect to which the board is at $\overrightarrow{r_b(t)} = [U_b, 0, W_b]$, the position of a bee i is defined as $\overrightarrow{r_i(t)} = [X_i(t), Y_i(t), Z_i(t)]$, and its displacement is defined as $[U_i(t), 0, W_i(t)] = \overrightarrow{r_i(t)} - \overrightarrow{r_i(0)} - \overrightarrow{r_b(t)}$. This allows us to track individual bees[3] along the surface of the cluster along the centerline $X_i(0) = 0$ (Fig. 2D, Movie S3), over a period of oscillation. Comparing trajectories of bees in an elongated cluster and a flat cluster, i.e. before and after shaking, show that relative displacement between the bees at the cluster tip and bees at the base is significantly larger for an elongated cluster. Snapshots of tracked bees highlight the decoupling of movement of the tip and base of the cluster, i.e. local deformations such as normal and shear strains are reduced in the mechani-

cally adapted state corresponding to a spread cluster. A similar trend is observed when the cluster is subjected to a single sharp shake (see signal at Fig. S2C), as shown in Movie S4. These measurements confirm that the adapted flattened structure is indeed more mechanically stable in the presence of dynamic horizontal loads.

Spreading of the cluster is a collective process, begging the question of how this collective spreading behavior is achieved. To study this, we tracked bees on the surface of the cluster during the process of adaptive spreading, particularly at the early stages. In Fig. 2E, Movie S5 we show how bees move from the tip-regions that are subject to large relative displacements towards the base-regions that are subject to small relative displacements, suggesting that the relative displacement U_i, may be a driver of shape adaptation.

3.3 A model of mechanical response at different aspect ratios

But what measure of the relative displacements might the bees be responding to? To understand this, we note that the fundamental modes of a pendant elastic cone are similar to those of a pendulum swinging from side to side, and a spring bouncing up and down, and their frequencies monotonically increase as a function of the aspect ratio of the cluster (Fig. B.3) (see SI Sec. C for details). To quantify the deviations from this simple picture due to the particulate nature of the assemblage, we turn to a computational model of the passive dynamics of a cluster and explore the role of shape on a pendant mechanical assemblage of passive particles used to mimic bees. We model each bee in the cluster as a spherical particle which experiences three forces: a gravitational force, an attractive force between neighboring particles, and a force that prevents inter-particle penetration (see SI Sec. C for further details). The bees at the base are assumed to be strongly attached to the supporting board, and those on the surface are assumed to be free. To study the passive response of the entire system, the board is oscillated at different frequencies and amplitudes, while we follow

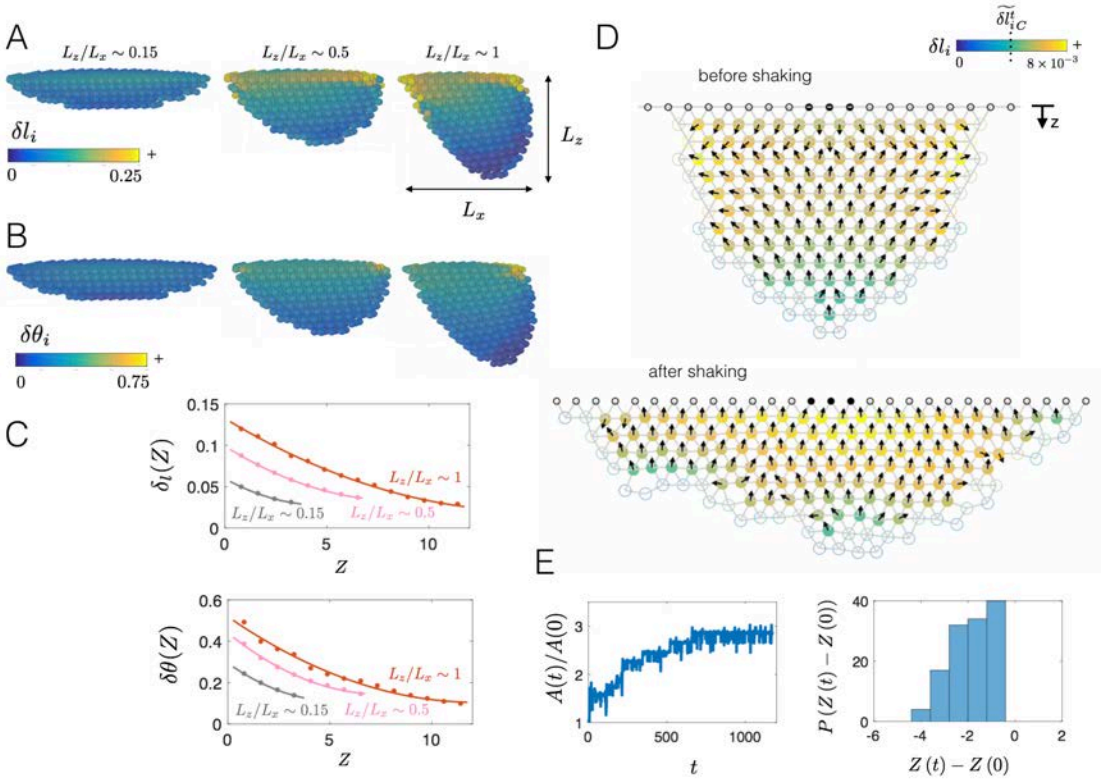

Figure 3.3: Computational model of mechanical adaptation: A cluster is modeled using particles that are linked via springs in a simple 2d triangular lattice. A) Clusters of different aspect ratios (L_z/L_x), shown at the extreme of a period of horizontal oscillation. Colors represent the local normal strain of each honeybee δl_i, as defined in the text. Elongated clusters (on the right) experience a larger deformation at the tip of the cluster, while flattened clusters (on the left) experience much less deformation. B) For the same state as in A), we also show the maximum shear strain, $\delta\theta_i$. C) Plots of the mean normal and shear strain ($\delta l(Z)$ and $\delta\theta(Z)$) as a function of the distance from the base, Z, and aspect ratio L_z/L_x. We see that the maximum magnitude of the strains decreases as the cluster becomes flattened. D) When we impose a behavioral rule that allows the bees to sense the strains around them and move in the direction of increasing strain when the magnitude crosses a threshold ($\widetilde{\delta l^t_{iC}}$), this leads to spreading. Colors represent the local integrated signal, $\widetilde{\delta l^t_i}$, and arrows point towards higher local signal. E) The scaled base contact area $A(t)/A(0)$ as a function of time, with the probability distribution function of vertical displacement shows a net negative response, i.e. bees move upwards on average, similar to experimental observations (see Fig. 2E).

the displacement of individual particles, $U_i(\overrightarrow{r_i})$, as well as the relative displacement between neighboring bees $\overrightarrow{l_{ij}(t)} = \overrightarrow{r_i(t)} - \overrightarrow{r_j(t)}$ (Fig. 3.3A). Decomposing the vector $\overrightarrow{l_{ij}(t)}$ into its magnitude and direction allows us to define two local deformation measures associated with the local normal

strain and shear strain. The local dynamic normal strain associated with a particle (bee) i relative to its extension at $t = 0$ is defined as $\delta l_i = \left\langle \max_{0\leq t\leq T} \left| \left|\overrightarrow{l_{ij}(t)}\right| - \left|\overrightarrow{l_{ij}(0)}\right| \right| \right\rangle$ where T is the duration from the onset of the applied mechanical shaking until the swarm recovers its steady state configuration, and the brackets $<>$ represent average over all bees j that are connected to bee i. The local shear strain is calculated from the changes in the angle $\left|\angle(\overrightarrow{l_{ij}(t)}, \overrightarrow{l_{ik}(t)})\right|$ between $\overrightarrow{l_{ij}(t)}$ and $\overrightarrow{l_{ik}(t)}$, connecting bees i and j, and bees i and k, respectively, with the shear strain, $\delta\theta_i$ defined as $\delta\theta_i = \left\langle \max_{0\leq t\leq T} \left| \angle(\overrightarrow{l_{ij}(t)}, \overrightarrow{l_{ik}(t)}) - \angle(\overrightarrow{l_{ij}(0)}, \overrightarrow{l_{ik}(0)}) \right| \right\rangle$ where the brackets $<>$ represent average over all pair of bees $j-k$ that are connected to bee i.

As expected, we see that for the same forcing, the maximum amplitude of the local strains increases as the cluster becomes more elongated (Fig. 3.3A,B, Movie S6). Therefore, these local strains can serve as a signal for the bees to move, and a natural hypothesis is that once the signal is above a certain critical value, the bees move. But how might they chose a direction ? While it may be plausible for the bees to simply move upwards against gravity, it is likely difficult to sense a static force (i.e., gravity) when experiencing large dynamic forcing (i.e., shaking) in a tightly packed assemblage. Instead, we turn to ask whether there are any local signals that would give honeybees a sense of direction. For all clusters, the strains are largest near the base (Fig. 3.3A,B, Movie S6) and decrease away from it, but in addition, as the cluster becomes more elongated, there are large local strains along the contact line where $x = \pm L_1/2$ where the bees are in contact with the baseboard. This is due to the effect of the pendular mode of deformation that leads to rotation-induced stretching in these regions. To quantify how the normal and shear strain vary as a function of the distance from the base, Z, we average δl_i and $\delta\theta_i$ over all bees that were at a certain Z position at $t = 0$ and define the following mean quantities: $\delta l(Z) = \langle \delta l_i \rangle$, and $\delta\theta(Z) = \langle \delta\theta_i \rangle$, where the bracket $<>$ indicate average over all spring connection at the vertical position $r_z^i(0) = Z$. Similar to the experimental data, the simulations show that the displacements U_i for horizontal shaking of elongated clusters are larger in comparison to flattened clusters. As both strains $\delta l(Z)$ and $\delta\theta(Z)$ are largest near the

base, $z = 0$ (Fig. 3.3C, Movie S6), and decrease away from the supporting baseboard, they may serve as local signals that bees at the tip of the cluster respond to by moving up the strain-gradient (Fig. B.3–5, Movie S7–8).

This passive signature of a horizontally-shaken assemblage suggests a simple behavioral hypothesis: bees can sense the local variations in the normal strain above a critical threshold, and move slowly up gradients collectively. We note that mechanical strain is invariant to translation and rotation of the whole assemblage, i.e. it is independent of the origin and orientation of the frame of reference, and thus a natural choice. This behavior will naturally lead to spreading of the cluster and thence smaller strains on the cluster. Noting that time scale of the response of the bees is of the order of minutes while the duration of a single period is seconds, it is natural to consider the integrated local normal strain signal: $\widetilde{\delta l_i^t} = \sum_{\tilde{t}=t-T_w}^{t} \delta l_i^{\tilde{t}} \times dt$, where T_w is chosen to be the period of the shaking (see detailed description in the SI Sec. C). Then our behavioral hypothesis is that when $\widetilde{\delta l_i^t} > \widetilde{\delta l_i^t}_C$ the bee becomes active, and moves in the direction of the time-integrated negative normal strain gradient (i.e. the active force is directed toward a higher local normal strain) according to the simple proportional rule $F^{\text{active}} = -f^{\text{active}} \overrightarrow{\widetilde{\delta l_i^t}}$. We note that moving up a gradient in time-integrated shear strain would also suffice to explain the observed mechanical adaptation.

We carry out our simulations of the active cluster in two dimensions for simplicity and speed (we do not expect any changes in 3D), allowing bonds to break and reform based on proximity similar to how bees form connections, and follow the shape of the cluster while it is shaken horizontally. We find that over time, the cluster spreads out to form a flattened cone (Fig. 3.3D,E, Movie S7), confirming that the local behavioral rule that integrates relative displacements that arise due to long-range passive coupling in the mechanical assemblage wherein bees actively move up the local gradient in normal strain δl_i does explain our observations.

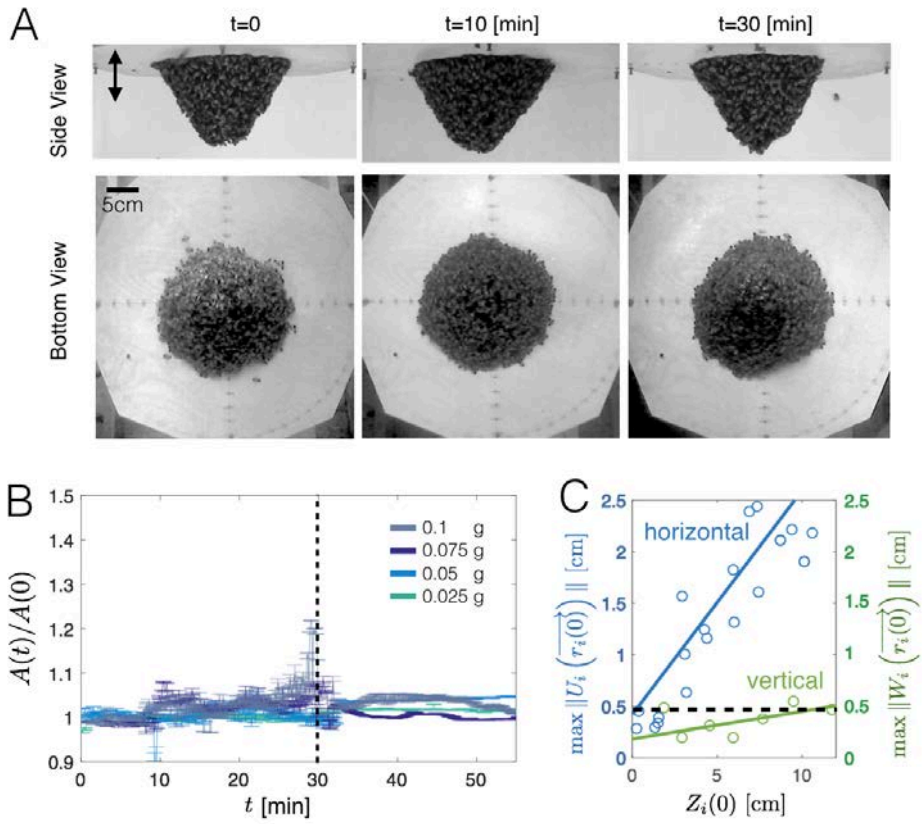

Figure 3.4: Response to Vertical Shaking. A) Vertical shaking (maximum acceleration 0.05 [g]) of the bee cluster leads to a very small displacement. This is consistent with our simulations (see Fig. S4, SI Sec. D) that vertical shakes do not destabilize the bees differentially. B) Contact area of the base of the cluster relative to its initial area $A(t)/A(0)$ vs. time. Areas are defined as in Fig. 1D. Colors represent results for different accelerations of continuous shaking. C) Maximum displacement at the tip of a tall cluster as a result of a single horizontal and vertical shake. Bees do not respond or change the shape of the cluster when subjected to vertical shaking (green), but do respond substantially when shaken horizontally (blue). Black dotted line represents the experimentally observed threshold value to initiate active behavior.

3.4 Vertical shaking

If sufficiently large dynamic normal strain gradients drive shape adaptation, different shaking protocols that result in lower local strains should limit adaptation. One way is to shake the cluster gently, and this indeed does not drive adaptation (Fig. 2B responding to 0.01g). Another is to shake the

cluster in a vertical direction, exciting the spring-like mode of the assemblage. For the same range of amplitudes and frequencies as used for horizontal shaking, our simulations of a passive assemblage show that vertical shaking results results in particles being collectively displaced up and down, with little normal strain. As expected, even in active clusters with the behavioral rule implemented, little or no adaptation occurs as the threshold normal strain gradient is not achieved (Fig. S5–6 and Movie S8). To test this experimentally, we shake the cluster vertically. We see that in this case the cluster shape remains approximately constant (Fig. 3.4A,B) until a critical acceleration is reached - at which time a propagating crack results in the detachment of the cluster from the board (Movie S9). Quantifying the displacements at the tip for vertical shaking and horizontal shaking are in agreement with our hypothesis that differential normal strain gradients drive adaptation (Fig. 3.4C, Movie S10).

3.5 Conclusion

Our study has shown how dynamic loading of honeybee swarm clusters leads to mechanical adaptation wherein the cluster spreads out in response to repeated shaking. We show that this morphological response increases the mechanical stability of the cluster. A computational model of the bee cluster treated as a passive mechanical assemblage suggests that there are strain gradients that can be used by bees as a local signal to drive movement in the direction of higher strains and causing the cluster to flatten. This behavioral response improves the collective stability of the cluster as a whole via a reversible shape change, at the expense of increasing the average mechanical burden experienced by the individual. Introducing elastic interactions between the bees naturally allows for long-range signaling via physical cues, complementing the more traditional view of collective behavior via stigmergy[84] wherein organisms respond to local chemical cues with little or no long range effects. Given the tensorial non-local nature of elastic interactions in assemblages of social insects, perhaps this is just the tip of an iceberg that hides the many ways in which organisms take advantage of physical

interactions and simple behavioral rules to adapt to changing mechanical environments.

4

Morphological responses of honeybee swarm clusters to dynamic ambient temperature perturbations

4.1 Introduction

In social animals, adaptive group-level behaviors can arise from the interactions between individuals acting on limited local information[10]. These interactions are often mediated by the environment. For example, the variations in branching patterns of pheromone trails formed by raiding army ants were once thought to be unique to particular species[9], but it was later demonstrated that subtle changes in the texture of the substrate could reproduce these variations given the same behavioral rules[26].

Many social hymenopterans (i.e., ants, wasps and bees) perform a unique class of collective behaviors in which individuals link their bodies together to form self-assembled structures such as rafts[54], bridges[69], escape droplets[7] and clusters[33]. These behaviors often serve adaptive functions,

aiding in flood survival, predator evasion, food transport, navigation of complex environments, etc. (see Anderson et al.[2] for a review). In self-assemblies, the microenvironment itself (within the self-assembly) is an extended phenotype of the colony. In some instances, this has allowed natural selection to shape the feedback between behavior and the microenvironment, resulting in dynamics that lead to adaptive homeostasis. Bivouacs and clusters formed by army ants[25] and honeybees[34], for example, are able to maintain stable internal temperatures despite dramatic fluctuations in ambient temperature. Studying these behaviors can provide insight into how the interplay between collective behavior and microenvironment can lead to adaptive super-organismal physiology.

Here we focus on thermoregulation in honeybee swarm clusters. When a honeybee colony is large enough to reproduce, as much as half of the workers ($\approx 10,000$ bees) and a fertilized queen leave the nest with finite honey stores and form a cluster on a nearby tree branch (Fig. 1A,B). The cluster remains here for days while scouts seek new nest sites[75]. Meanwhile the swarm maintains near stable core temperatures ($\approx 35°$C) despite fluctuating ambient conditions (Fig. 1C)[33]. When ambient temperature is below $\approx 17°$C, the surface temperature of the cluster is actively maintained at $\approx 17°$C through shivering in order to prevent chill coma (i.e., cold-induced immobility). When ambient temperature is above $\approx 17°$C the surface temperature is maintained a few degrees above ambient. These dynamics are reflected in the metabolic rate of the colony, with oxygen consumption increasing linearly as temperatures rise above $\approx 17°$C (Fig. 1D)[34]. Such collective thermoregulation allows the swarm to avoid lethal temperatures, prevents the colony from exhausting its honey stores too quickly, and allows bees to quickly mobilize in response to threats (bees must warm their flight muscles to $\approx 35°$ C in order to fly)[32].

Although this phenomenon has been described in some detail, empirical studies have provided little mechanistic understanding of how the behavior of individual bees gives rise to the global behavior of expansion and contraction of the cluster, and ultimately to thermoregulation. Many theoretical studies have explored how a group of individual bees might interact to give rise to global

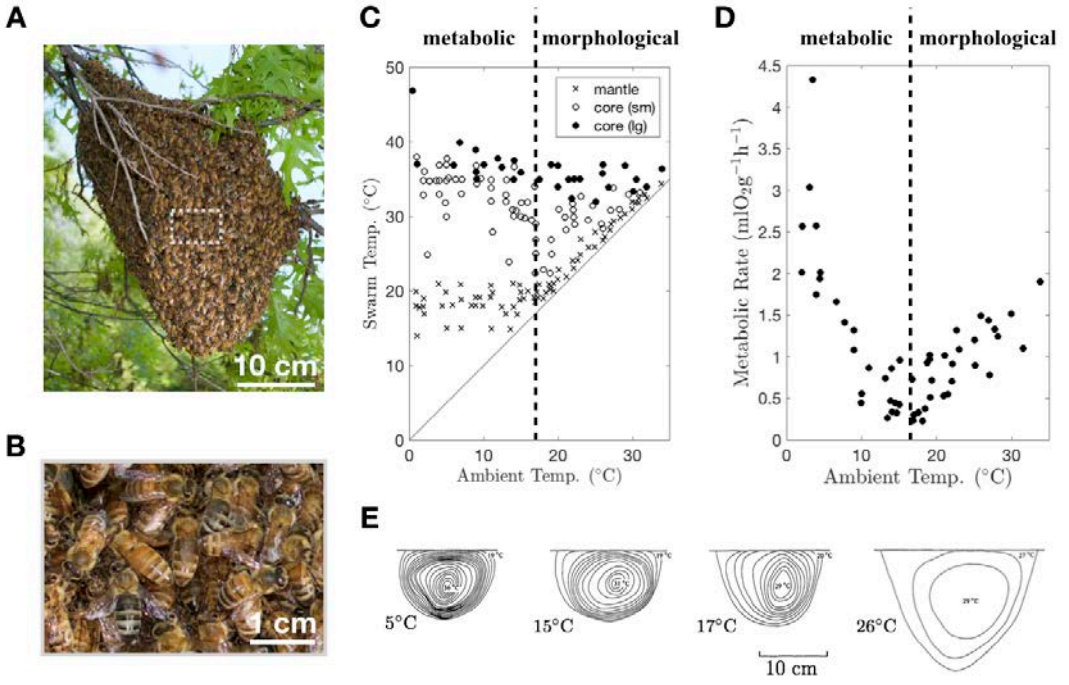

Figure 4.1: (A) A feral honeybee swarm cluster hanging from an oak tree at Concord Field Station in May 2016. (B) An expanded view from (A) showing individual bees on the surface of the swarm. (C) Measured temperatures of the core and mantle of a swarm at various ambient temperatures. (D) The metabolic rate of swarms at various ambient temperatures. (E) Drawings of the profile shape of swarms hanging from a flat horizontal surface at various ambient temperatures. C-E are adapted from Heinrich[34].

thermal stability through feedback between the density of bees and heat diffusion, in the context of both winter clusters and reproductive swarms[61,22,79,88,57,47,64,65]. Early models of thermoregulation in winter clusters focused on the coupling between the density of bees and temperature, which was determined both by prescribed metabolic activity and heat diffusion[64,65]. These models typically assume that bees know their position within the swarm. However, it is thought that collective thermoregulation emerges from the actions of individual bees attempting to regulate their own body temperature within a tolerable range, without reference to global information (e.g., without regard to relative position within the swarm). Meyerscough[57] proposed a model based on a nonlinear heat production-diffusion equation in which both density and heat production varied as a function only of local temperature. Extensions of this model introduced a "thermotaxis" rule, whereby the movement of individual bees toward each other is dependent on local temperature[88,79]. In these models, temperature-dependent density is not prescribed, but is an emergent property of individual bees' movements. Ocko and Mahadevan[61] proposed a model in which the movement of bees is described by a "behavioral pressure", which is a function of both temperature and the local packing fraction. This model also included an additional mode of heat transfer, convection.

Despite intense interest among both experimentalists and theorists in the mechanistic underpinnings of collective thermoregulation in honeybee swarm clusters, we do not yet have detailed measurements of (1) the movements of individual bees within clusters, or (2) global morphological responses of clusters to ambient temperature fluctuations. In fact, all experimental studies to date have focused on instantaneous measurements of the steady state behavior of clusters at fixed ambient temperatures[33]. Hence, all current mathematical and computational models of thermoregulation consider only the density, temperature and behavior of the cluster at equilibrium[61]. To address this gap in our understanding of honeybee swarm clusters, here we measure the dynamic, global morphological responses of swarm clusters to controlled, time-varying temperature perturbations.

4.2 Methods

The artificial swarm clusters used in experiments consisted of packages of honeybees purchased from New England Beekeeping in Tyngsboro, Massachusetts between March and April 2017. These packages consisted of approximately 1 kg of bees and a caged Italian queen. For at least two days prior to the experiments the bees were fed *ad libitum* sugar solution, which is known to induce the swarm state.

The experimental setup consisted of a $1.2 \times 1.5 \times 1.2$ m box constructed from 3.8×8.9 cm dimensional lumber and insulated with a double layer of press-fit 2.5-cm Styrofoam sheets. Two window air conditioners were inserted into holes at the bottom left and right corners of one of the walls of the box, and three small space heaters were placed in the corners of the box. Four temperature sensors were suspended in the airspace of the box and connected to an Arduino microcontroller. The heaters and air conditioners were toggled on and off in response to this temperature feedback in order to maintain a desired set-point temperature. This set-point temperature was modulated by a MATLAB program to achieve controlled heating and cooling cycles.

Two wooden struts were used to support a scale (scale info) approximately 10 cm from the roof of the box, and a 60-cm, circular wooden board was hung from the scale. The caged queen was fixed to the underside of this board with wires. The rest of the bees were allowed to form a cluster around the queen until the mass reported by the scale was stable. The bees were allowed to fly freely, both within the box and out of a 0.25×1 m window in the side of the box which connected to the outside world. This allowed the swarm to send scouts in search of new nest sites. Without this freedom of movement, the bees would continuously search for an opening in the box to escape, and the mass of the cluster would not stabilize.

A Point Grey camera was placed 50 cm from the board supporting the cluster and an LED back light (50×100 cm) was placed orthogonal to the camera on the other side of the swarm. During

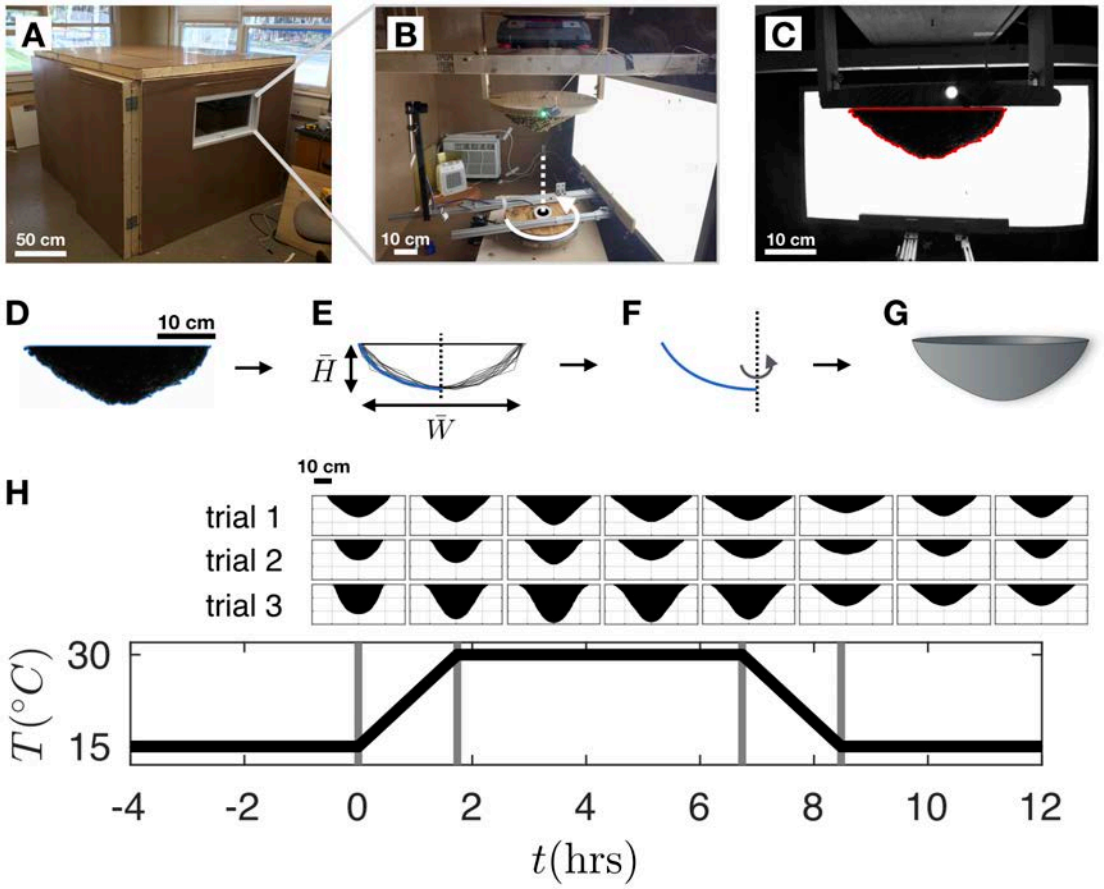

Figure 4.2: Experimental setup for quantifying the thermoregulatory response of swarm clusters. (A) Swarms were housed in a large insulated box, outfitted with heaters and coolers that were toggled on and off to produce controlled temperature perturbations. (B) Within the box, a board with the swarm attached was suspended from a scale. A motor was used to revolve a camera and an opposing back light 360° around the swarm. (C) During each rotation, 40 images of the swarm were captured from different angles. (D) The swarm was segmented from the background of each image using thresholding. (E) The silhouettes of the 40 images were transformed so that their height and width matched the average values for the whole set, $\bar{H}$ and $\bar{W}$. (F) An average shape was calculated from the 40 silhouettes, and this shape was revolved around the z-axis to obtain (G) a 3D approximation of the swarm's shape. (H) The dynamic temperature perturbation applied in Treatment 1 is shown. The silhouette of the swarm (averaged over all 40 views) is shown for trials 1-3. Each image is centered at its corresponding time stamp in the panel below, beginning at $t = 0$.

each data collection bout, the back light was turned on and 40 images were captured as both the camera and the back light were revolved around the swarm. When the revolution was complete, the back light was turned off to avoid luring bees away from the cluster. This filming routine was executed every 4 minutes during the experiment.

Each experiment was 10-12 hours long. Initially, the air temperature in the box was held at 15°C for 4 hours, then raised to 30°C for 5 hours, and finally lowered back to 15°C for an additional 4 hours. Two different heating and cooling rates were tested, with air temperature changing by 8°C/hr for 3 of the trials (Treatment 1) and by 32°C/hr for 3 trials (Treatment 2).

Prior to analysis, each image of the swarm was undistorted using MATLAB's checkerboard calibration tool (to correct for wide-angle lens geometry). The checkerboard was placed orthogonal to the camera at the axis of rotation so that images in that plane could be converted from pixels to centimeters. A custom MATLAB program was then used to define a wire frame silhouette of the cluster in each of the 40 views. Because the cluster was rarely centered at the camera's axis of rotation, the silhouette of the cluster appeared to loom and recede during the camera's rotation. To correct for this, each silhouette was transformed such that its dimensions (i.e., height and width) equaled the average dimensions of the set of 40 silhouettes. The silhouettes were then averaged to achieve a single 2D approximation of the profile shape of the cluster centered at the axis of rotation. This average silhouette was revolved around the vertical axis to create a 3D approximation of the shape of the cluster, and to determine its surface area and volume. We also attempted to perform hull reconstruction of the swarm to obtain a true 3D reconstruction, but this method was less robust to bees flying in front of the camera (which was a persistent problem). Ultimately, we chose to use the radially symmetric shape approximations in our analyses to prevent errors associated with such camera occlusions.

Quantifying expansion/contraction rates

To calculate peak expansion/contraction rates during heating and cooling phases of the experiments, time series data of swarm volume, height and width for each treatment were standardized (to account for size differences between swarms) by dividing by their initial value at t = 0. A moving average filter (window size $\approx$ 40 min) was then applied to smooth the data. We computed the numerical derivative of each time series over a window size of $\approx$ 40 min and found the peaks associated with the most extreme positive and negative values, which correspond to the peak expansion and contraction rates, respectively. The hypothesis that expansion and contraction rates are equal (within each metric, i.e., volume, height, width) was tested using a paired T-test. Within each treatment (i.e. heating/cooling rate), we compared expansion/contraction rates in height vs. width, using an unpaired two-sample T-test.

4.3 Results

Swarm mass

During some trials, the mass of the swarm was somewhat volatile due to the activity of the bees, but it generally stabilized once the experiments began (Fig. 3, Panel 1). Over the course of a heating/cooling experiment, the swarm clusters in treatments 1 and 2 lost an average of 10% and 5%, respectively. We cannot determine the source of this weight loss, but several factors may contribute to it. First, we noticed that wax scales accumulated on the floor of the box during the experiments. Honeybees regularly produce wax scales in preparation for colonizing a new nest site[30]. In addition, some of the loss may be attributed to attrition of bees, as some dead bees accumulated on the floor of the box. However, this did not appear to be enough to account for the 5-10% weight loss. It is also possible that some of the weight loss resulted from bees leaving the box and failing to return to

the swarm, though scouts appeared to move in and out of the box with ease. In fact, on a few occasions between experiments, the entire swarm flew out the window (likely toward a newly selected nest sight), only to return to the box after discovering that their queen was not with them. In these instances, the mass of the swarm was similar before and after its departure, suggesting that the bees did not struggle to find their way back to the box.

Morphing response

Continuous measures of the volume, density, surface area, height and width of swarm clusters during imposed temperature perturbations are shown in Figure 4 (see Table 1 for summary statistics). The clusters nearly doubled in volume when raised from 15°C to 30°C ($\langle \hat{V}_h \rangle = 1.89$ and 1.81 for treatments 1 and 2, respectively). We expected that the cluster would expand to a steady state size at 30°C, but the volume never reached a plateau value within the 4-hour heating phase. However, when the temperature was dropped to 15°C during the cooling phase, the volume V returned to the initial volume V_0 within 2 hours (quantify time to saturation?). Similar dynamics were observed for surface area ($\langle \hat{S}_h \rangle = 1.89$ and 1.81), although surface area saturated more slowly during the cooling phase and on average did not quite return to its initial value by the end of the experiment ($\langle \hat{S}_c \rangle = 1.11$ and 1.08). The initial density of the clusters ρ_0 was 0.06 g/cm^3. For reference, we measured the average mass of a honeybee to be 0.11 g, so the steady state density of the clusters at 15°C is about 0.5 bees/cm^3. As expected given the doubling in cluster volume, the density of the clusters was approximately halved by the end of the heating phase ($\langle \hat{\rho}_h \rangle = 0.50$ and 0.55).

Although the volume and surface area of the clusters do not reach a steady state during the heating phase, the height of the swarm does reach a maximum value 2-3 hours after the onset of expansion. In some cases (i.e., trials 2 and 3), the swarm even begins to shorten again before the cooling phase begins. Despite this apparent limit on expansion in the vertical direction, the swarm continues to expand radially at its base throughout the heating phase, reaching a base width that is over

40% larger than the initial width ($\langle \hat{W}_h \rangle = 1.46$ and 1.41). This anisotropy in the expansion of the cluster suggests that expansion and contraction in the vertical vs. horizontal directions may occur by different mechanisms, and may be subject to different physical constraints.

Hysteresis

The expansion/contraction dynamics show strong hysteresis, with swarm expansion occurring more slowly than contraction (Fig. 4.4A). For instance, for both treatment 1 and 2, the mean peak expansion rate across trials ($\langle \Delta \hat{V}/hr \rangle$ = 0.31 and 0.30, respectively) was slower than the mean peak contraction rate ($\langle \Delta \hat{V}/hr \rangle$ = -0.50 and -0.60). Note that the peak expansion rates for both treatments were similar, but the mean peak contraction rate of treatment 2 was $\approx$ 20% slower than treatment 1. The swarm cluster tended to shorten during cooling much faster than it lengthened during warming (Fig. 4.4B). This was especially true for the Treatment 2 which had a faster heating/cooling rate. However, the rate of change in width of the cluster during heating and cooling was approximately equivalent (Fig. 4.4C). As a result, the aspect ratio of the swarm ($\hat{W}/\hat{H}$) spikes during cooling (Fig. 4.4D,E). This suggests that the rate at which the cluster narrows may be constrained, and that bees overcome this constraint to some extent by shortening more rapidly. However, the discrepancy between lengthening and shortening rates suggests that the overall hysteresis in expansion/contraction dynamics of the cluster is driven by mechanical differences between the lengthening vs. shortening processes.

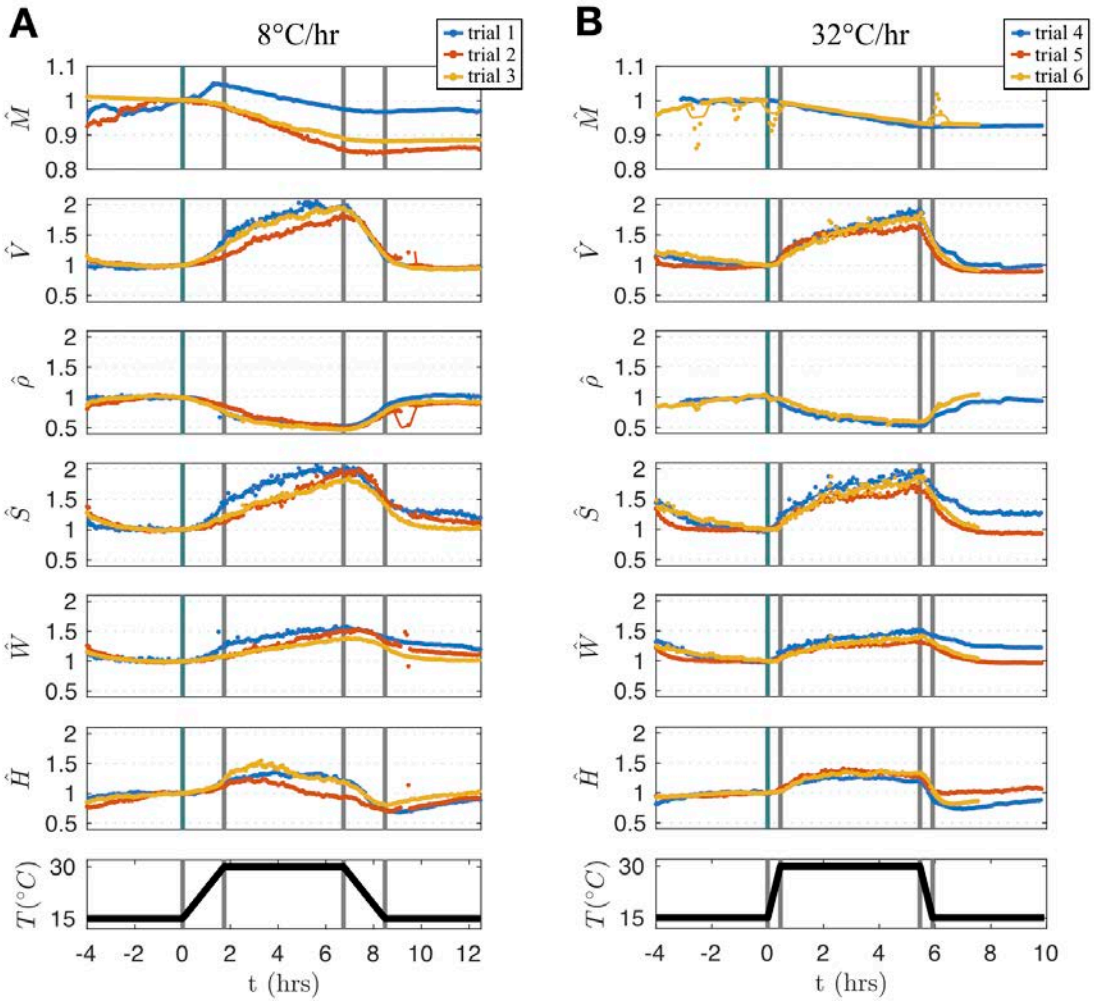

Figure 4.3: Measurements of cluster size and shape over time for treatment 1 (A) and treatment 2 (B). Mass $\hat{M}$, volume $\hat{V}$, density $\hat{\rho}$, surface area $\hat{S}$, width $\hat{W}$ and height $\hat{H}$ are calculated relative to their value at $t = 0$ and therefore do not have units (e.g., $\hat{M} = M/M_0$). Raw values are represented by circles and the filtered data (moving average) are indicated with solid lines. The bottom panel shows the imposed ambient temperature and the vertical gray bars refer to key transitions.

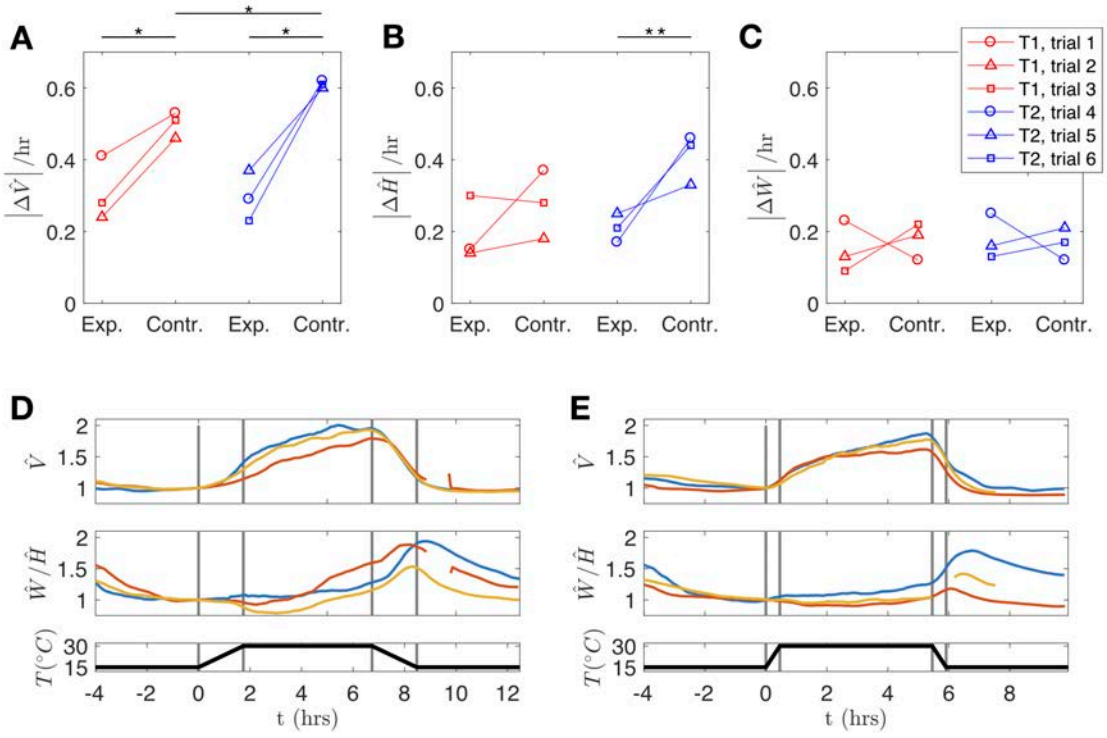

Figure 4.4: Hysteresis in expansion and contraction of the swarm. (A) Peak expansion and contraction rates measured during each trial, in terms of volume $\left|\Delta\hat{V}\right|/\mathrm{hr}$, where $\left|\Delta\hat{V}\right| = |V/V_0|$. Swarms from both treatment groups consistently expanded more slowly than they contracted. (B) Peak lengthening and shortening rates expressed as $\left|\Delta\hat{H}\right|/\mathrm{hr}$, where $\Delta\hat{H} = H/H_0$. Swarms also tended to lengthen more slowly (during expansion) than they shortened (during contraction). (C) Peak broadening and narrowing rates expressed as $\left|\Delta\hat{W}\right|/\mathrm{hr}$, where $\Delta\hat{W} = W/W_0$. In contrast to the directional differences seen in volume and length changes, there was no clear difference in the rate at which swarms broadened vs. narrowed during expansion and contraction. (D, E) Time course of changes in the aspect ratio ($\hat{W}/\hat{H}$) of swarms (middle panel), along with temperature and volume changes, for treatment 1 (D) and treatment 2 (E). Swarm aspect ratio peaks during the contraction response, when temperature is dropping or has dropped back to $15°$C. This suggests that the rate at which the cluster narrows may be constrained, and that bees overcome this constraint (to some extent) by shortening more rapidly. However, the discrepancy between lengthening and shortening rates suggests that the overall hysteresis in expansion/contraction dynamics of the cluster is driven by mechanical differences between the lengthening vs. shortening processes. $*$ indicates $p < 0.05$ and $**$ indicates $p < 0.001$.

4.4 Discussion

Previous empirical studies on the thermoregulation of honeybee swarm clusters have focused on measuring the metabolic rates and temperature profiles of swarms at static ambient temperatures[33,34]. These studies showed that swarm clusters adapt their size and shape to the ambient temperature in order to modulate how much metabolic heat is dumped to the environment, allowing the cluster to maintain a relatively stable core temperature and reduce the rate of honey consumption. However, little is known about the proximate mechanisms of this collective behavior or about the individual-level behaviors that allow for such collective thermoregulation. This knowledge gap is not surprising, given that the observer can see only the behavior of bees at the surface of the cluster. The process by which thousands of interlinked bees interact with the local microclimate within a swarm to achieve a thermally stable global structure has been the subject of many theoretical studies[61], with individual bees sensing and responding only to local temperature within the swarm and modulating their movements and/or metabolic rates through shivering. However, all theoretical work currently in the literature is based on equilibrium models, which consider the behavior of the model at steady state and compare the results of the model to static measurements from empirical studies. The measurements presented here of the dynamics of cluster size and shape changes in response to controlled temperature perturbations improve our understanding of collective thermoregulation in this system, and point to the need for new modeling approaches.

Hysteresis

Perhaps the most surprising result of our experiments is that swarm expansion in response to rising ambient temperatures is remarkably slow, particularly in comparison to contraction when temperatures fall. We designed our experiments with a 4-hr gap between ramping the ambient temperature up to 30°C and ramping it back down 15°C, expecting that within this time frame the cluster

would reach an equilibrium size and shape. However, the volume of the swarm continued to increase throughout this period without reaching a plateau. The contraction of the swarm during the cooling phase was much faster, saturating within $\approx$ 2 hrs after the onset of cooling. This hysteresis suggests that expansion and contraction are subject to different physical constraints. Swarm expansion and contraction require the breaking and reforming of connections between individual bees. Given that individuals within the swarm are supporting not only their own weight but also the weight of other bees within the assembly, one might expect that contraction – which primarily requires forming new connections between individuals – would be easier to accomplish quickly without risking mechanical failure. On the other hand, expansion requires bees to relinquish connections with other individuals, so this task may require more careful coordination to avoid mechanical failure. For instance, if too many bees relinquish connections at the same time, the swarm may fracture as the load distribution changes. An alternative to systematic coordination between individuals is to simply decrease the rate at which bees rearrange their connections, thereby decreasing the risk of fracture. This may explain why swarm clusters expand more slowly during warming than they contract during cooling.

It is also possible that the rates of these processes differ because contraction during cooling is likely more critical to the fitness of the swarm than expansion during heating. When the ambient temperature drops below chill coma temperature ($\approx$ 15°C), bees near the surface of the cluster shiver using their flight muscles to avoid cold-induced immobilization. This comes at a potentially large metabolic cost. If the swarm fails to mitigate cooling through contraction, more bees are at risk of chill coma and more bees have to shiver to avoid immobilization and possible mortality. Although our experiment did not go below 15°C and likely did not force the bees to shiver, swarm clusters may avoid any lag in their contraction response in order to mitigate future risk, in case the ambient temperature continues to fall below 15°C. It is not clear that expansion during heating is as urgent of a task for the swarm. While it may have been possible for some parts of the swarm to reach

adversely high temperatures (i.e, above $\approx$ 36°C) during the heating phase of our experiment, it is unlikely that there was immediate risk lethal temperatures $\approx$ 52°C)[10]. Having higher average temperatures within the swarm would lead to higher metabolic rates and excessive use of honey reserves, but this poses no immediate risks, and therefore expansion may be less urgent.

Anisotropy

During the heating phase of the experiment, the height of the cluster reached saturation within 2-3 hours (and in some cases started to decrease again), whereas the width continued to increase steadily without reaching saturation. This anisotropy in expansion suggests that lateral and vertical expansion may be subject to different constraints. Obviously, the bees are loaded vertically and therefore must maintain vertical connectivity in order to avoid breakage. While lateral connections between bees help distribute the load within the cluster, lateral gaps between bees are tolerable. In fact, Heinrich[33] noted that the bees in the interior of the swarm are arranged in columns, and that vertical channels form between the these columns at high temperatures. He suggested that these channels may form to facilitate airflow, but this channelization may also simply result from differential lateral vs. vertical constraints on connectivity between individuals.

We found that swarm clusters in the faster treatment group (Treatment 2) subjected to falling temperatures were able to contract $\approx$ 2.5 times faster in the vertical direction than in the horizontal direction. This difference may also be associated with the "columnar" organization of the cluster. Unloaded bees on the surface of the swarm may be able quickly climb up these columns to decrease the height off the cluster.

Conclusions

Our study demonstrates that the expansion and contraction dynamics of swarm clusters in response to dynamically varying ambient temperatures are slower and more complex than previously appreciated, and that the mechanics of the cluster may limit the rate at which clusters can respond to changes in the environment. Existing models of cluster thermoregulation do not consider the structure of the cluster or the mechanical constraints that limit its ability to modulate its density, nor do they incorporate dynamic changes in temperature and cluster morphology. We hope that our data will contribute to improvement of these models. Towards a complete understanding collective thermoregulation, future experimental work should focus on tracking the movements of individuals in response to local temperature and mechanical cues.

Table 4.1: Summary table of parameters describing the size/shape of the swarm throughout each trial. Parameters measured at the end of the phase 0 (i.e., the beginning of the experiment) are given the subscript $_0$ and have units (e.g., V_0 (cm^3)). Parameters measured at the end of the heating/cooling phase are given the subscript $_{h/c}$. These parameters are measured relative to the initial value at the end of phase 0 and therefore do not have units (e.g., $\hat{V}_h = V_h/V_0$). This scheme is used so that values can be easily compared across trials which have different initial sizes and shapes.

Trial	Rate (°C/hr)	M_0 (g)	$\hat{M}_c$	V_0 (cm^3)	$\hat{V}_h$	$\hat{V}_c$	ρ_0 (g/cm^3)	$\hat{\rho}_h$	$\hat{\rho}_c$	A_0 (cm^3)	$\hat{A}_h$	$\hat{A}_c$	H_0 (cm)	$\hat{H}_h$	$\hat{H}_c$	W_0 (cm)	$\hat{W}_h$	$\hat{W}_c$
1	8	660.48	0.97	12.69×10^3	1.93	0.97	0.06	0.53	0.99	3.22×10^3	2.01	1.20	22.53	1.21	0.89	36.79	1.54	1.20
2	8	402.12	0.86	7.11×10^3	1.79	0.97	0.06	0.51	0.90	2.40×10^3	1.92	1.12	14.64	0.95	0.92	34.37	1.48	1.11
3	8	821.83	0.88	12.81×10^3	1.95	0.95	0.07	0.47	0.92	4.02×10^3	1.79	1.02	15.74	1.20	1.04	46.41	1.37	1.02
Mean		628.14	0.90	10.87×10^3	1.89	0.96	0.06	0.50	0.94	3.21×10^3	1.90	1.11	17.64	1.12	0.95	39.19	1.46	1.11
SD		211.71	0.06	3.25×10^3	0.09	0.01	0.01	0.03	0.05	0.8×10^3	0.11	0.09	4.27	0.15	0.08	6.37	0.09	0.09
4	32	733.20	0.93	12.81×10^3	1.94	1.01	0.06	0.52	0.92	3.37×10^3	2.03	1.30	20.59	1.25	0.91	39.17	1.51	1.23
5	32	898.80	na	15.34×10^3	1.62	0.90	na	na	na	4.3×10^3	1.63	0.92	17.56	1.28	1.07	46.73	1.31	0.96
6	32	1205.31	0.96	25.88×10^3	1.87	0.92	0.05	0.59	1.04	6.06×10^3	1.87	1.03	22.26	1.33	0.86	55.42	1.42	1.04
Mean		945.77	0.94	18.01×10^3	1.81	0.94	0.06	0.55	0.98	4.58×10^3	1.84	1.08	20.14	1.29	0.95	47.11	1.41	1.08
SD		239.53	0.02	6.93×10^3	0.17	0.06	0.01	0.05	0.09	1.37×10^3	0.20	0.19	2.38	0.04	0.11	8.13	0.10	0.13

Table 4.2: Expansion and contraction rates (with respect to volume, height and width) broken down by treatment group and trial.

		Expansion and Contraction Rates					
	heat-/cooling rate	$\Delta\hat{V}$/hr		$\Delta\hat{H}$/hr		$\Delta\hat{W}$/hr	
Trial	°C/hr	Exp.	Cont.	Exp.	Cont.	Exp.	Cont.
1	8	0.41	-0.53	0.15	-0.37	0.23	-0.12
2	8	0.24	-0.46	0.14	-0.18	0.13	-0.19
3	8	0.28	-0.51	0.30	-0.28	0.09	-0.22
Mean		0.31	-0.50	0.20	-0.28	0.15	-0.18
SD		0.09	0.04	0.09	0.10	0.07	0.05
5	32	0.29	-0.62	0.17	-0.46	0.25	-0.12
6	32	0.37	-0.60	0.25	-0.33	0.16	-0.21
7	32	0.23	-0.61	0.21	-0.54	0.13	-0.17
Mean		0.30	-0.61	0.21	-0.44	0.18	-0.17
SD		0.07	0.01	0.04	0.11	0.06	0.05

A

Supplementary Information for Chapter 2

A.1 Study Site

All hives observed were located at Concord Field Station, Harvard University, Bedford, Massachusetts.

A.2 Study Organisms

All colonies were originally started from packages derived from Rossman Apiaries in Georgia. The colonies were started with an Italian queen.

A.3 Manual measurements

Fig. A.1 and Fig. A.2 contain the results of manual measurements of fanner distribution, air velocity and temperature at the nest entrance of 4 hives from 07/21/2015 to 07/23/2015. These data complement Fig. 1.

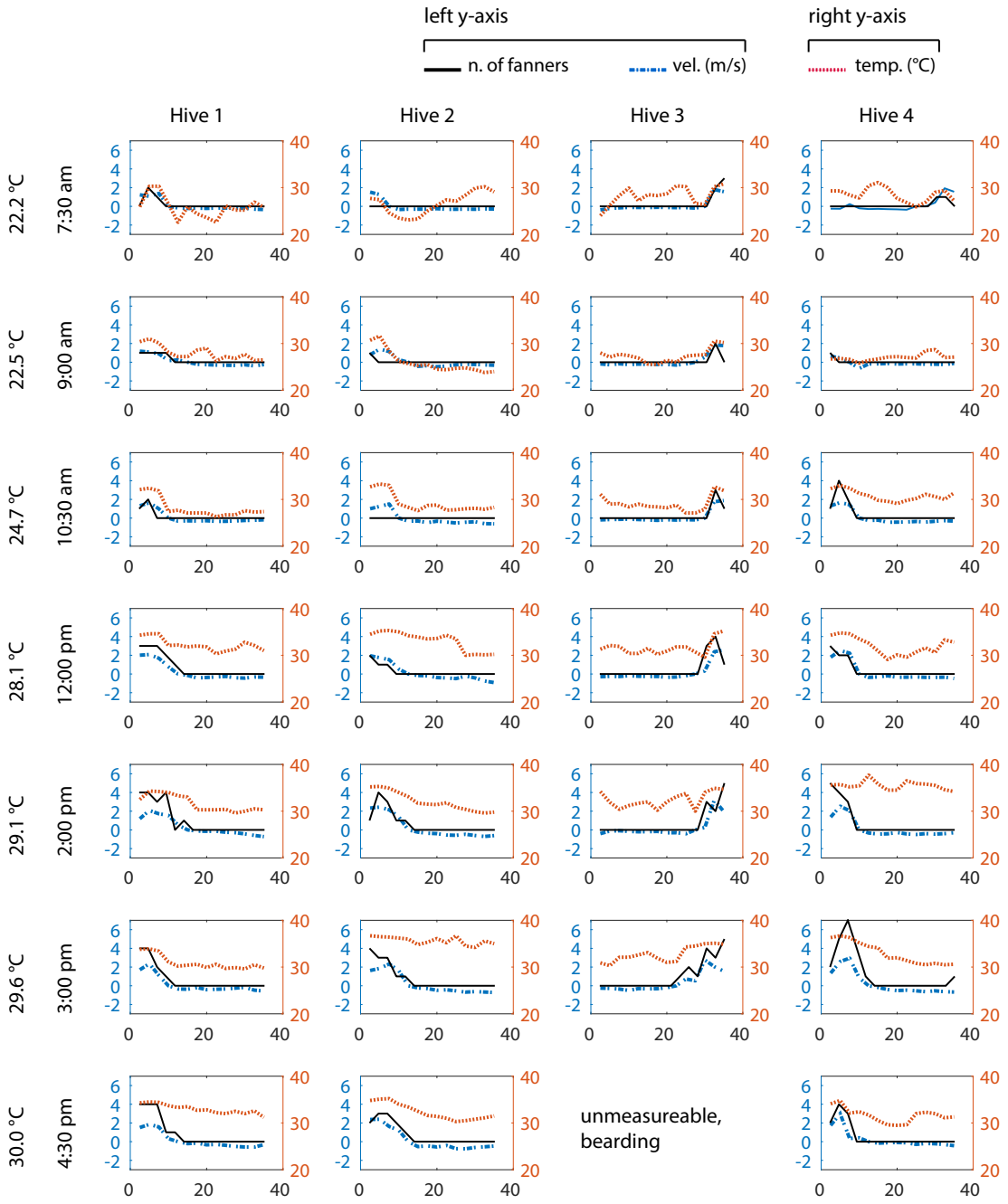

Figure A.1: Fanning activity, air velocity and air temperature as measured along the nest entrance (x-axis, cm). Measurements were made from 4 hives at 7 times throughout the day (07/21/2015). The density of fanning bees, air velocity and air temperature were spatially coupled.

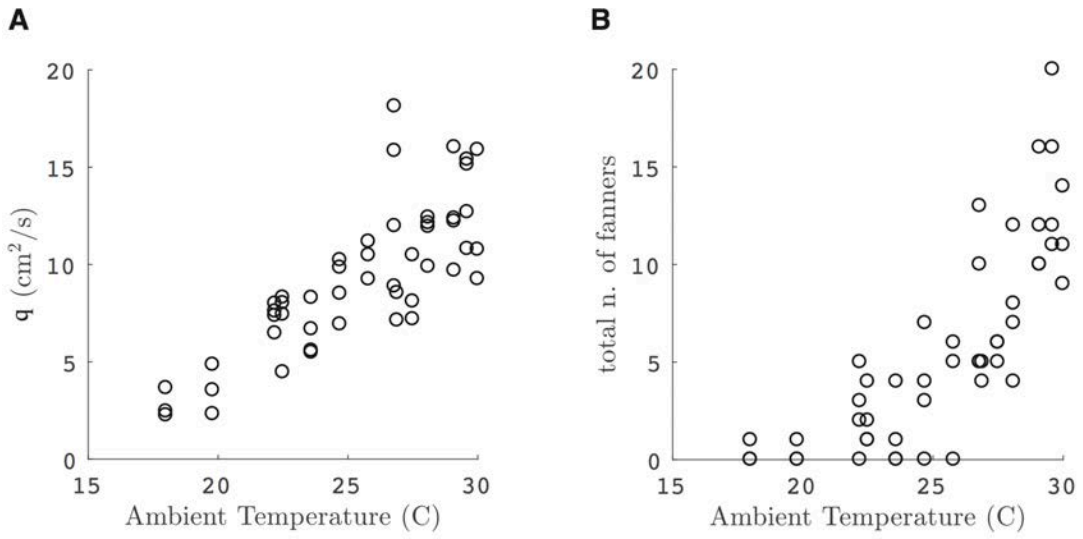

Figure A.2: The relationship between ventilation behavior and ambient temperature according to manual measurements made from 4 colonies from 07/21/2015 to 07/23/2015. (A) Flux of air at the nest entrance ($q = \frac{\int |v| dx}{2}$). Note that because our measurements were sampled from a 1D space, we report flow rate in cm^2/s rather than cm^3/s. (B) Total number of fanners visible at the nest entrance as a function of ambient temperature.

A.4 Numerical simulations

The MATLAB code used to generate the data in all figures presented in this paper is available on GITHUB (ENTER STABLE LINK HERE).

Parameter choices

Our simulations tracked the change of local density (ρ), local temperature (T) and local velocity (v) at every position along the nest entrance over each iteration (time). These values were held in three arrays of length L/l_b. L was fixed at 38cm, the approximate width of the nest entrance in the experimental setup and l_b was set to 2cm, the approximate wingspan of a fanning bee. We chose to fix T_h to 36 °C which is the temperature at which honeybees are known to regulate their core nest temperature[46]. Ambient temperature was was fixed throughout each simulation, but was varied

across simulations to explore the effects of varying ΔT. D_v and D_T for Fig. 2 and 3 were 1×10^{-4} and 4×10^{-5}, respectively. These choices were used to fit the simulations to the observed behavior. We explore the effect of these diffusion coefficients on the model's behavior in FigurFig.e A.3.

In the continuous form of the model, K_{on} and K_{off} relate the rate at which bees begin to fan and cease fanning to the local air temperature. In the context of the simulations, these values describe the probability that a bee will fan or cease fanning at a given temperature and are governed by the following equations: $k_{\text{on}} = k_0 \frac{\tanh(m*(T-36))+1}{2}$ and $k_{\text{off}} = k_0 - k_{\text{on}}$. The parameter m controls the slope of this sinusoidal function. Cook et al. 2013 report the distribution of temperature thresholds above bees will fan when heated in groups of 1, 3 and 10 bees over a range of temperatures[14]. They found that the distribution of temperatures at which individuals are induced to fan is dependent on group size. For the purposes of our study we assumed that the distribution associated with groups of 10 bees was most similar to that which would be found at the hive entrance. We used $m = 0.1$ because it approximately replicates this distribution. This value also adequately reproduced the same dynamics that we observed at the nest entrance. See SI Fig. A.4 to see the effects of m on ventilation dynamics.

Implementation

We used a finite difference scheme to solve the differential equations. All simulations began with the following initial conditions: T was set to 36 °C across the entire entrance, ρ was a uniform distribution (1 bee per bin), and v was an array of zeros. At each iteration (or time step) in the simulations, an x position was randomly selected. A single bee was allowed to make a decision about whether to begin fanning and one bee was allowed to decide whether to cease fanning according to Equation 1. Equations 2 and 3 were then solved to update the velocity and temperature arrays given the new density array. These steps were then repeated in subsequent loops, each time randomly choosing a position to update.

Boundary conditions

Bees were not allowed to fan at the boundaries, so $\rho = 0$ at $x = 1$ at $x = L/l_b$. Velocity at the boundaries was also fixed at 0 to enforce the nonslip condition with the walls of the nest entrance. Finally, the diffusion of heat along x requires a boundary condition that accounts for the thermal conductivity of the boundaries (the walls of the nest entrance), which depends on the thickness and material properties. We implemented a Robin Boundary Condition in which the conductivity of the boundary is controlled by the parameter α. When $\alpha \approx 0$, the wall of the nest entrance behaves as a perfect conductor. When $\alpha = 1$, the wall behaves as a perfect insulator. See SI Fig. A.5 to see the effect of this parameter choice on ventilation dynamics.

A.5 Mechanisms of self-organization

Our basic model is derived from the equations of mass and momentum conservation of air flow, recognizing that this flow is driven by bee fanning. We denote the direction parallel to the hive entrance using a coordinate x, and the direction perpendicular to the hive entrance by y, the fluid velocity components in the two direction by $u(x, y, t), v(x, y, t)$ respectively, and the temperature by $T(x, y, t)$. Since there are no flows in the x direction, and no variations in the temperature and flow velocity in the y direction, we have $u = 0, v = v(x, t), T = T(x, t)$. Then, momentum balance in the y direction reads $\rho_f(\partial v/\partial t + v\partial v/\partial y) = -\partial p/\partial y + f + \mu\partial^2 v/\partial x^2$, where ρ_f is the fluid density, and f is the body force that consists of the fluid friction with the floor of the hive entrance, i.e. $f = -\zeta v$, where ζ is the friction factor. If the flow reaches steady state relatively quickly compared to any changes in the environment associated with diurnal variations, momentum balance reduces to a simple equation that now reads $-\zeta v + \mu\partial v/\partial x^2 - \partial p/\partial y = 0$. Since the pressure gradient is predominantly an active one generated by the bees over their length, a simple expression suggests that $\partial p/\partial y \sim \rho\rho_f v_b^2$ in the active region where ρ is the linear density of fanning bees, and v_b is the

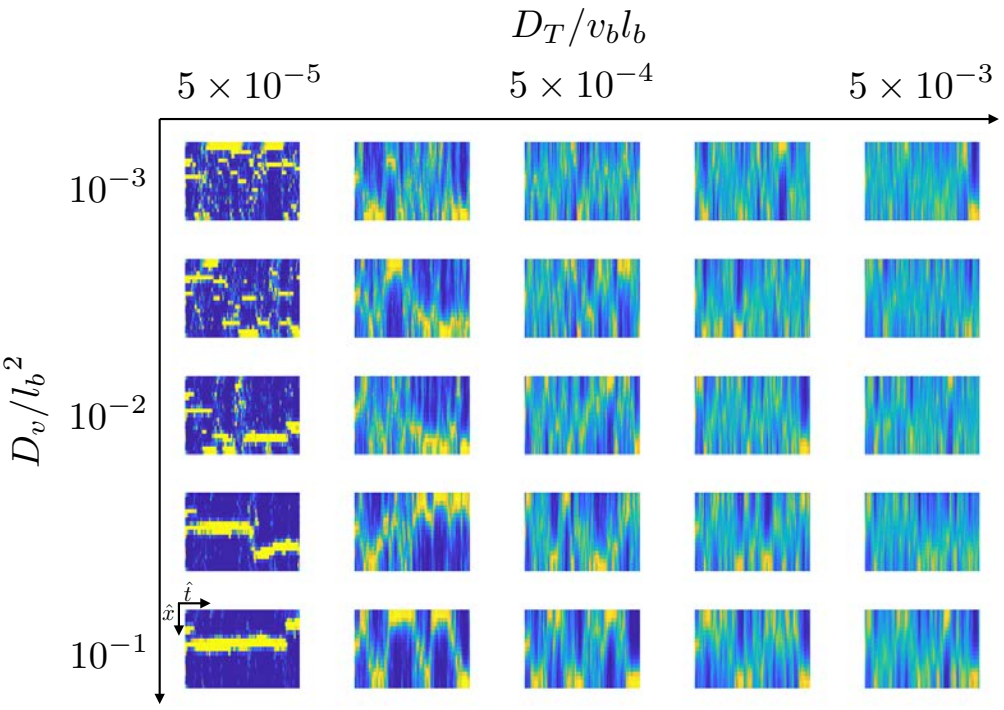

Figure A.3: Effects of diffusion coefficients, D_V and D_T, on ventilation dynamics. At low D_V and D_T, there is minimal shear imposed by velocity gradients (effective diffusion of velocity) and minimal diffusion of heat through x. In this condition, the positive feedback between fanning behavior, air velocity and temperature occurs only locally and there is not short-range attraction between fanning groups. This leads to the formation of many small fanning groups. As D_V and D_T increase, positive feedback occurs in both space and time. This leads to fewer, larger fanning groups. $\hat{x} \in [0, 19]$ and $\hat{t} \in [0, 2 \times 10^4]$.

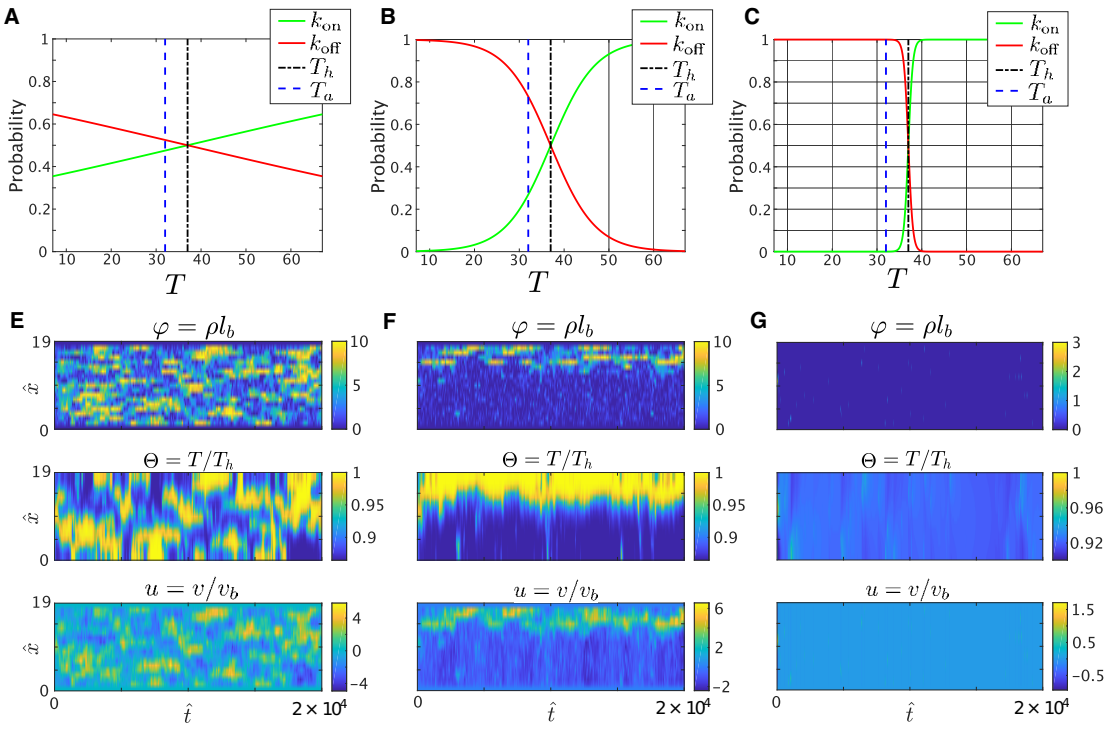

Figure A.4: Effect of slope of behavioral switch functions on ventilation dynamics. K_{on} and K_{off} prescribe the probability of a given bee to begin fanning or cease fanning at a given local air temperature. The slope of these functions is controlled by the parameter m. (A,E) When m is extremely low ($m = 0.01$), fanning behavior is weekly coupled to temperature and no distinct fanning group forms. This leads to high fluid friction and poor ventilation efficiency. (C,E) When m is extremely high ($m = 1$), fanning behavior will occur only over a narrow range of temperatures. (B,F) At moderate m ($m = 0.1$), ventilation can occur over a broad range of temperatures and a stable fanning group will form, except when T is very close to $T_{\text{hive}}(\Delta T < 2)$. Because the slope of these switch functions is the only behavioral parameter in our model–the others pertaining only to the properties of the physical environment–it is likely that natural selection has acted on this parameter to ensure efficient ventilation. We selected $m = 0.1$ for our simulations because it most adequately fits data on the diversity of fanning temperature thresholds reported in the literature[14,38]. $\hat{x} \in [0, 19]$ and $\hat{t} \in [0, 2 \times 10^4]$

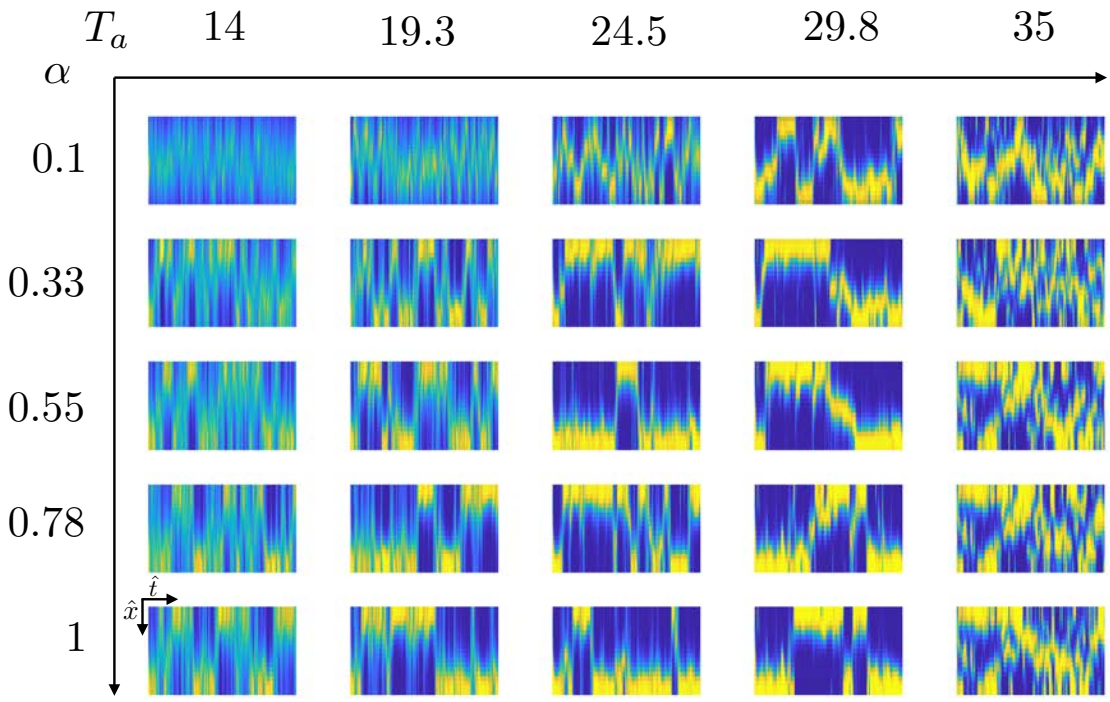

Figure A.5: Effects of ambient temperature and boundary conductivity on ventilation dynamics. The parameter α controls the thermal conductivity of the boundaries of the nest entrance. When α is near 0, the boundary is perfectly conductive. When α is 1, the boundary is a perfect insulator. When α is small, the fanning group is more likely to occupy the center of the nest entrance. This occurs because heat is being continually lost to the environment through the boundary (if $T_a < T_h$) and the warmest region of the entrance where bees are most likely to fan is the center of the entrance. When α is high, the system loses no heat through the boundary. Therefore, when the fanning group is positioned at near the boundary, heat diffuses toward the opposite side of the entrance (where inflow is occurring) but not through the boundary. This condition is relatively stable and the fanning bees are more likely to continue fanning near the boundary than they are away from the boundary. $\hat{x} \in [0, 19]$ and $\hat{t} \in [0, 2 \times 10^4]$.

constant flow velocity generated by a bee. In the passive region, the pressure gradient is reversed by an amount that is dictated by mass balance. Indeed, integrating the equation for mass balance over the length of the hive entrance L, we must have $\int_0^L v dx = 0$ for global mass balance (assuming that the dominant flow into the hive occurs only at the entrance). Then final equation for fluid flow at the entrance then reads

$$\zeta v = \rho_f v_b^2 \left[\rho(x,t) - \frac{1}{L} \int_0^L \rho(x,t) dx \right] + \mu \frac{\partial^2 v(x,t)}{\partial x^2}. \tag{A.1}$$

Dividing both sides by ζ and defining a characteristic length scale $l_b = \rho_f v_b / \zeta$ and a scaled momentum diffusivity (with dimensions of the inverse length squared), $D_v = \mu/\zeta$, we obtain Eq. (2) in the main text.

For heat balance at the hive entrance, we may write an equation that accounts for advection, diffusion and sources as $\partial T/\partial t + u\partial T/\partial x + v\partial T/\partial y = D(\partial^2 T/\partial x^2 + \partial^2 T/\partial y^2) + q$. Again, with the assumptions of variations only in x and $u = 0$, along with a simple cooling law that assumes $q = -cv\Delta T$, i.e. the cooling rate is linearly proportional to the temperature difference and the fluid velocity (neglecting any complex dependence on the Nusselt number), we find that the resulting equation for heat balance at the entrance reads

$$\frac{\partial T(x,t)}{\partial t} = -cv(x,t)\Delta T + D_T \frac{\partial^2 T(x,t)}{\partial x^2} \tag{A.2}$$

If we use the dimensionless variables defined by $\hat{x} = x/l_b, \hat{t} = tv_b/l_b, u = v/v_b, \phi = \rho l_b, \Theta = T/T_a$, we are led to a dimensionless set of our original equations with four dimensionless parameters, given by:

$$u = \left[\phi - \frac{l_b}{L} \int_0^{L/l_b} \phi d\hat{x} \right] + \frac{D_v}{l_b^2} \frac{\partial^2 u}{\partial \hat{x}^2}. \tag{A.3}$$

$$\frac{\partial \Theta}{\partial \hat{t}} = -c l_b u \Delta\Theta + \frac{D_T}{v_b l_b} \frac{\partial^2 \Theta}{\partial \hat{x}^2} \tag{A.4}$$

In Fig. S6, we elaborate on the succinct mathematical description indicated in Eqn S1 that describes the dynamics of airflow in and out of the nest entrance. The first term (A) denotes the outward airflow due to the actively fanning bees. However, since the nest volume is fixed, this outflow must be balanced by inflow elsewhere. This simple consequence of fluid conservation demands the presence of the second term (B), which serves as an inhibitor of flow (as it reverses the flow direction). Finally, the last term (C) characterizes the effect of flow entrainment due to the shear induced by motion in and out of the nest; the net effect is that of penalizing large velocity gradients. The accompanying figures show how a population of active fanners leads to a local actively driven outflow, that via conservation of fluid demands passive inflow in those regions where there are no active fanners. The resulting increase in fluid friction due to shear gradients in these regions causes additional entrainment of flow from the nest. This leads to the bees there sensing the nest temperature, driving local recruitment of bees and creating a positive feedback that drives the clusters to coarsen into a single one when the temperature difference between the nest and the environment is large. The different schematics 1,2,3, show how fluid flow can serve as both activator and inhibitor depending on the spatial heterogeneity of the initial density of fanning bees.

A.6 Long-term hive monitoring

Thermistors were uniformly distributed along the nest entrance ((1.8 x 37cm), leading to a 1.17cm spacing between thermistors. The thermistors were suspended from rigid lead wires so that the bead of the thermistor was isolated from the circuit board and suspended in the airflow generated by the

$$v(x,t) = \underbrace{l_b v_b}_{\text{A. fanning behavior}} \underbrace{\left[\rho(x,t) - \frac{1}{L}\int_0^L \rho(x,t)dx\right]}_{\text{B. fanning behavior + conservation of volume}} + \underbrace{D_v \frac{\partial^2 v(x,t)}{\partial x^2}}_{\text{C. fanning behavior + conservation of volume + friction}}$$

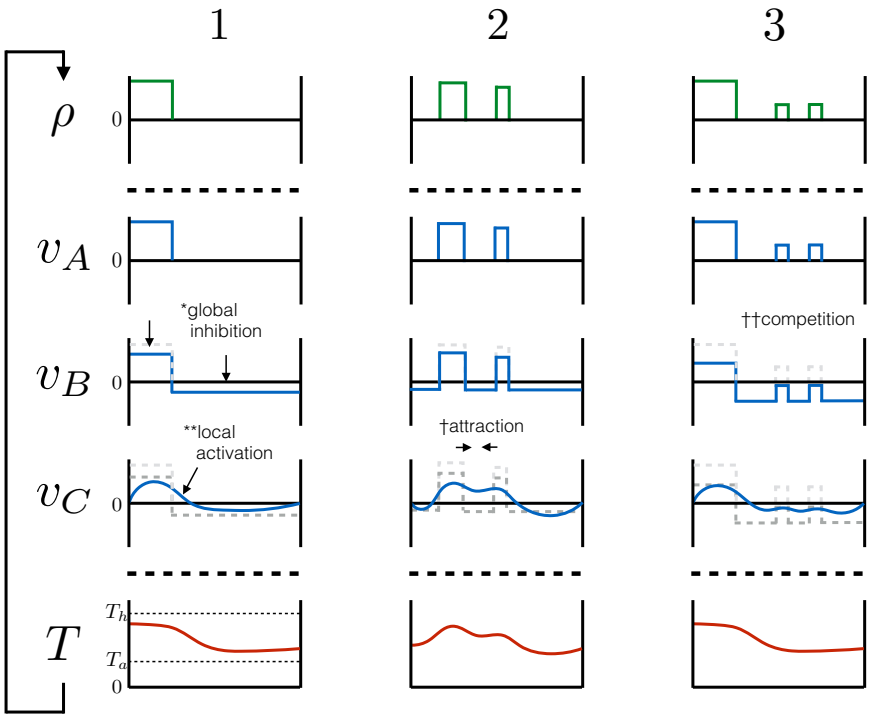

Figure A.6: A schematic illustrating the mechanisms of self-organization which emerge from the model. Equation 2 is broken down into components: (A) the direct result of fanning behavior, (B) conservation of volume, and (C) friction (or effective diffusion of velocity). Below, the following variables are plotted: the distribution of fanners (ρ), velocity calculated considering only fanning behavior (v_A), velocity calculated considering fanning and conservation (v_B), velocity considering fanning, conservation and friction (v_C), and the temperature profile (T). Scenario 1 is a simple example which illustrates how conservation of volume contributes to global inhibition of fanning behavior (*) and friction (as well as the diffusion of heat) contribute to local activation (**). That is, bees are more likely to fan adjacent to other fanning bees due to friction and diffusion. Scenario 2 illustrates a case in which this friction/diffusion drives attraction between adjacent fanning groups (†). Fanners are more likely to fan between fanning groups as a result of friction/diffusion. Finally, Scenario 3 illustrates the potential for conservation of volume to act as a global inhibitor which ultimately drives competition between fanning groups (††). Large fanning groups are more likely to grow and smaller groups are likely to shrink and disappear due to this competition.

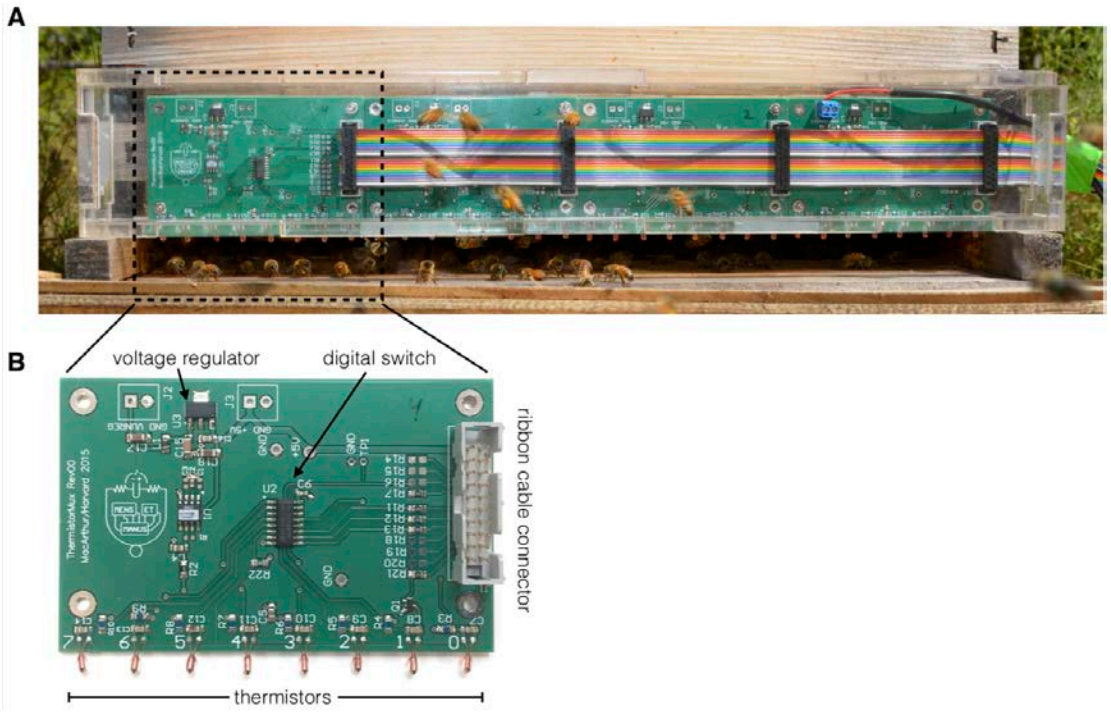

Figure A.7: Custom sensor array. A) The ThermistorMUX circuit installed at the nest entrance. B) One of four PCB modules.

Table A.1: Dimensionless parameters and constants. Values reported here were used in simulations unless otherwise specified in the figure captions. $L = 0.38m, l_b = 0.02m, v_b = 1m/s, c = 0.05/m, D_T = 4 \times 10^4 m^2/s, D_v = 1 \times 10^{-4} m^2$.

Parameter	Description	Value
L/l_b	scaled entrance length	19
D_v/l_b^2	scaled fluid friction	0.25
$D_T/v_b l_b$	scaled thermal diffusivity	4×10^{-4}
cl_b	scaled fanning length	1×10^{-3}
m	behavioral switch response	$0.1/^oC$
α	scaled boundary conductivity	0.2

bees. The thermistors were occasionally contacted by the wings of fanning bees but they were typically not directly touching the bodies of the bees (see Fig. A.8A and SI Movie 2). A Logitech c920 web cam was mounted approximately 3 ft above the nest entrance pointing down such that an orthogonal view of the ”porch” was visible. Four-second videos of fanning activity were collected every 5 minutes from 9/16/15 to 9/24/15. Temperature measurements from each of the 32 thermistors was acquired every 5 seconds over this period. An additional Parallax SHT11 digital temperature sensor was placed nearby in the shade in order to measure the ambient temperature. This protocol was repeated for two additional hives from 7/7/2016 to 7/19/2016 (Fig. A.8 for complete dataset). The position of all fanning bees visible on the outside of the nest entrance during the videos taken during daylight hours were digitized by mouse click using a custom MATLAB program (See SI Movie 3). Fanning activity also occurs just inside the entrance of the hive, however these bees were not visible in our videos and are not represented in our data. We assume that analyzing the position and number of fanning bees visible in the videos is sufficient to capture the phenomena that we are interested in.

The sensor array used in this study was designed by Jim MacArthur to continuously measure air temperature at the nest entrance with high spatial and temporal resolution. The sensor array consists of four PCB modules bearing 8 thermistors each (Fig. A.7). The circuit board is covered with an acrylic case. During data collection an opaque covering was used to prevent radiative heating from the sun. The thermistors were suspended in the flow stream in order to acquire an accurate air temperature without directly contacting the bees (See SI Movie 3). Each PCB module has a voltage regulator to ensure a consistent reference voltage. A digital switch allows a single digital signal to switch between each of the 8 thermistors which are read through a common analog pin. When a given thermistor is not being read, it is not receiving current, preventing self-heating. Each of modules has a ribbon cable connector allowing them to interface with the Arduino. The Arduino was programed using the Arduino IDE to select and read each thermistor in sequence. Data was

transfered to a MATLAB program using a USB-Serial connection. Schematics, drawings, and code required to reproduce this setup are available on GITHUB (ENTER STABLE LINK HERE).

A.7 In large colonies CO_2 and temperature at the nest entrance are coupled in space but are decoupled in time

Heat is thought to be the primary cue that induces the fanning response in honeybees. However, Seeley (1974) observed that a small colony (approximately 10,000 bees) experienced dramatic spikes in CO_2 concentrations which were abated by a proportional fanning response by the colony[74]. Over a 52 hours of CO_2 measurements from the brood nest of a small (10,000 bees) and large colony (35,000 bees), Seeley reported that the large colony had a lower mean CO_2 concentration (0.44%) than did the small colony (0.78%). In addition, the larger colony showed much less variation in CO_2 concentration (0.16%) than did the small colony (0.34%). Seeley suggested that this better homeostasis in CO_2 concentration in the large colony was likely due to near continuous thermoregulatory ventilation rather than fanning in response to CO_2.

In our model, we assumed that the fanning response at the nest entrance would primarily track the local air temperature given because we were using large, mature colonies. We tested this assumption by measuring both CO_2 and temperature at the nest entrance of Hive 3. Because CO_2 sensors are larger and much more expensive than thermistors, we were not able to make a high resolution sensor array as we did for the temperature measurements. Instead, we partitioned the nest entrance into two discrete regions by placing a 15cm wooden partition in the center of the nest entrance to block airflow in this region (Fig. A.9A). This allowed use to study the spatial dynamics of the fanning group while using only two CO_2 sensors. The bees established an outflow region on the left of the partition allowing air to passively move into the hive on the right side. This segregation of inflow and outflow emerged from the behavior of the bees and the physical constraints imposed by

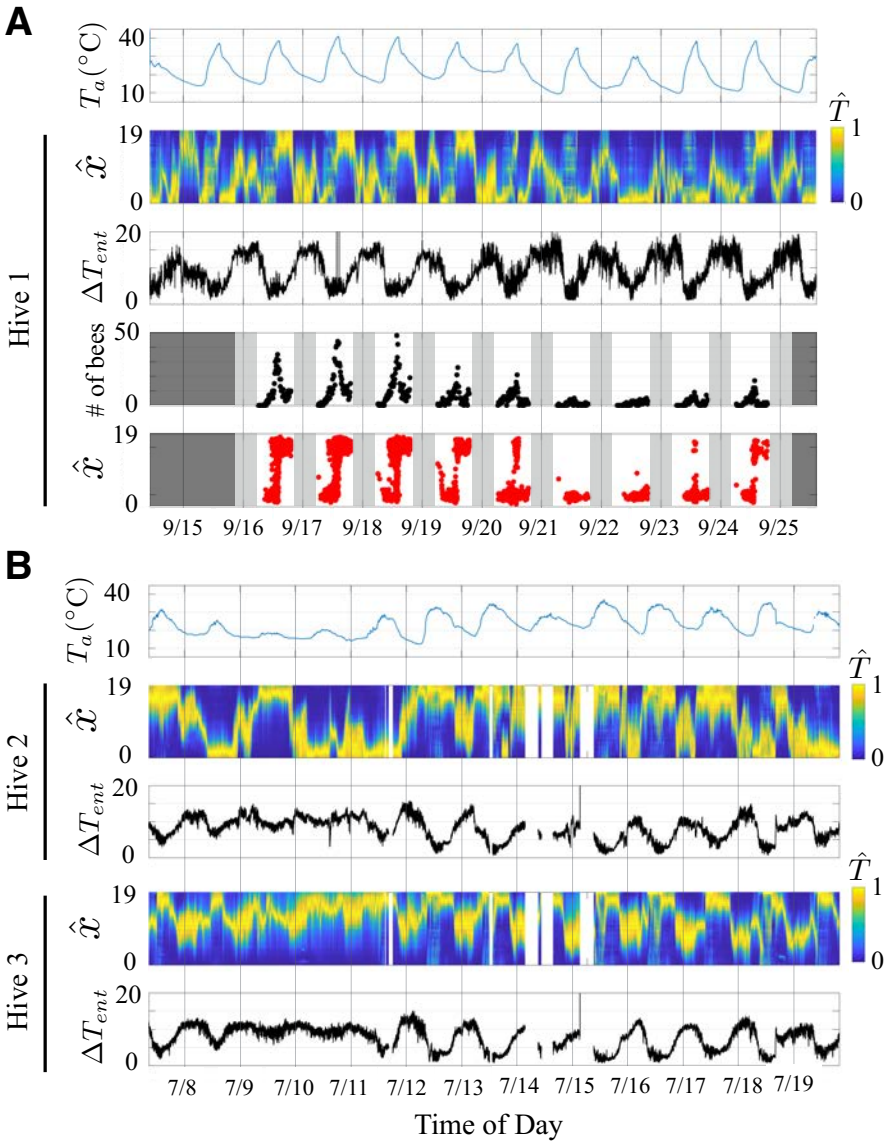

Figure A.8: Complete dataset of fanning behavior at nest entrance of three colonies in response to ambient temperature oscillations. A1) Ambient temperature, T_a, oscillations measured in the apiary from 9/14/2015 to 9/25/2015. A2) Normalized entrance temperature, $\hat{T} \in [0, 1]$, as measured by 32 thermistors distributed across the nest entrance. A3) The differential, ΔT_{ent}, between the maximal (outflow) and minimal (inflow) temperature readings measured at the nest entrance at a given time. A4) The number of fanners visible at the nest entrance over time. Dark gray regions indicate times when video data was not available. Light gray regions indicate times when it was too dark to collect accurate data. A5) The position of fanning bees along the nest entrance. B1) Ambient temperature, T_a, oscillations measured in the apiary from 9/14/2015 to 9/25/2015. B2-5) Entrance temperature data for Hive 2 and Hive 3.

the partition (Fig. A.9B). This configuration persisted for the three day period over which data was collected.

As expected, temperature and CO_2 were coupled in space–outflowing air was enriched in both CO_2 and heat relative to inflowing air (Fig. A.9C). However, the temperature and CO_2 concentration of outflow were decoupled in time. The temperature of outflowing air tracked the ambient temperature. During the heat of the day when thermoregulatory ventilation was peak, CO_2 was at a minimum. When thermoregulatory fanning decreased during the the night, CO_2 was maximal. There are two possible explanations for this: 1) the number and density of bees in the nest at night is higher during the night resulting in higher CO_2 production, and 2) as the thermoregulatory fanning response decreases at night, CO_2 is evacuated at a lower rate. It seems likely that both mechanisms contribute. We also noticed an interesting dip in the CO_2 concentration at around 6am which was reproducible across days that we cannot yet explain.

These measurements bolster our assumption that temperature is the dominant cue inducing the fanning response in large, mature colonies. A probability function for the CO_2-induced fanning response could be added to our model once it is resolved by future experimental work, but it is unlikely to qualitatively change the dynamics of the model because CO_2 and temperature are spatially coupled at the nest entrance.

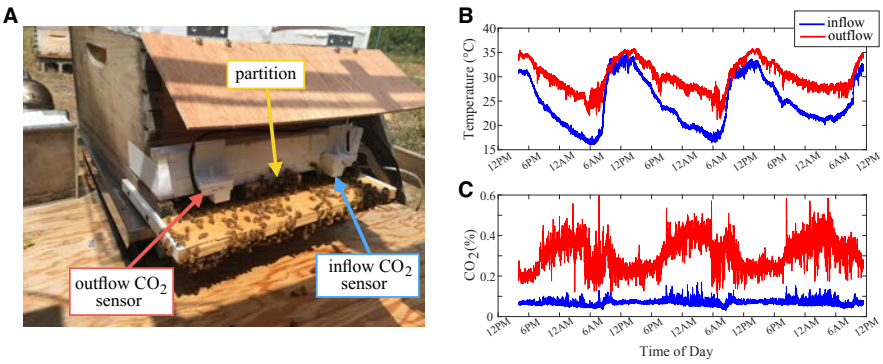

Figure A.9: A) Setup for acquiring CO_2 concentration data. B) Temperature of outflowing air was consistently higher than inflowing air, but varied with the ambient temperature. C) Similarly, CO_2 was higher in outflow than in inflow. However, CO_2 was decoupled from temperature, reaching a minimum during the heat of the day and a maximum at night.

B

Supplementary Information for Chapter 3

B.1 Experimental Methods

B.1.1 Study site.

All clusters were studied at Harvard University, Concord Field Station, Bedford, Massachusetts (42°30N, 72°10W).

B.1.2 Cluster preparation.

All of the clusters studied were artificial clusters were bought from honeybee suppliers (New England Beekeeping LTD, and Gold Star bees LTD), where the colony (10,000 worker/drone bees and a queen) is confined in a wooden box. Bees were a mix of Russian, Italian, and Carniolan bees. Clusters were prepared by separating the queen from the rest of the colony. The queen is placed in a small queen cage (3.2 x 10.0 x 1.6 cm). Next, the cluster box was opened and the queen (still in her own cage) was fastened to a cluster mount at position $U_i = V_i = W_i = 0$. The worker bees were

then shaken onto the base of the mount whereupon they clustered around their queen.

B.1.3 Apparatus.

To analyze the mechanisms of mechanical stress adaptation, the clusters were mounted on a cluster mount (see Fig. 1B and Fig. B.1A,B) which consists of a horizontal wooden board. The board was controlled by a motor (purchased from Applied Motion) that produced periodic movement in the horizontal or vertical axis at different frequencies and forces. The shape of the cluster was recorded via cameras (Logitech C270) positioned at three orthogonal locations (front, bottom, and side). Positions of individual bees were recorded using a high-speed frontal camera (SA3, Fastec Imaging) recording at 500 fps, and an $8-$megapixel iSight camera recording at 240 fps. Ambient temperature was recorded using a digital thermometer (A150Q Tech Instrumentation) that was fixed to the cluster mount, 2 cm above the clustered bees. Forces were measured using an accelerometer (SparkFun ADXL335) mounted on the wooden board.

B.1.4 Procedure.

A trial recording lasted 60 minutes, where shaking was applied for 30 minutes, and then no shaking was applied for additional 30 minutes. Equilibration period of 1 hour was applied within trials. During this time, the bees were fed ad libitum with a sugar solution (1:1 by volume, granulated sucrose: liquid water) by spraying it onto the cluster with a squirt bottle. Unless stated otherwise, single shaking response was recorded before the trial, and after 30 minutes. The responses to each mechanical shaking condition were replicated three times. Experiments were performed at $22 \pm 2^{\circ}$C.

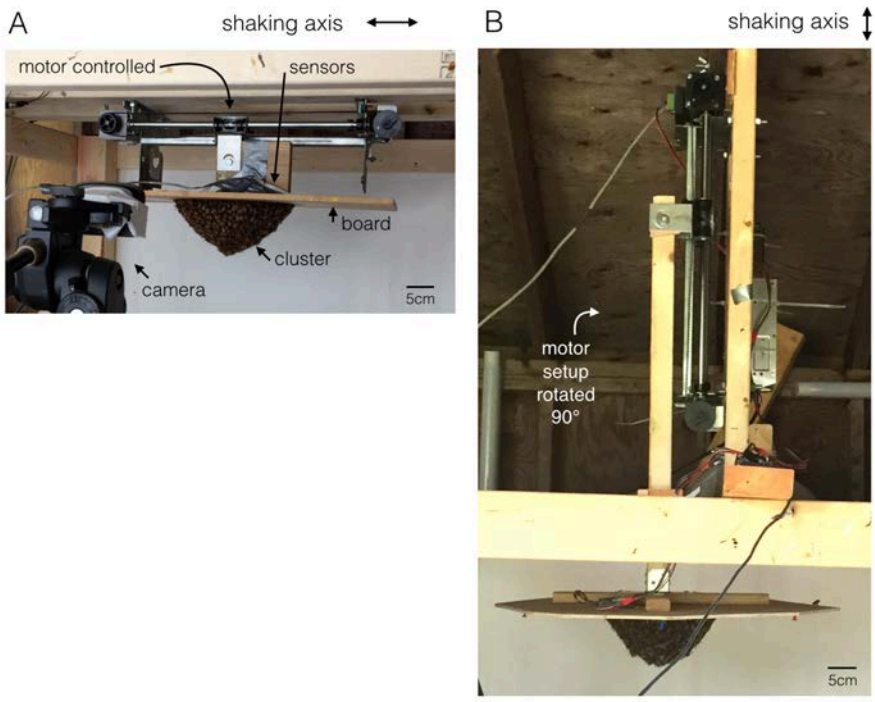

Figure B.1: Experimental Setup: A) Horizontal shaking B) Vertical shaking. For the vertical shaking, the motor setup was rotated 90° to produce movement along the z axis.

B.1.5 Video analysis.

The shape of the cluster was extracted using the image analysis tool box of MATLAB 2016a. In particular, the base area, $A(t)$ was identified using image segmentation with a threshold value to turn the gray-scale image into a binary image. The number of pixels belonging to the base segment were translated to area using the pixel to cm^2 conversion via a calibration object. Individual honeybee positions were digitized using a freely available MATLAB application, DLTdv5[?].

B.2 Continuous vs. Discontinous Shakings

The measured accelerations during shaking events were recorded using an accelerometer mounted on the wooden board, and are shown in Fig. B.2A, and Fig. B.2B, for periodic and discontinuous shaking, respectively.

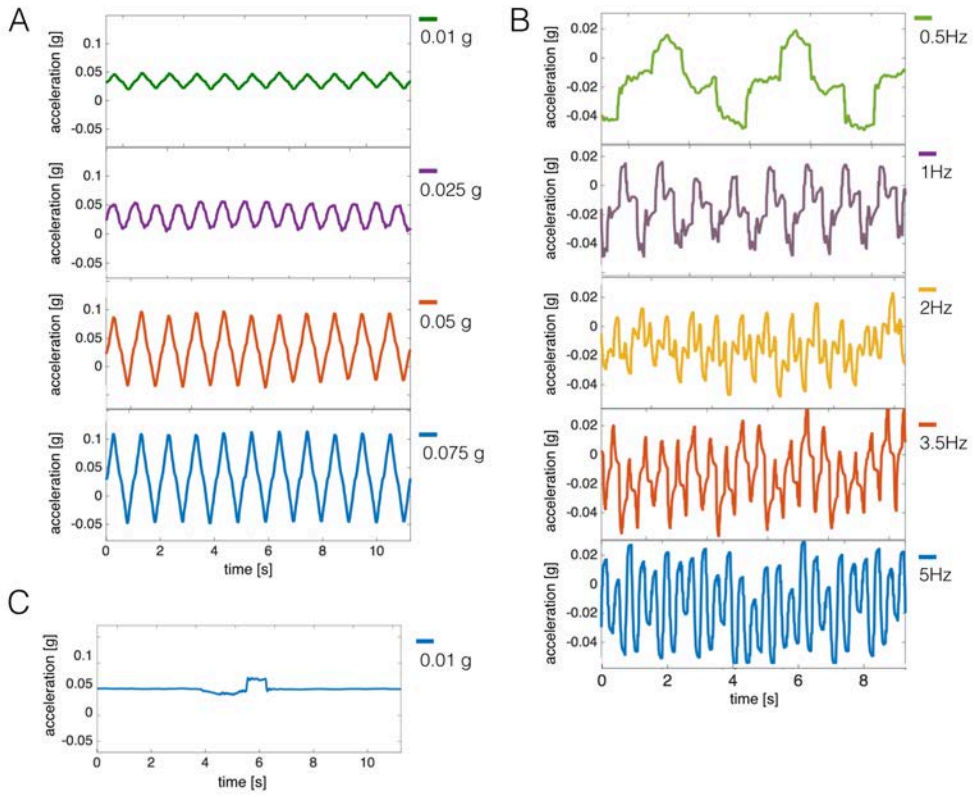

Figure B.2: Mechanical Shaking Signals. A) Continuous shaking in which the frequency is kept constant and the acceleration is modified. B) Discontinuous shaking in which the acceleration is kept constant and the frequency is modified. C) A single sharp shake. Maximal acceleration or frequency values for each shaking signal appear in the legend.

Trial	Swarm	Stimulus type	Intensity	Direction	Date
1	1	discontinous	2 Hz	horizontal	23-Apr-15
2	1	discontinous	5 Hz	horizontal	23-Apr-15
3	1	discontinous	0.5 Hz	horizontal	24-Apr-15
4	1	discontinous	1 Hz	horizontal	24-Apr-15
5	1	discontinous	2 Hz	horizontal	24-Apr-15
6	1	discontinous	3.5 Hz	horizontal	24-Apr-15
7	1	discontinous	1 Hz	horizontal	25-Apr-15
8	1	discontinous	3.5 Hz	horizontal	25-Apr-15
9	1	discontinous	0.5 Hz	horizontal	26-Apr-15
10	1	discontinous	5 Hz	horizontal	26-Apr-15
11	1	discontinous	3.5 Hz	horizontal	26-Apr-15
12	1	discontinous	0.5 Hz	horizontal	27-Apr-15
13	1	discontinous	5 Hz	horizontal	27-Apr-15
14	1	discontinous	1 Hz	horizontal	27-Apr-15
15	1	discontinous	2 Hz	horizontal	27-Apr-15
16	2	continuous	0.075 g	vertical	10-Jun-15
17	2	continuous	0.1 g	vertical	10-Jun-15
18	2	continuous	0.075 g	vertical	10-Jun-15
19	2	continuous	0.075 g	vertical	11-Jun-15
20	2	continuous	0.1 g	vertical	11-Jun-15
21	2	continuous	0.025 g	horizontal	11-Jun-15
22	2	continuous	0.025 g	horizontal	11-Jun-15
23	2	continuous	0.01 g	horizontal	11-Jun-15
24	2	continuous	0.075 g	horizontal	12-Jun-15
25	2	continuous	0.025 g	horizontal	12-Jun-15
26	2	continuous	0.01 g	horizontal	12-Jun-15
27	2	continuous	0.075 g	horizontal	12-Jun-15
28	2	continuous	0.01 g	horizontal	12-Jun-15
29	2	continuous	0.075 g	horizontal	13-Jun-15
30	2	continuous	0.05 g	horizontal	13-Jun-15
31	2	continuous	0.05 g	horizontal	13-Jun-15
32	2	continuous	0.05 g	horizontal	13-Jun-15
33	2	continuous	0.025 g	horizontal	13-Jun-15
34	2	continuous	0.05 g	horizontal	13-Jun-15
35	2	continuous	0.025 g	vertical	15-Jun-15
36	2	continuous	0.05 g	vertical	15-Jun-15
37	2	continuous	0.025 g	vertical	16-Jun-15
38	2	continuous	0.025 g	vertical	16-Jun-15
39	2	continuous	0.05 g	vertical	16-Jun-15
40	2	continuous	0.05 g	vertical	16-Jun-15

Table B.1: A description of the experimental trials, the particular swarm used (swarm 1 or swarm 2), the stimulus type (continuous or discontinous), intensity (frequency or acceleration), direction (horizontal or vertical) and the date they were performed.

B.3 Statistical Tests

In this section we describe a series of statistical tests we perform to compare the observed experimental results across the varied experimental parameters.

We consider the time series of the ratio of the contact area of the base of the cluster divided by its original area $A(t)/A(0)$ as a function of time. We calculated the Pearson correlation coefficient between the time series of the continuous shaking, the horizontal and vertical case, for intensities 0.025g, 0.050g, and 0.075g. P–values for testing the hypothesis that there is no relationship between the observed time series (null hypothesis) are summarized in Table S3. This shows that all pairs of horizontal trails are significantly different, all pairs of vertical trails are not significantly different ($p < 0.05$). At low shaking intensities (0.025 g), the horizontal and vertical results are not significantly different, as in both cases the swarm doesn't flatten. As the intensity increases the horizontal and vertical results differ significantly $p < 0.01$ (for the 0.05 intensity) and $p < 0.001$ (for the 0.075 intensity).

		Horizontal			Vertical		
		0.025g	0.050g	0.075g	0.025g	0.050g	0.075g
Horizontal	0.025g	1	$2 \times 10^{-110***}$	$7.44 \times 10^{-105***}$	0.51	0.81	$9.56 \times 10^{-34***}$
	0.050g		1	$1.92 \times 10^{-160***}$	0.26	0.02^{**}	$1.31 \times 10^{-50***}$
	0.075g			1	0.75	0.01^{**}	$5.13 \times 10^{-45***}$
Vertical	0.025g				1	0.09^{*}	0.11
	0.050g					1	0.11
	0.075g						1

Table B.2: P–values for testing the hypothesis that there is no relationship between the observed time series of the cluster divided by its original area ($A(t)/A(0)$). Significant p–values are highlighted via asterisk: $p < 0.1(^{*})$, $p < 0.05(^{**})$, and $p < 0.001(^{***})$.

B.4 Numerical Model

Each honeybee is modeled as a $3D$ spherical particle of diameter a. Clusters at time $t = 0$ consisted of 1000 bees connected by linear springs arranged in a face centered lattice over a volume defined by a half-ellipsoid volume at different aspect ratios (i.e. different L_z/L_x values, as defined in Fig. 3.3A). The board is represented as an additional layer of bees that serve as a physical non-permiable barrier. Their position is fixed as the position of the board $\overrightarrow{r_b(t)} = [U_b, V_b, W_b]$, and they are not subjected to Newton's equation of motion.

The rest of the bees (not represented on the board) experience three types of forces in the simulation. The first is the truncated Lennard Jones (LJ) defined as:

$$F^{\text{LJ}}(\|\vec{r}\|) = \begin{cases} \dfrac{12\epsilon}{a}\left[\left(\dfrac{a}{\|\vec{r}\|}\right)^{13} - \left(\dfrac{a}{\|\vec{r}\|}\right)^{7} - \left(\dfrac{a}{\|\vec{r}^{\text{LJ}}_{\text{cutoff}}\|}\right)^{13} + \left(\dfrac{a}{\|\vec{r}^{\text{LJ}}_{\text{cutoff}}\|}\right)^{7}\right]\hat{r} & \|\vec{r}\| \leq r^{\text{LJ}}_{\text{cutoff}} \\ 0 & \text{o/w} \end{cases} \tag{B.1}$$

where $\vec{r}$ is the vector connecting the centers of the two particles; ϵ is the amplitude of the LJ potential; the force is truncated at the cutoff so that $F^{\text{LJ}}(r^{\text{LJ}}_{\text{cutoff}}) = 0$. The second force is a spring force defined as:

$$F^{\text{s}}(\|\vec{r}\|) = \begin{cases} k(\|\vec{r}\| - a)\hat{r} & \|\vec{r}\| < r^{\text{s}}_{\text{cutoff}} \\ 0 & \text{o/w} \end{cases} \tag{B.2}$$

where k is the spring coefficient. The third force is gravity, defined as:

$$F^{\text{g}} = -mg\hat{y} \tag{B.3}$$

where g is the gravitational constant and m is the mass of a particle.

B.4.1 Normal modes.

To characterize the frequency of the lowest mode of the cluster, we perform Normal Mode Analysis (NMA)[3] on clusters of different aspect ratios. The free motion described by the normal modes takes place at fixed frequencies that depend on its structure, materials and boundary conditions. In this context, the lower the frequency, the less energy it takes to invoke its associated mode of motion and thus more likely to occur.

We force the top layer of bees to remain stationary. We assume small deformations of the network ($X_i << 1$) and Taylor expand the potential V. We take into consideration elements up to power 2 of X_i, where X_i is the length of spring i minus its equilibrium length. The corresponding force on particles connected by spring i is:

$$F_i = \nabla_i V = \left(\frac{\partial^2 V}{\partial^2 X_i}\right) X_i + \sum_{j \neq i} \left[\left(\frac{\partial^2 V}{\partial X_i X_j}\right) X_j\right] \tag{B.4}$$

The harmonic potential of the spring connecting particles i and j is defined as:

$$V_{i,j} = \frac{1}{2} k \left(\left[(X_j - X_i)^2 + (Y_j - Y_i)^2 + (Z_j - Z_i)^2\right]^{1/2} - a\right)^2 \tag{B.5}$$

where X_i and X_j are the $x-$positions of particle i and j, respectively; Y_i and Y_j are the $y-$positions of particle i and j, respectively; Z_i and Z_j are the $z-$positions of particle i and j, respectively; a is the equilibrium length of the spring and k is the spring coefficient. In the general case of N particles connected by M springs in a $3D$ system, the second derivatives of the overall potential are organized

in the $3N \times 3N$ Hessian matrix $\mathbb{H}$. $\mathbb{H}$ is composed of $N \times N$ super–elements of size 3×3, i.e. ,

$$\mathbb{H} = \begin{pmatrix} \mathrm{H}_{1,1} & \mathrm{H}_{1,2} & \cdots & \mathrm{H}_{1,n} \\ \mathrm{H}_{2,1} & \mathrm{H}_{2,2} & \cdots & \mathrm{H}_{2,n} \\ \vdots & \vdots & \ddots & \vdots \\ \mathrm{H}_{n,1} & \mathrm{H}_{n,2} & \cdots & \mathrm{H}_{n,n} \end{pmatrix} \tag{B.6}$$

where

$$\mathrm{H}_{ij} = \begin{pmatrix} \frac{\partial^2 V}{\partial X_i X_j} & \frac{\partial^2 V}{\partial X_i Y_j} & \frac{\partial^2 V}{\partial X_i Z_j} \\ \frac{\partial^2 V}{\partial Y_i X_j} & \frac{\partial^2 V}{\partial Y_i Y_j} & \frac{\partial^2 V}{\partial Y_i Z_j} \\ \frac{\partial^2 V}{\partial Z_i X_j} & \frac{\partial^2 V}{\partial Z_i Y_j} & \frac{\partial^2 V}{\partial Z_i Z_j} \end{pmatrix} \tag{B.7}$$

The equation of motions can then be written as $\mathrm{F} = \mathbb{H} \cdot \mathrm{D}$, where

$$\mathrm{D} = (X_1, Y_1, Z_1, X_2, Y_2, Z_2 \cdots X_n, Y_n, Z_n) \tag{B.8}$$

is vector of all X, Y and Z positions of particles in the system. We solve $\mathrm{M}\ddot{\mathrm{D}} - \mathbb{H}\mathrm{D} = 0$ by converting it to the following Eigen value problem of the Hessian matrix: $(\mathbb{H} - \lambda \mathrm{I}) = 0$, where λ is a set of the Eigen values and I is a unit matrix. The Eigen values represent frequencies of motion, and the Eigen vectors represent displacement of all particles in the system.

As expected, the pendular motion is the lowest frequency normal mode of the elongated cluster (Fig. B.3). It is the most likely to occur naturally (under the NMA assumptions) and thus also the most relevant stimulus the honeybees experience. The frequency associated with the pendular mode increases monotonically as a function of the aspect ratio of the cluster, L_z/L_x. Therefore, modulation of the aspect ratio suffices to reduce the strain.

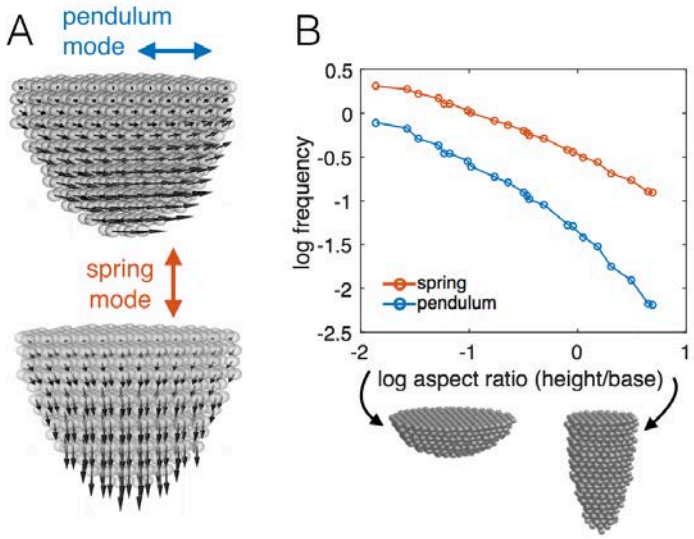

Figure B.3: Normal mode analysis show that the primary deformation modes are associated with spring and pendulum modes - consistent with experimental observations. A) Illustration of the displacements associated with pendulum (top) and spring (bottom) modes. B) The normal mode's frequencies as a function of aspect ratio.

B.4.2 Passive simulations to extract local strains.

To extract the local strains, the positions of the top bees were manipulated to produced periodic movement in the horizontal or vertical axis at different frequencies and forces (similarly to the experiments, e.g., Fig. ??C). The rest of the bees obey the Langevin equations of motion: $\dot{\mathrm{r}}_i = \mathrm{p}_i/m$, and $\dot{\mathrm{p}}_i = -\zeta \mathrm{p}_i + \mathrm{f}_i$, where $\dot{\mathrm{r}}_i$ is the velocity of particle i; ζ is the friction; f_i is the force acting on the particle. The bees experience all three forces mentioned above: F^{LJ}, F^{s}, and F^{g} with associated parameters listed in Table S2.

Local instantaneous strains were measured relative to a reference configuration in the absence of shaking at $t = 0$, as shown in Fig. 3.3A–C and Fig. B.3, according to the definitions in the main text.

Time integrated local strains presented in Fig. 3.3D–E, Fig. B.3 and Fig. B.4 were defined using a

modified instantaneous signal:

$$\delta l_i^t = \sqrt{\left(\sum_{\forall j \in i} l_{ij}^x(t+1) - l_{ij}^x(t)\right)^2 + \left(\sum_{\forall j \in i} l_{ij}^y(t+1) - l_{ij}^y(t)\right)^2} \tag{B.9}$$

for each neighbor j of particle i that is connected via spring. The time integrated signal is defined as $\widetilde{\delta l_i^t} = \sum_{\tilde{t}=t-T_w}^{t} \delta l_i^{\tilde{t}} \times dt$, where T_w is the time duration in which the signal is integrated and is chosen to be the period of the shaking.

B.4.3 Active stochastic simulations to follow active behavior

We performed a Stochastic Dynamics simulations to follow the active behavior of bees. The bees obey the over–damped equations of motion: $\dot{\mathrm{r}}_i = -\mathrm{f}_i + \tilde{\mathrm{r}}_i$, where $\tilde{\mathrm{r}}_i$ is a Gaussian random number with mean zero and variance η. f_i is the force acting on the particle which include F^{LJ}, F^{s}, and an active force F^{active}, with associated parameters listed in Table S2.

When $\widetilde{\delta l_i^t} > \widetilde{\delta l_{iC}^t}$ the honeybee becomes active, and experiences an additional force in the direction of the time integrated negative normal stain gradient (i.e. the active force is directed toward a higher local strain):

$$F^{\mathrm{active}} = -f^{\mathrm{active}} \overrightarrow{\widetilde{\delta l_i^t}} \tag{B.10}$$

The direction, $\overrightarrow{\widetilde{\delta l_i^t}}$, is calculated as:

$$\overrightarrow{\widetilde{\delta l_i^t}} = \left(\sum_{\tilde{t}=t-T_w}^{t} \delta l_i^x(\tilde{t}) \times dt\right) \widehat{x} + \left(\sum_{\tilde{t}=t-T_w}^{t} \delta l_i^y(\tilde{t}) \times dt\right) \widehat{y} \tag{B.11}$$

where the instantaneous signal is defined as $\delta l_i^x(t) = \sum_{\forall j \in i} \delta l_{ij} \widehat{l_{ij}^x(t)}$, $\delta l_i^y(t) = \sum_{\forall j \in i} \delta l_{ij} \widehat{l_{ij}^y(t)}$, $\delta l_{ij} = \left|\left|\overrightarrow{l_{ij}(t)}\right| - \left|\overrightarrow{l_{ij}(0)}\right|\right|$.

If an active honeybee has less than 6 spring bonded interactions it would have a tendency to move

towards one of its neighbors and could lead to pathological expansion of cavities in the cluster. To prevent this, we allow bees to become active only if they have 6 spring bonded interactions.

			Unitless Value		
Parameter	Description	Type	Passive	Active	NMA
a	honeybee diameter	length	$2^{1/6} \sim 1.122$	$2^{1/6} \sim 1.122$	$2^{1/6} \sim 1.122$
k	spring coefficient	force/length	5×10^2	5×10^2	5×10^2
ϵ	Lennard-Jones (LJ) amplitude	length	1	2×10^2	–
g	gravitational coefficient	force	10^{-2}	–	–
η	amplitude of stochastic noise	length	0	2×10^{-2}	–
ζ	friction	force	5	–	–
f^{active}	active force	force	–	2.5×10^2	–
$r^{\text{LJ}}_{\text{cutoff}}$	cutoff for LJ force	force	a	3.5	–
$r^{\text{s}}_{\text{cutoff}}$	cutoff for spring force	length	inf	1.2	–
dt	time integration constant	time	3×10^{-2}	5×10^{-5}	–
$\widetilde{\delta l^t_{iC}}$	local strain threshold to become active	–	–	4×10^{-3}	–

Table B.3: Simulation parameters values for both the passive and active simulations described in section B.4, as well as the Normal Mode Analysis (NMA).

B.5 Response to Horizontal vs. Vertical Shakings

To test the differential strain hypothesis, we simulate the active model and compare the response of the cluster to horizontal and vertical shaking. Both the maximal instantaneous normal strain (Fig. B.4) as well as the integrated normal strain (Fig. B.4) are higher in response to a horizontal shaking. Therefore, there exists an activation threshold $\widetilde{\delta l_{iC}^{t}}$, such that most bees will not respond to vertical shaking but would respond to horizontal shaking. Indeed, we see that in this case the cluster shape remains approximately constant when vertical shaking are applied (Fig. B.4C–D), while the the bees adapt by spreading themselves into a squatter conical form when horizontal shaking are applied (Fig. B.4A–B).

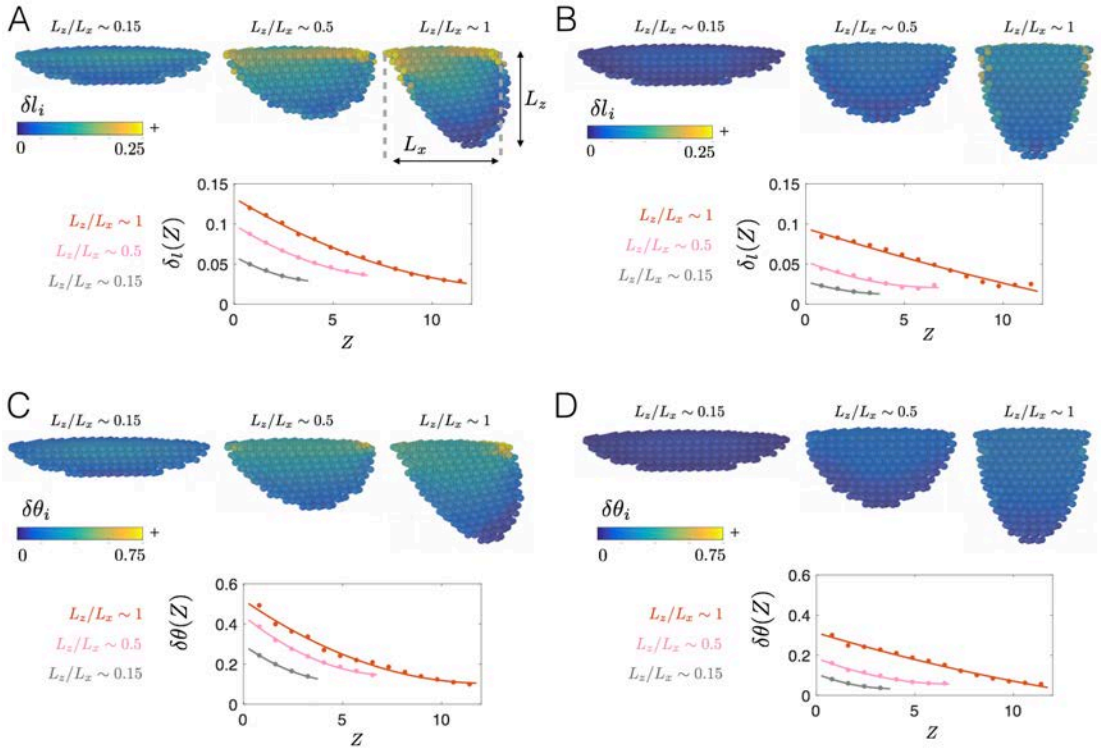

Figure B.4: Dynamic simulations of a 3D clusters. A) Clusters of different aspect ratios (L_z/L_x), shown at an extreme end of an oscillation associated with largest normal strains. Colors represent the local normal strain of each honeybee δl_i. Elongated clusters (on the right) experience a larger deformation at the tip of the cluster, while squat clusters (on the left) experience low deformations. Fountain plots show the mean normal strain ($\delta l(Z)$) as a function of the distance from the base, Z, and aspect ratio L_z/L_x. B) Same as A for a vertical shaking. C,D) same as A,B for the mean shear strain ($\delta\theta(Z)$).

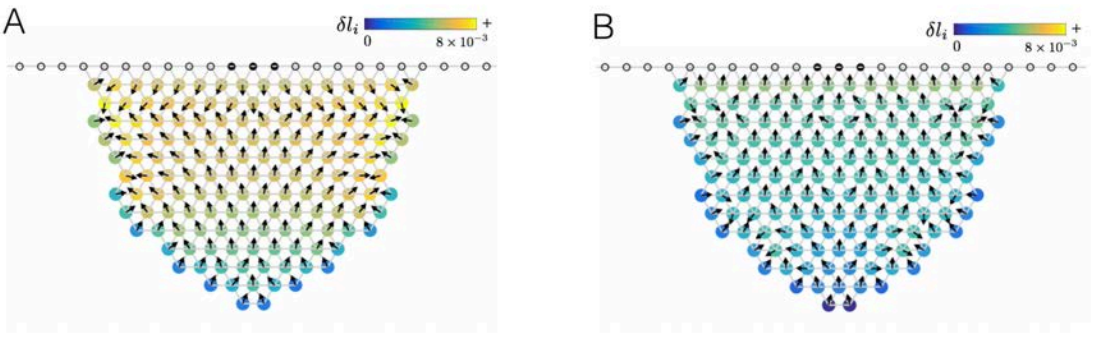

Figure B.5: Local integrated normal strains resulting from one shaking period. A) When horizontal shaking is applied. B) When vertical shaking is applied. Colors represent the local integrated signal, $\widetilde{\delta l_i^t}$, and arrows represent the direction towards higher local signal.

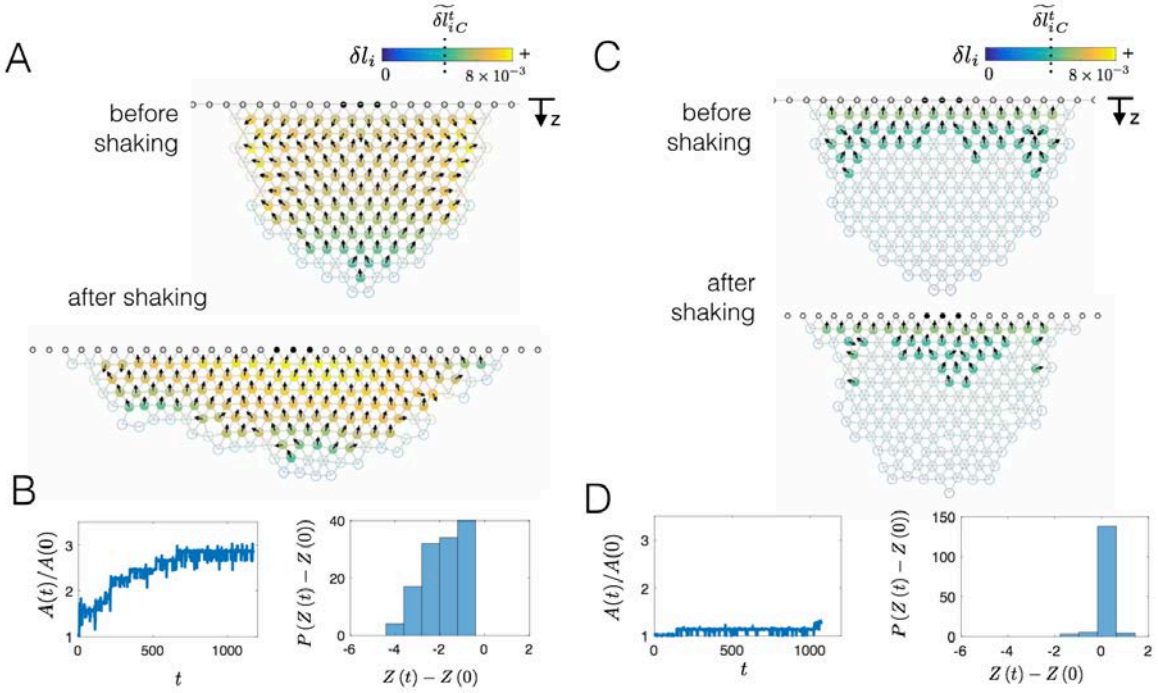

Figure B.6: Simulation of an active cluster in which the bees monitor their local deformation and follow a local rule in which once the deformation is larger than a certain threshold, the honeybee has a bias to move toward a region of higher local deformation. In agreement with experimental results, spreading occurs during horizontal shaking (A) but not during vertical shaking (C), in agreement with the experimental results. Colors represent the local integrated signal, $\widetilde{\delta l_i^t}$, and arrows represent the direction towards higher local signal. B,D) The relative base area as a function of time is similar to the results of experiments, with the probability distribution function of vertical displacement shows a net negative response, i.e. bees move upwards on average, for horizontal and vertical shaking respectively.

References

[1] Altshuler, D. L., Dickson, W. B., Vance, J. T., Roberts, S. P., & Dickinson, M. H. (2005). Short-amplitude high-frequency wing strokes determine the aerodynamics of honeybee flight. *Proceedings of the National Academy of Sciences*, 102(50), 18213–18218.

[2] Anderson, C., Theraulaz, G., & Deneubourg, J. L. (2002). Self-assemblages in insect societies. *Insectes Sociaux*, 49(2), 99–110.

[3] Beekman, M., Fathke, R. L., & Seeley, T. D. (2006). How does an informed minority of scouts guide a honeybee swarm as it flies to its new home? *Animal Behaviour*, 71(1), 161–171.

[4] Berdahl, A., Torney, C. J., Ioannou, C. C., Faria, J. J., & Couzin, I. D. (2013). Emergent sensing of complex environments by mobile animal groups. *Science*, 339(6119), 574–576.

[5] Bollazzi, M. & Roces, F. (2007). To build or not to build: circulating dry air organizes collective building for climate control in the leaf-cutting ant *Acromyrmex ambiguus*. *Animal Behaviour*, 74(5), 1349–1355.

[6] Bonabeau, E., Theraulaz, G., Deneubourg, J., Franks, N. R., Rafelsberger, O., Joly, J., & Blanco, S. (1998a). A model for the emergence of pillars, walls and royal chambers in termite nests. *Philosophical Transactions of the Royal Society of London B: Biological Sciences*, 353(1375), 1561–1576.

[7] Bonabeau, E., Theraulaz, G., Deneubourg, J.-L., Lioni, A., Libert, F., Sauwens, C., & Passera, L. (1998b). Dripping faucet with ants. *Physical Review E*, 57(5), 5904.

[8] Buck, J. & Buck, E. (1968). Mechanism of rhythmic synchronous flashing of fireflies: Fireflies of Southeast Asia may use anticipatory time-measuring in synchronizing their flashing. *Science*, 159(3821), 1319–1327.

[9] Burton, J. L. & Franks, N. R. (1985). The foraging ecology of the army ant *Eciton rapax*: an ergonomic enigma? *Ecological Entomology*, 10(2), 131–141.

[10] Camazine, S. (2003). *Self-organization in biological systems*. Princeton University Press.

[11] Camazine, S., Deneubourg, J. L., Franks, N., Sneyd, J., Theraulaz, G., & Bonabeau, E. (2002). *Self-organization in biological systems*.

[12] Cardinal, S. & Danforth, B. N. (2011). The antiquity and evolutionary history of social behavior in bees. *PLoS one*, 6(6), e21086.

[13] Cartar, R. V. (1992). Morphological senescence and longevity: An experiment relating wing wear and life span in foraging wild bumble bees. *The Journal of Animal Ecology*, 61(1), 225.

[14] Cook, C. N. & Breed, M. D. (2013). Social context influences the initiation and threshold of thermoregulatory behaviour in honeybees. *Animal Behaviour*, 86(2), 323–329.

[15] Cook, C. N., Durzi, S., Scheckel, K. J., & Breed, M. D. (2016). Larvae influence thermoregulatory fanning behavior in honeybees (*Apis mellifera* L.). *Insectes Sociaux*, (pp. 1–8).

[16] Couzin, I. D. (2009). Collective cognition in animal groups. *Trends in Cognitive Sciences*, 13(1), 36–43.

[17] Cully, S. M. & Seeley, T. D. (2004). Self-assemblage formation in a social insect: the protective curtain of a honey bee swarm. *Insectes Sociaux*, 51(4), 317–324.

[18] Dudley, R. (2002). *The biomechanics of insect flight*. Form, Function, Evolution. Princeton University Press.

[19] Dukas, R. & Dukas, L. (2011). Coping with nonrepairable body damage: effects of wing damage on foraging performance in bees. *Animal Behaviour*, 81(3), 635–638.

[20] Ellington, C. P. (1984). The aerodynamics of hovering insect flight. III. Kinematics. *Philosophical Transactions of the Royal Society of London B: Biological Sciences*, 305(1122), 41–78.

[21] Ellington, C. P. (1999). The novel aerodynamics of insect flight: applications to micro-air vehicles. *The Journal of Experimental Biology*, 202(23), 3439–3448.

[22] Eskov, E. K. & Toboev, V. A. (2009). Mathematical modeling of the temperature field distribution in insect winter clusters. *Biophysics*, 54(1), 85–89.

[23] Foster, D. J. & Cartar, R. V. (2011). What causes wing wear in foraging bumble bees? *The Journal of Experimental Biology*, 214(11), 1896–1901.

[24] Foster, P. C., Mlot, N. J., Lin, A., & Hu, D. L. (2014). Fire ants actively control spacing and orientation within self-assemblages. *The Journal of Experimental Biology*, 217(12), 2089–2100.

[25] Franks, N. R. (1989). Thermoregulation in army ant bivouacs. *Physiological Entomology*, 14(4), 397–404.

[26] Franks, N. R., Gomez, N., Goss, S., & Deneubourg, J. L. (1991). The blind leading the blind in army ant raid patterns: Testing a model of self-organization (Hymenoptera: Formicidae). *Journal of insect behavior*, 4(5), 583–607.

[27] Gilbert, C., Robertson, G., Lemaho, Y., Naito, Y., & Ancel, A. (2006). Huddling behavior in emperor penguins: Dynamics of huddling. *Physiology & Behavior*, 88(4-5), 479–488.

[28] Grassé, P.-P. (1959). La reconstruction du nid et les coordinations interindividuelles chezBellicositermes natalensis etCubitermes sp. la théorie de la stigmergie: Essai d'interprétation du comportement des termites constructeurs. *Insectes Sociaux*, 6(1), 41–80.

[29] Greenewalt, C. H. (1960). The wings of insects and birds as mechanical oscillators. In *Proceedings of the American Philosophical Society*.

[30] Grozinger, C. M., Richards, J., & Mattila, H. R. (2013). From molecules to societies: mechanisms regulating swarming behavior in honey bees (*Apis* spp.). *Apidologie*, 45(3), 327–346.

[31] Hedrick, T. L. (2008). Software techniques for two- and three-dimensional kinematic measurements of biological and biomimetic systems. *Bioinspiration & Biomimetics*, 3(3), 034001.

[32] Heinrich, B. (1981a). Energetics of honeybee swarm thermoregulation. *Science*, 212(4494), 565–566.

[33] Heinrich, B. (1981b). Energetics of honeybee swarm thermoregulation. *Science*, 212(4494), 565–566.

[34] Heinrich, B. (1981c). The mechanisms and energetics of honeybee swarm Temperature Regulation. *The Journal of Experimental Biology*, 91(1), 25–55.

[35] Higginson, A. D. & Gilbert, F. (2004). Paying for nectar with wingbeats: a new model of honeybee foraging. *Proceedings of the Royal Society of London B: Biological Sciences*, 271(1557), 2595–2603.

[36] Jackson, W. B. (1957). Microclimatic patterns in the army ant bivouac. *Ecology*, 38(2), 276–285.

[37] Jones, J. C., Helliwell, P., Beekman, M., Maleszka, R., & Oldroyd, B. P. (2005). The effects of rearing temperature on developmental stability and learning and memory in the honey bee, Apis mellifera. *Journal of Comparative Physiology B*, 191(12), 1121–1129.

[38] Jones, J. C., Myerscough, M. R., Graham, S., & Oldroyd, B. P. (2004). Honey bee nest thermoregulation: Diversity promotes stability. *Science*, 305(5682), 402–404.

[39] Jones, J. C. & Oldroyd, B. P. (2006a). Nest thermoregulation in social insects. *Advances in Insect Physiology*, 33, 153–191.

[40] Jones, J. C. & Oldroyd, B. P. (2006b). Nest thermoregulation in social insects. In *Advances in Insect Physiology Volume 33* (pp. 153–191). Elsevier.

[41] Josephson, R. K. (1981). Temperature and the mechanical performance of insect muscle. In B. Heinrich (Ed.), *Insect Thermoregulation* (pp. 19–44). New York: John Wiley and Sons.

[42] Jost, C., Verret, J., Casellas, E., Gautrais, J., Challet, M., Lluc, J., Blanco, S., Clifton, M. J., & Theraulaz, G. (2007a). The interplay between a self-organized process and an environmental template: corpse clustering under the influence of air currents in ants. *Journal of The Royal Society Interface*, 4(12), 107–116.

[43] Jost, C., Verret, J., Casellas, E., Gautrais, J., Challet, M., Lluc, J., Blanco, S., Clifton, M. J., & Theraulaz, G. (2007b). The interplay between a self-organized process and an environmental template: corpse clustering under the influence of air currents in ants. *Journal of The Royal Society Interface*, 4(12), 107–116.

[44] Khuong, A., Gautrais, J., Perna, A., Sbaï, C., Combe, M., Kuntz, P., Jost, C., & Theraulaz, G. (2016). Stigmergic construction and topochemical information shape ant nest architecture. *Proceedings of the National Academy of Sciences*, 113(5), 1303–1308.

[45] King, H., Ocko, S., & Mahadevan, L. (2015). Termite mounds harness diurnal temperature oscillations for ventilation. *Proceedings of the National Academy of Sciences*, 112(37), 11589–11593.

[46] Kronenberg, F. & Heller, H. C. (1982). Colonial thermoregulation in honey bees (*Apis mellifera*). *Journal of Comparative Physiology B*, 148(1), 65–76.

[47] Lemke, M. & Lamprecht, I. (1990). A model for heat production and thermoregulation in winter clusters of honey bees using differential heat conduction equations. *Journal of Theoretical Biology*, (142), 261–273.

[48] Loudon, C. & Koehl, M. A. (2000). Sniffing by a silkworm moth: wing fanning enhances air penetration through and pheromone interception by antennae. *The Journal of Experimental Biology*, 203(19), 2977–2990.

[49] Lushi, E., Wioland, H., & Goldstein, R. E. (2014). Fluid flows created by swimming bacteria drive self-organization in confined suspensions. *Proceedings of the National Academy of Sciences*, 111(27), 9733–9738.

[50] Marchetti, M. C., Joanny, J. F., Ramaswamy, S., Liverpool, T. B., Prost, J., Rao, M., & Simha, R. A. (2013). Hydrodynamics of soft active matter. *Reviews of Modern Physics*, 85(3), 1143–1189.

[51] Marden, J. H., O'Donnell, B. C., Thomas, M. A., & Bye, J. Y. (2015). Surface-skimming stoneflies and mayflies: The taxonomic and mechanical diversity of two-dimensional aerodynamic locomotion. *Physiological and Biochemical Zoology*, 73(6), 751–764.

[52] Marras, S., Batty, R. S., & Domenici, P. (2011). Information transfer and antipredator maneuvers in schooling herring. *Adaptive Behavior*, 20(1), 44–56.

[53] Miller, L. A. & Peskin, C. S. (2009). Flexible clap and fling in tiny insect flight. *The Journal of Experimental Biology*, 212(19), 3076–3090.

[54] Mlot, N. J., Tovey, C. A., & Hu, D. L. (2011). Fire ants self-assemble into waterproof rafts to survive floods. *Proceedings of the National Academy of Sciences*, 108(19), 7669–7673.

[55] Mountcastle, A. M., Alexander, T. M., Switzer, C. M., & Combes, S. A. (2016). Wing wear reduces bumblebee flight performance in a dynamic obstacle course. *Biology Letters*, 12(6), 20160294.

[56] Mountcastle, A. M. & Combes, S. A. (2014). Biomechanical strategies for mitigating collision damage in insect wings: structural design versus embedded elastic materials. *The Journal of Experimental Biology*, 217(7), 1108–1115.

[57] Myerscough, M. R. (1993). A simple model for temperature regulation in honeybee swarms. *Journal of Theoretical Biology*, 162(3), 381–393.

[58] Nachtigall, W. & Wilson, D. M. (1967). Neuro-muscular control of dipteran flight. *The Journal of Experimental Biology*, 47(1), 77–97.

[59] Nachtigall, W., Wisser, A., & Eisinger, D. (1998). Flight of the honey bee. VIII. Functional elements and mechanics of the "flight motor" and the wing joint – one of the most complicated gear-mechanisms in the animal kingdom. *Journal of Comparative Physiology B*, 168(5), 323–344.

[60] Neuhaus, W. & Wohlgemuth, R. (1960). Über das Fächeln der Bienen und dessen Verhältnis zum Fliegen. *Zeitschrift für vergleichende Physiologie*, 43(6), 615–641.

[61] Ocko, S. & Mahadevan, L. (2014). Collective thermoregulation in bee clusters. *Journal of The Royal Society Interface*, 11(91), 20131033–20131033.

[62] Ocko, S. & Mahadevan, L. (2015). Feedback-induced phase transitions in active heterogeneous conductors. *Physical Review Letters*, 114(13), 134501.

[63] Oldroyd, B. P. & Wongsiri, S. (2009). *Asian honey bees*. Biology, Conservation, and Human Interactions. Harvard University Press.

[64] Omholt, S. W. (1987). Thermoregulation in the winter cluster of the honeybee, *Apis Mellifera*. *Journal of Theoretical Biology*, 128(2), 219–231.

[65] Omholt, S. W. & Lonvik, K. (1986). Heat production in the winter cluster of the honeybee, *Apis mellifera*. A theoretical study. *Journal of Theoretical Biology*, (120), 447–456.

[66] Peeters, C. & De Greef, S. (2015). Predation on large millipedes and self-assembling chains in *Leptogenys* ants from Cambodia. *Insectes Sociaux*, 62(4), 471–477.

[67] Peters, J. M., Gravish, N., & Combes, S. A. (2017). Wings as impellers: honey bees co-opt flight system to induce nest ventilation and disperse pheromones. *The Journal of Experimental Biology*, 220(12), 2203–2209.

[68] Phonekeo, S., Mlot, N., Monaenkova, D., Hu, D. L., & Tovey, C. (2017). Fire ants perpetually rebuild sinking towers. *Royal Society Open Science*, 4(7), 170475.

[69] Reid, C. R., Lutz, M. J., Powell, S., Kao, A. B., Couzin, I. D., & Garnier, S. (2015). Army ants dynamically adjust living bridges in response to a cost–benefit trade-off. *Proceedings of the National Academy of Sciences*, 112(49), 15113–15118.

[70] Ribands, C. R. & Speirs, N. (1953). The adaptability of the homecoming honeybee. *The British Journal of Animal Behaviour*, 1(2), 59–66.

[71] Rieucau, G., Holmin, A. J., Castillo, J. C., Couzin, I. D., & Handegard, N. O. (2016). School level structural and dynamic adjustments to risk promote information transfer and collective evasion in herring. *Animal Behaviour*, 117, 69–78.

[72] Schaap, P. (2011). Evolution of developmental cyclic adenosine monophosphate signaling in the Dictyostelia from an amoebozoan stress response. *Development, Growth & Differentiation*, 53(4), 452–462.

[73] Schmitz, H. (1994). Thermal characterization of butterfly wings—1. Absorption in relation to different color, surface structure and basking type. *Journal of Thermal Biology*, 19(6), 403–412.

[74] Seeley, T. D. (1974). Atmospheric carbon dioxide regulation in honey-bee (*Apis mellifera*) colonies. *Journal of insect physiology*, 20(11), 2301–2305.

[75] Seeley, T. D. (2010). *Honeybee democracy*. Princeton University Press.

[76] Seeley, T. D. & Morse, R. A. (1976). The nest of the honey bee (*Apis mellifera L.*). *Insectes Sociaux*, 23(4), 495–512.

[77] Southwick, E. E. & Moritz, R. F. A. (1987). Social control of air ventilation in colonies of honey bees, Apis mellifera. *Journal of Insect Physiology*, 33(9), 623–626.

[78] Srygley, R. B. & Thomas, A. L. R. (2002). Unconventional lift-generating mechanisms in free-flying butterflies. *Nature*, 420(6916), 660–664.

[79] Sumpter, D. J. T. & Broomhead, D. S. (2000). Shape and dynamics of thermoregulating honey bee clusters. *Journal of Theoretical Biology*, 204(1), 1–14.

[80] Tennenbaum, M., Liu, Z., Hu, D., & Fernandez-Nieves, A. (2016). Mechanics of fire ant aggregations. *Nature Materials*, 15(1), 54–59.

[81] Theraulaz, G., Bonabeau, E., & Deneubourg, J. L. (1998a). The origin of nest complexity in social insects. *Complexity*.

[82] Theraulaz, G., Bonabeau, E., & Denuebourg, J.-N. (1998b). Response threshold reinforcements and division of labour in insect societies. *Proceedings of the Royal Society of London B: Biological Sciences*, 265(1393), 327–332.

[83] Theraulaz, G., Bonabeau, E., Nicolis, S. C., Solé, R. V., Fourcassié, V., Blanco, S., Fournier, R., Joly, J.-L., Fernández, P., Grimal, A., Dalle, P., & Deneubourg, J.-L. (2002). Spatial patterns in ant colonies. *Proceedings of the National Academy of Sciences*, 99(15), 9645–9649.

[84] Theraulaz, G., Gautrais, J., Camazine, S., & Deneubourg, J.-L. (2003). The formation of spatial patterns in social insects: from simple behaviours to complex structures. *Philosophical Transactions of the Royal Society of London A: Mathematical, Physical and Engineering Sciences*, 361(1807), 1263–1282.

[85] Tomoyasu, Y., Arakane, Y., Kramer, K. J., & Denell, R. E. (2009). Repeated co-options of exoskeleton formation during wing-to-elytron evolution in beetles. *Current Biology*, 19(24), 2057–2065.

[86] Vance, J. T., Altshuler, D. L., Dickson, W. B., Dickinson, M. H., & Roberts, S. P. (2015). Hovering flight in the honeybee *Apis mellifera*: Kinematic Mechanisms for Varying Aerodynamic Forces. *Physiological and Biochemical Zoology*, 87(6), 870–881.

[87] von Frisch, K. & Lindauer, M. (1956). The "language" and orientation of the honey bee. *Annual Review of Entomology*, 1(1), 45–58.

[88] Watmough, J. & Camazine, S. (1995). Self-organized thermoregulation of honeybee clusters. *Journal of Theoretical Biology*, 176(3), 391–402.

[89] Weis-Fogh, T. (1973). Quick estimates of flight fitness in hovering animals, including novel mechanisms for lift production. *The Journal of Experimental Biology*, 59(1), 169–230.

[90] Zitterbart, D. P., Wienecke, B., Butler, J. P., & Fabry, B. (2011). Coordinated movements prevent jamming in an emperor penguin huddle. *PLoS one*, 6(6), e20260.